

ADVERTIMENT. La consulta d'aquesta tesi queda condicionada a l'acceptació de les següents condicions d'ús: La difusió d'aquesta tesi per mitjà del servei TDX (www.tesisenxarxa.net) ha estat autoritzada pels titulars dels drets de propietat intel·lectual únicament per a usos privats emmarcats en activitats d'investigació i docència. No s'autoritza la seva reproducció amb finalitats de lucre ni la seva difusió i posada a disposició des d'un lloc aliè al servei TDX. No s'autoritza la presentació del seu contingut en una finestra o marc aliè a TDX (framing). Aquesta reserva de drets afecta tant al resum de presentació de la tesi com als seus continguts. En la utilització o cita de parts de la tesi és obligat indicar el nom de la persona autora.

ADVERTENCIA. La consulta de esta tesis queda condicionada a la aceptación de las siguientes condiciones de uso: La difusión de esta tesis por medio del servicio TDR (www.tesisenred.net) ha sido autorizada por los titulares de los derechos de propiedad intelectual únicamente para usos privados enmarcados en actividades de investigación y docencia. No se autoriza su reproducción con finalidades de lucro ni su difusión y puesta a disposición desde un sitio ajeno al servicio TDR. No se autoriza la presentación de su contenido en una ventana o marco ajeno a TDR (framing). Esta reserva de derechos afecta tanto al resumen de presentación de la tesis como a sus contenidos. En la utilización o cita de partes de la tesis es obligado indicar el nombre de la persona autora.

WARNING. On having consulted this thesis you're accepting the following use conditions: Spreading this thesis by the TDX (www.tesisenxarxa.net) service has been authorized by the titular of the intellectual property rights only for private uses placed in investigation and teaching activities. Reproduction with lucrative aims is not authorized neither its spreading and availability from a site foreign to the TDX service. Introducing its content in a window or frame foreign to the TDX service is not authorized (framing). This rights affect to the presentation summary of the thesis as well as to its contents. In the using or citation of parts of the thesis it's obliged to indicate the name of the author



UNIVERSITAT POLITÈCNICA
DE CATALUNYA

DOCTORAL PROGRAMME ON
BIOMEDICAL ENGINEERING

**Mathematical models and
multiscale simulations of
cellular secretion processes**

Thesis presented by

Virginia González-Vélez

to obtain the qualification of Doctor

Supervisor:

Dra. Amparo Gil-Gómez

Dept. Matemática Aplicada y C.C.

Universidad de Cantabria

Barcelona, Spain, July 26th, 2011

Acknowledgements

Quiero agradecer profundamente a Amparo, que además de dirigir esta tesis, me ha dado su confianza, su tiempo y su apoyo en todo momento, incluso antes de conocerme. Le doy las gracias por hacer posible este proyecto de estudios y de vida.

Agradezco también a los investigadores Iván Quesada, Luis Miguel Gutiérrez y Almudena Albillos por darle sentido fisiológico a este trabajo, y por lo mucho que he disfrutado y aprendido al trabajar con ellos.

Many thanks to Geneviève for her patience, her knowledge, and the great moments working (and not working) together.

Gracias a Dionisio, mi amado esposo y compañero de vida, porque sin él, sin su apoyo incondicional y su gran amor, este trabajo nunca se hubiese iniciado (y mucho menos, culminado).

Gracias a Marlén por sus correcciones lingüísticas, pero sobre todo, por su maravillosa amistad.

Dedico este trabajo a mis hijos, Sofi y Eli, que alegran cada día de mi vida.

Finalmente, agradezco a la Universidad Autónoma Metropolitana Azcapotzalco y a CONACyT México por el apoyo económico otorgado para la realización de esta tesis.

Abstract

Exocytosis is the cellular process whereby a product such as a hormone or a neurotransmitter is released as a response to stimulation. There are a lot of exocytotic cells in mammals, and each cell type has their specific subcellular mechanisms, needed to achieve the final substance release. Therefore, unveiling the role of subcellular mechanisms in secretion processes is highly relevant to understand disease evolution and possible therapies.

The efficiency of the coupling between stimulus and secretion is mainly managed by an intracellular Ca^{2+} signal. In the present thesis, a modeling approach of Ca^{2+} -triggered secretion is presented for some different cellular types. In particular, cells with different characteristic time scales were chosen in order to discuss about a multiscale approach for studying spatiotemporal features of secretion processes. The object of this piece of research ranges from a short temporal scale (fast secretion) up to a long temporal scale (slow secretion). The study also discuss the intermediate temporal scale, and the joining point between theoretical methodologies. Cellular Ca^{2+} and secretion dynamics have been studied in the abovementioned timescales for the calyx of Held presynaptic terminal, the pancreatic alpha cell, and the adrenal chromaffin cell, respectively.

The aim of this work has been twofold: first, to develop mathematical models that follow actual sub-cellular mechanisms involved in secretion, and second, to make simulations on these models in order to reproduce the experimentally observed Ca^{2+} and secretory behaviour. The ultimate goal is to propose common methodologies and algorithms to support the theoretical approach for studying multiscale cellular processes.

KEYWORDS: cellular secretion, exocytosis, modeling, simulation, computational cell biology.

Preface

Calcium is mainly concentrated in teeth and bones in higher organisms as mammals, and it is moved through the body as a divalent ion (Ca^{2+}). This ion is the most ubiquitous cell signaler that nature uses to trigger and control a lot of vital processes such as muscular contraction, genetic transcription, cell proliferation and differentiation, and regulated secretion of hormones and neurotransmitters, between many others [193]. Ca^{2+} homeostasis is carefully kept inside the body to maintain fixed amounts of Ca^{2+} in the intracellular and extracellular liquids. For example, in resting conditions, the ratio between extracellular and intracellular calcium concentrations is of four orders of magnitude i.e., ten thousand times. This difference guarantees an endless source for cells, and at the same time, it makes cells highly sensitive to very small changes (even of few ions) in the internal calcium ion concentration [48]. The huge gradient of Ca^{2+} between both sides of a cell is kept thanks to a cell membrane that acts as a barrier and to some specific mechanisms that work all the time to take out any excess, named extrusion mechanisms. However, there are other mechanisms that allow Ca^{2+} to enter into the cell in a selective manner, mainly calcium channels. Calcium channels are proteins located across the cell membrane that are normally closed (i.e., not allowing Ca^{2+} to go from the outside to the inside), but they can open in response to a specific stimulus (voltage, ligand or emptying of intracellular stores) [48]. Since ions are charged particles, when some ions are crossing the cell membrane they can be detected as an ionic (electric) current. Using two electrodes, one in the cell inside and one in the external side, it is possible to measure an electrical current. It is common, in biophysics experiments, that currents going from the exterior to the interior are conceived as, and plotted as, negative currents.

In 1968, the term *stimulus-secretion coupling* was coined to describe the vital role of Ca^{2+} as the coupling agent between the stimulus and the secretion process, based on observations in neuroendocrine cells [37]. In other words, the particular physiological process starts by producing an adequate stimulation that opens some calcium channels, produces a calcium current, and consequently increases the intracellular calcium level. As will be detailed in the next sections, the presence of incoming Ca^{2+} is decoded to trigger secretion through its binding to specific Ca^{2+} sensors located in the cell membrane and/or in the vesicles [11]. To always keep the vital calcium gradient, the extrusion mechanisms will work constantly to take out all the extra Ca^{2+} which is inside the cell. However, some ions will have time to diffuse into the cell core to trigger other processes. Thus, the temporal dynamics of intracellular calcium concentration ($[Ca^{2+}]_i$) is strongly related to the corresponding dynamics of those physiological processes that such a behaviour activates, as is the case of Ca^{2+} -triggered secretion (also named *exocytosis*) [193].

The optimal functioning of the nervous system strongly depends on neurotransmission, that is, the whole process of passing a signal from one neuron (presynapse or presynaptic) to another (postsynaptic) by releasing a substance (neurotransmitter) into the synapse, i.e., the junction between them. The efficiency of neurotransmitter release, depends in turn on the number of active zones (releasing areas) located in the presynaptic neuron, as well as on the speed of vesicle fusion on time. Vesicles are the small bags inside the cell that contain the releasing substance. Once the

secretion process is started, it is finished when the vesicle fuses its membrane with the cellular one, opening a pore through which its contents are released to the cell exterior. Not only secretion depends on vesicles, but it is also influenced by the organization of the exocytotic machinery, including Ca^{2+} channels and other relevant proteins; they all shape the spatiotemporal dynamics of the stimulus-secretion coupling [7]. Presynaptic terminals of the central nervous system are characterized for their high efficiency because the secretory response appears just a few milliseconds after a single action potential stimulates the presynaptic neuron. Fast secretion is possible thanks to effective geometrical and physiological factors such as the spatial coupling of vesicles and Ca^{2+} channels, and the availability of a pool of vesicles. Indeed, calcium channels are known to play a key role in the control of neurotransmitter release, in particular, those that open in response to cell depolarization (voltage-gated channels). Vesicles are also important to have a fast response, but there needs to be enough of them and they have to be ready to be fused, so as to have an efficient stimulus-secretion coupling [121]. Despite the great relevance of neurotransmitter release in the adequate functioning of the nervous system in mammals, the study of the stimulus-secretion coupling has enormous experimental restrictions since fast, microscopic, and not invasive systems are needed to simultaneously record a stimulus and its corresponding response. Theoretical modeling and simulation are very useful tools for complementing experimental studies in such a way that their combination allows a more thorough interpretation of results.

It is important to emphasize that secretion is not only observed in the central nervous system, where neurotransmitters such as glutamate or acetylcholine, are the released substances [157]. Neuroendocrine cells are peripheral cells that secrete hormones needed to start vital process like glucose regulation, fat metabolism, stress control, etc. In this case, secretion is also triggered by Ca^{2+} , in a similar manner to neurotransmitter release. However, the main differences are: one, the time delay in-between stimulus and release, which is much longer; two, the sources for $[Ca^{2+}]_i$ elevations; and three, the associated $[Ca^{2+}]_i$ dynamics [130]. In neuroendocrine cells, Ca^{2+} elevations do not occur as fast as in neurons, but they occur more slowly (lasting milliseconds to seconds), or they even appear as oscillations (lasting seconds to minutes). On the other hand, the intracellular calcium elevation could be due to the opening of calcium channels but also to the release from intracellular stores in a variable proportion; this combination may lead to calcium oscillations. Thus, the relevant time scales of Ca^{2+} dynamics and release are in the range of seconds up to minutes and they frequently appear as rhythmic secretion levels [24]. Again, theoretical modeling and simulation may help experimental studies to unveil how $[Ca^{2+}]_i$ is being increased and how it is decoded to trigger secretion, as well as which the main factors affecting the secretory response are. Moreover, since dynamic variables are hard to be recorded in experiments, modeling could serve for testing some experimental protocols to predict cellular responses to stimulation. Also, experiments can be suggested by the model to test the possible influence of a mechanism, or the benefits of a drug therapy.

Although synaptic terminals and neuroendocrine cells share the vital function of Ca^{2+} -triggered exocytosis, some crucial differences have been found [130]: 1) Neuroendocrine cells can be considered approximately spherical but neurons and synapses are usually elongated (since they are branches of the axon); 2) Vesicle release in synapses has a very fast component, lasting below 3 ms, while neuroendocrine cells exhibit a

delayed response at least 10 to 20 ms after they were stimulated; and 3) Distance and correlation between Ca^{2+} channels and ready releasable vesicles are completely different, being clustered and close in synapses, and being vesicles far away from channels in neuroendocrine cells. These important differences in time scales and spatial organization of the secretory machinery impose the need for defining the relevant time periods for studying the stimulus-secretion coupling; defining specific models that closely describe main mechanisms participating in exocytosis; converting models to equations; choosing the adequate mathematical methods to solve models considering time scales and experimental data; building algorithms to simulate real protocols that complement experimental observations; and, sharing common models and algorithms, and complementing results from them to reach a multiscale simulation. These have been the main stages we have followed during the development of the present project in order to reach the main goal: studying Ca^{2+} -triggered secretion processes in three cell types (calyx of Held, chromaffin and alpha cells), which present time scale differences, on the basis of a multiscale approach. Among many intermediate and interesting objectives reached throughout the development of the present work, the ultimate goal has been exploring solutions for diseases associated with impaired exocytosis in the chosen cell types; that is, hearing impairment, related to the calyx presynaptic terminal [174]; impaired adrenaline secretion, associated with adrenal chromaffin cells [58]; and diabetes, partly due to alpha cells [141].

Contents

1	Introduction	1
2	Modeling tools and mathematical methods	4
2.1	Studying Ca^{2+} dynamics	4
2.1.1	Modeling Ca^{2+} influx through voltage-dependent ionic channels	5
2.1.2	Modeling calcium diffusion	12
2.1.3	Modeling biochemical reaction kinetics	14
2.1.4	Modeling calcium extrusion	17
2.2	Developed models	17
2.2.1	Active-zone model	17
2.2.2	Cytoskeleton-cage model	19
2.2.3	Shell model	19
2.3	Mathematical and numerical methods	20
2.3.1	Stochastic methods	20
2.3.2	Deterministic methods	23
3	The calyx of Held presynapsis: Studying fast secretion	27
3.1	Introduction	27
3.2	Modeling	29
3.2.1	P-type Ca^{2+} channel model	30
3.3	Simulations	30
3.3.1	Influence of exogenous buffers on fast release	33
3.3.2	Vesicle-fusion models and cooperativity of release	35
3.3.3	Spatial channel organization and kinetic cooperativity	37
3.4	Discussion of results	38
4	Bovine chromaffin cells: Studying spatiotemporal features	41
4.1	Introduction	41
4.2	Experimental data	42

4.3	Modeling	43
4.3.1	L- and P/Q-type Ca^{2+} channel models	45
4.4	Simulations	45
4.4.1	Spatio-temporal distribution of $[Ca^{2+}]_i$	45
4.4.2	Modeling cytoskeleton influence on exocytosis	48
4.5	Discussion	48
5	Human chromaffin cells:	
	Studying intermediate secretion	51
5.1	Introduction	51
5.2	Experimental data	52
5.3	Modeling	54
5.3.1	Intermediate secretion	56
5.3.2	Fast secretion	57
5.4	Results	57
5.4.1	Multiscale aspects	58
5.5	Discussion	62
6	Alpha cells:	
	Studying slow secretion	66
6.1	Introduction	66
6.2	Experimental data	68
6.3	Modeling glucagon secretion based on calcium oscillations	70
6.3.1	Frequency of oscillations	70
6.3.2	Model description	71
6.4	Results	78
6.4.1	Secretion induced at low and high glucose	78
6.4.2	Secretion induced by constant $[Ca^{2+}]_i$ levels	82
6.4.3	Effect of oscillation frequency and mean $[Ca^{2+}]_i$ levels on secretion	83
6.5	Discussion	84
7	Alpha cells:	
	Electrical activity related to glucagon secretion	88
7.1	Introduction	88
7.2	Modeling ionic channels and electrical currents relevant to glucagon secretion	88
7.2.1	A-type K^+ channels	90
7.2.2	DR-type K^+ channels	91
7.2.3	Na^+ channels	91
7.2.4	T-type Ca^{2+} channels	91
7.2.5	N-type Ca^{2+} channels	92
7.3	Discussion	94
8	Conclusions	96
A	Publications derived from this thesis	103

B Algorithms	106
B.1 Routines for parameter estimation of channel models	106
B.2 Routines for the Stochastic models	107
B.3 Routines for the Deterministic model	109

List of Figures

2.1	Two, three, and four state models and associated differential equations.	6
2.2	Flow diagram for finding best parameter set for channel models	9
2.3	Comparison of static and dynamic parameter estimations.	10
2.4	The Active-zone model.	18
2.5	The Cytoskeleton-cage model.	19
2.6	The Shell model.	19
2.7	Random walk	21
2.8	Flow diagram for solving the stochastic models.	22
2.9	Flow diagram for solving the deterministic model.	24
3.1	The calyx of Held presynaptic terminal	27
3.2	Model for the P-type Ca^{2+} channel	32
3.3	Influence of exogenous buffers (BAPTA and EGTA) on fast release . .	34
3.4	Delay of peak release rates due to exogenous buffers	34
3.5	Influence of BAPTA buffer on accumulated secretion for high and low Ca^{2+} influx	34
3.6	Accumulated secretion predicted by different kinetic schemes	36
3.7	Estimated Ca^{2+} thresholds of secretion	36
3.8	Release rates for the cooperative and non-cooperative schemes	37
3.9	Spatial random and clustered distribution of Ca^{2+} channels and vesicles	38
3.10	Secretion predicted by a Ca^{2+} -channel cluster and a non-cooperative kinetic scheme	39
3.11	Kinetic cooperativity at low Ca^{2+} influx	39
4.1	Localization of adrenal glands which are composed of chromaffin cells .	41
4.2	Spatial heterogeneity in the distribution of Ca^{2+} influx and Ca^{2+} channels in bovine chromaffin cells	42
4.3	Model of spatial arrangements of channel clusters and the secretory machinery in bovine chromaffin cells	44
4.4	Simulation of spatial Ca^{2+} distribution in bovine chromaffin cells	47

4.5	Tested cluster-vesicle positions used to investigate cytoskeleton influence on secretion	47
4.6	Ca^{2+} dynamics and secretion for the tested cluster-vesicle arrangements in a cytoskeleton cage	49
5.1	Experimental equipment used for the "patch-clamp" technique	52
5.2	Experimental measurements of secretion and Ca^{2+} currents in human chromaffin cells	53
5.3	Relationship between cell secretion and pulse duration in human chromaffin cells	53
5.4	Secretion model for chromaffin cells	56
5.5	Dynamic simulation of Ca^{2+} concentration and secretion for human chromaffin cells	59
5.6	Theoretical and experimental secretion in human chromaffin cells	59
5.7	Spatial relationship between the Shell (S) and the Active-zone (AZ) model in human chromaffin cells	60
5.8	Relevance of Ca^{2+} channel density on $[Ca^{2+}]_i$ spatial distribution	61
5.9	Comparison of accumulated secretion predicted by the stochastic and the deterministic models for human chromaffin cells	61
5.10	Ca^{2+} -dependence of capacitance increments in human chromaffin cells	63
5.11	Pool contribution to secretion in human chromaffin cells	65
6.1	Location of pancreas within the human body	66
6.2	Immunofluorescence image of a mouse pancreatic α -cell	69
6.3	Some experimental Ca^{2+} oscillations from α -cells	69
6.4	How the Ca^{2+} oscillation frequency is computed	70
6.5	Stages proposed for glucagon secretion	71
6.6	Intracellular Ca^{2+} dynamics in an α -cell	72
6.7	Parameter dependence of the glucagon secretion model	76
6.8	Secretion dynamics of 14 α -cells along 20 minutes	79
6.9	Continue from Figure 6.8	80
6.10	Summary of α -cell secretion rates for 20 minutes	81
6.11	α -cell secretion rate per hour induced by Ca^{2+} oscillations	82
6.12	Mean Ca^{2+} level of the 14 α -cells	83
6.13	α -cell secretion rates per hour induced by a constant Ca^{2+} level	83
6.14	Computed frequency for the 14 Ca^{2+} oscillations	84
6.15	Secretion rate as a function of oscillation frequency in α -cells	85
6.16	Secretion rate as a function of individual mean Ca^{2+} level in α -cells	85
7.1	Simulated current-to-voltage curves and dynamic currents in α -cells	93

List of Tables

3.1	Parameter values used to simulate secretion in the calyx of Held, using the Active-zone model	31
3.2	Continue from Table 3.1.	32
4.1	Parameter values used to simulate secretion in bovine chromaffin cells, using the Cytoskeleton-cage model	46
5.1	Average data from experiments in human chromaffin cells	55
5.2	Parameter values of the secretion model for human chromaffin cells	58
5.3	Parameter values used to simulate $[Ca^{2+}]_i$ dynamics, in human chromaffin cells, using the Shell (S) and the Active-zone (AZ) model	62
6.1	Parameter values to estimate membrane Ca^{2+} concentration in pancreatic α -cells.	74
6.2	Parameter values of the glucagon secretion model.	78
6.3	Distribution of individual α -cell secretion.	83
7.1	Fixed values for ionic channel models of pancreatic α -cells	89
7.2	Fitted values for ionic channel models of pancreatic α -cells	89
7.3	Estimated conductances and channel densities in α -cells	94
8.1	Studied cell types and modeled ionic channels	102
8.2	Models and solving methods	102
8.3	Cell types, spatiotemporal scales, and models	102

CHAPTER 1

Introduction

Exocytosis, the process of releasing a substance contained inside vesicles or granules out of the cell membrane, is tightly regulated by Ca^{2+} in many cells as is the case of the cell types studied in this thesis. During the exocytotic pathway, vesicles traverse several steps: trafficking or moving them through the intracellular space (*cytosol*) helped by the *cytoskeleton* (the supporting structure of the cytosol); tethering or attaching them near the membrane; docking or tightly attaching them to release sites; priming or activating vesicles to be ready; fusion of vesicle membrane with cell membrane; release of vesicle contents; and finally, vesicle membrane retrieval. In Ca^{2+} -regulated exocytosis, Ca^{2+} participates in some of these steps along with other substances like ATP [24]. For the present study, the main effort is made in order to study those stages controlled by Ca^{2+} , namely, resupply or trafficking, priming, fusion and release. For each cellular case examined in this thesis (the calyx of Held, the chromaffin cell and the alpha cell), a model that includes one or more of these stages in a detailed manner, connecting it to $[Ca^{2+}]_i$ dynamics, is developed.

Models are becoming an important research tool in biology. Simulations based on biological models can reveal relevant roles of microscopic mechanisms that affect macroscopic behaviour. The multiscale approach tries to connect the microscopic events to the macroscopic physiological phenomenon by developing models and software tools, which can cross the spatial and temporal scales [1]. One of the main steps to reach this goal is to select the adequate mathematical and computational methods to solve each particular model. These methods range from those suitable for simulating microscopic events occurring in short time periods, as the discrete Monte Carlo methods, up to those able to simulate more macroscopic issues taking place in longer intervals, as continuous or deterministic methods [145]. In the present case, i.e., the study of secretion in different cellular environments, the multiscale perspective allows us to recognize similarities and relevant differences, towards sharing common models and algorithms, in order to reach a multiscale simulation of cellular exocytosis.

As far as we know, there have been no previous multiscale studies of secretion processes in several cell types. However, modeling works about secretion on a specific

cell type have been reported. There are some works on synapses, where fastest secretion (shortest timescale) takes place, which propose kinetic models for secretion and calcium influx based on experimental data [59, 78, 86, 109, 172, 198]. There are some others which study neurotransmitter release using Monte Carlo methods, but not in the calyx of Held [60, 72, 84]. With regard to the calyx of Held, there are simulations of neurotransmitter modulation to analyze possible channel-vesicle localizations in the active zones [119, 120], and simulations that evidence the influence of Ca^{2+} influx in neurotransmitter release [13, 163]. Nevertheless, there is no a global model which considers all factors (vesicle population, channel-vesicle configuration, calcium influx, secretion profiles and mobile buffers), that simulates glutamate release at a microscopic level. On neuroendocrine chromaffin cells, secretion has been modeled as a compartmental process, or a kinetic reaction, assuming that vesicles belong to different pools that are triggered by calcium to be fused, which is based on experimental findings [97]. There are modeling works on secretion that relate calcium concentrations to secretion proposing kinetic models [98, 115, 189], and a microscopic study about channel-vesicle localization in chromaffin cells [160]. There is also one simulation study using open software environments [192]. Being a broadly used cell model for research on exocytosis, chromaffin cells are still valuable to understand stimulus-secretion coupling. Moreover, proposed models were developed for chromaffin cells in an animal species that may not be applicable to other species. On pancreatic alpha cells, there is no modeling work about glucagon secretion. In fact, the only modeling work about alpha cells is the one reported by [34] that simulates electrical activity associated with glucagon secretion, trying to predict glucose influence on secretion.

Objectives

The main goal of the present thesis is to study cellular secretion in various cell types covering different time scales. For this purpose, the following aspects have been considered:

- The choice of cellular types that exhibit secretion in different time scales, from milliseconds to minutes i.e., from fast to slow secretion.
- The modeling of real mechanisms present in the cell and known to be strongly involved in Ca^{2+} -controlled secretion.
- The modeling of secretion dynamics based on experimental findings.
- The simulation of intracellular calcium and secretion dynamics including spatiotemporal cell features, using adequate numerical methods and algorithms.

Cellular secretion is mainly controlled by calcium in the studied cells, but displays particular differences in the way it does. This hypothesis makes sense since calcium-triggered secretion follows similar steps: An external stimulus is translated into an intracellular calcium increase that initiates buffered calcium diffusion in the cytosol; intracellular calcium triggers secondary processes like secretion. Secretion is activated because the calcium sensor associated with exocytosis binds calcium ions, so vesicles

are fused, and then, they release their contents to the extracellular medium. However, crucial differences are found in each cell type: 1) The nature and characteristics of a stimulus able to produce exocytosis; 2) The levels of intracellular calcium needed to trigger secretion; 3) The localization, quantity and readiness of vesicles; and, 4) The dynamic behaviour of intracellular calcium that determines the timescale of secretion.

The study of three cell types (calyx of Held, chromaffin cell, and alpha cell), comprehends exocytosis taking place in milliseconds, (fast secretion), seconds (intermediate secretion), and minutes (slow secretion). This set of cases covers fast, intermediate and slow dynamic behaviours of calcium and release, which requires to model an active zone up to the whole cell, and that finally require short, medium and long time scale simulations. Then, we will discuss a multiscale perspective of exocytosis. The multiscale approach adds complementary tools that improve the simulating task by sharing mathematical methods and algorithms suitable for each set of models.

Since the present thesis has been developed in the framework of a Biomedical Engineering doctoral programme, our approach has been intended to cover goals in two main areas of research: biomedicine and engineering. Within the former, the present work addresses the cellular secretion topic that belongs to the *Cell Biology* discipline; this discipline studies cell behaviour at different spatial and temporal levels. Within the latter, this work makes use of mathematical and computational tools to study the biomedical problem from a theoretical perspective. Therefore, the present thesis is an example of an interdisciplinary study developed to integrate experimental biomedical data to spatiotemporal models and simulations. The term *Computational cell biology* was coined some years ago to describe this research area [167].

Modeling tools and mathematical methods

2.1 Studying Ca^{2+} dynamics

Secretion is one of the most important and sophisticated processes in which a cell can exhibit its magnificent capabilities. Theoretical studies on the spatiotemporal Ca^{2+} dynamics in a cell are useful to predict main Ca^{2+} controlling processes, and to understand their impact on secretion [129]. Ca^{2+} dynamics is severely affected by Ca^{2+} buffers that slow down the free movement of incoming calcium ions, and each cell type has its particular kind of buffers, each one with specific kinetic characteristics [14]. Moreover, in many experiments, external Ca^{2+} buffers are added to allow fluorescent images (like Fura-2 fluorescent dye), or to study the Ca^{2+} -dependence of secretion (like BAPTA or EGTA buffers) [173]. Thus, to predict a correct intracellular Ca^{2+} behaviour along time and space, and to quantify how the presence of calcium ions start a secretion process, it is necessary to consider the following mechanisms:

1. Calcium ions that enter into the cell, in response to a stimulus.
2. Calcium diffusion in the intracellular space.
3. Buffers (internal or external) and barriers that would modify intracellular calcium diffusion.
4. Calcium binding by the Ca^{2+} sensor involved in vesicle fusion.
5. Calcium extrusion.

It is important to emphasize that each cell type will exhibit dramatic differences in the spatiotemporal characteristics of these five processes. Moreover, depending on the spatial and temporal scale of the theoretical study, some of these sub-cellular processes may become more or less relevant for studying cell secretion.

Intracellular calcium dynamics can be modeled as a set of differential equations that represent the spatiotemporal dependence of Ca^{2+} concentration. This set of differential

equations should include equations that describe the particularities of the calcium influx (to model point 1), the diffusion (point 2), the kinetic reactions leading to calcium buffering (point 3), the calcium-binding steps associated with the vesicle calcium sensor (point 4), and the extrusion of calcium (point 5). In terms of fluxes and following mass conservation of Ca^{2+} , the rate of change of free calcium ions, in space and time, must equal the algebraic sum of incoming and outgoing cellular fluxes and diffusion, as stated in the following diffusion equation:

$$\frac{\partial C(\mathbf{r}, t)}{\partial t} = D_{Ca} \nabla^2 C(\mathbf{r}, t) + J_{in} - J_{on} + J_{off} - J_{out} \quad (2.1)$$

where $C(\mathbf{r}, t)$ denotes the quantity of free Ca^{2+} in the position described by the vector \mathbf{r} (in any coordinates) at time t ; D_{Ca} is the diffusion coefficient of Ca^{2+} in the cytoplasm and it is used to calculate the free diffusion term; ∇^2 is the spatial Laplacian operator; J_{in} is the influx generated by the incoming Ca^{2+} in response to a stimuli; J_{out} is the efflux due to the Ca^{2+} -extrusion mechanisms; and J_{on}, J_{off} are the fluxes resulting from the calcium binding and unbinding, respectively, associated with buffers and the vesicle calcium sensor. As will be explained later, these fluxes could be modeled using similar equations and solution methods considering them as biochemical reactions.

Each one of the fluxes included in Equation 1.1 could be described by one or more equations. Thus, the complete set of equations to be solved includes all those needed to calculate each specific flux coupled to all the others. The suitable method to solve them depends on the characteristics of the solution we are interested in; for example: 1) The temporal and spatial dependence of each flux, including the relevant resolution scales; 2) The time scale associated with the kinetic rates for the buffers and the vesicle calcium sensor; 3) The homogeneity of the media; and, 4) The geometry shape of the cellular area to be modeled. Although the combination of these conditions may lead to many possibilities and also, to many suitable methods, two main families of mathematical approaches have been used in the present work: The stochastic, in particular, the Monte Carlo numerical methods, and the continuous or deterministic numerical methods. In the following sections, there is a brief introduction for each family of mathematical methods, including some up-to-date reported applications to the cell biology area, and then, there is a detailed explanation of our approach to solve the four points listed above, based on these methods. Notice that although we separate the equations associated with each flux in sections, to be solved, they need to be coupled i.e., to be solved together in each time step at each spatial point.

2.1.1 Modeling Ca^{2+} influx through voltage-dependent ionic channels

Cell depolarization induces Ca^{2+} entrance from the external medium, which occurs via two main pathways: influx from the extracellular medium through open Ca^{2+} channels located in the plasma membrane, and release from internal stores to the cytoplasm [14]. An usual experimental protocol is to depolarize the cell with pulses of defined amplitude and duration that provoke channels opening. Calcium influx due to depolarization is mainly conducted through voltage-dependent Ca^{2+} channels [199], so to correctly simulate intracellular Ca^{2+} dynamics it is necessary to pose a correct model for them.

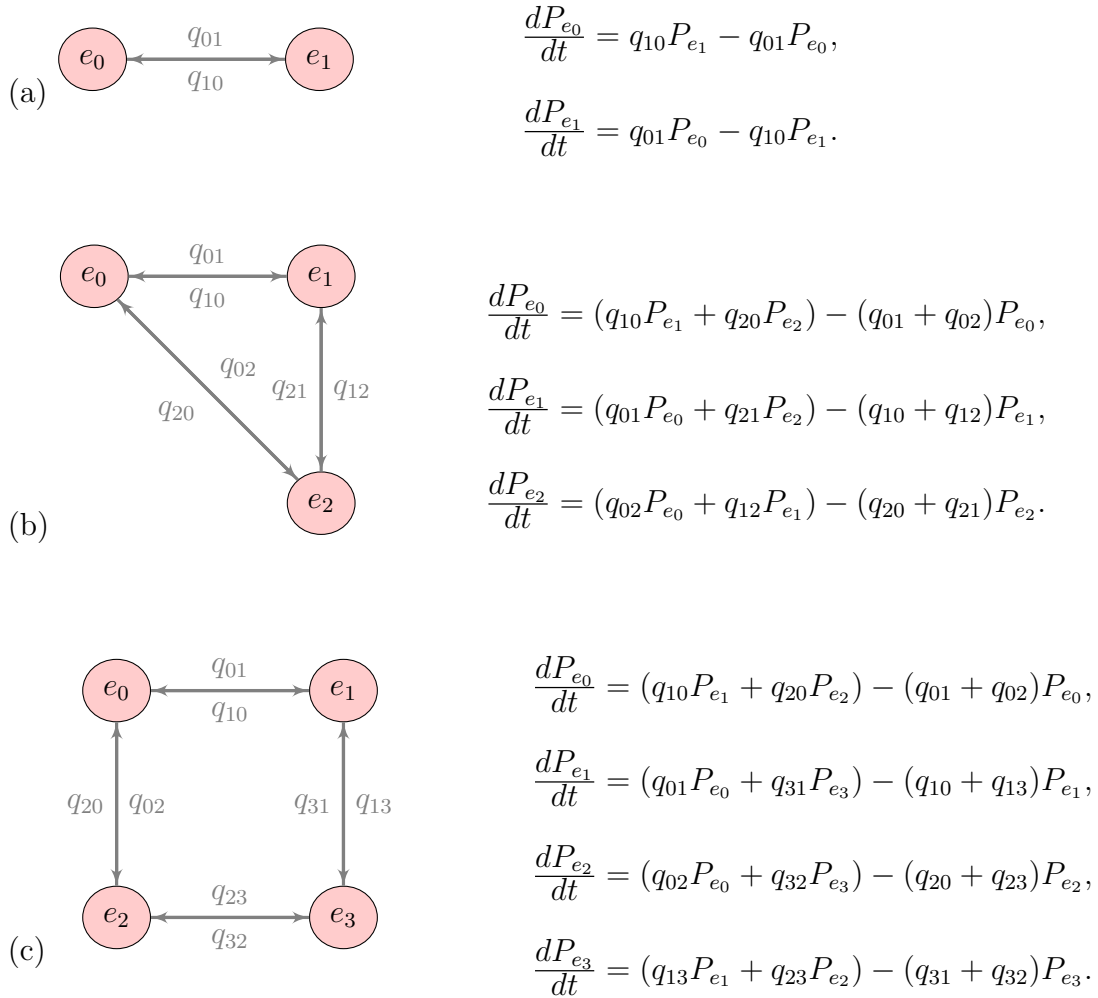


Figure 2.1: State models for all channels used in simulations. (a) Two-state model for potassium channels associated with $I_{K_{DR}}$ in alpha cells. e_0 and e_1 represent *Open* and *Closed* channel states, respectively. (b) Three-state model for calcium channels found in the calyx of Held, in chromaffin cells, and in alpha cells. e_0 , e_1 , e_2 correspond to *Open*, *Closed* and *Inactive* states, respectively. (c) Four-state model for sodium and potassium channels associated with I_{Na} and I_{KA} currents in alpha cells. e_0 , e_1 , e_2 , e_3 correspond to *Open but Inactive*, *Closed and Inactive*, *Open*, and *Closed* states, respectively. The system of ordinary differential equations corresponding to each state model is shown in its right. The values for transition rates between states are given in the tables shown in each chapter, since they are specific to each cell type.

Ca^{2+} influx is managed by different Ca^{2+} channel subtypes, depending on the cell type [26]. In the present thesis, we developed models for the L-type and P-type voltage-dependent calcium channels, for the calyx and for bovine chromaffin cells, and for the N-type and T-type, for pancreatic alpha cells.

For the above-mentioned cell types, we developed channel state models, and estimated their parameters for those channels associated with secretion. Once the models were developed and the related parameters established, a set of differential equations for each model were obtained and solved using numerical methods, as we discuss later. In this section we present a state-modeling approach for ionic channels, intended to simulate the dynamics of ionic currents commonly measured in voltage-clamp experiments, coupled to diffusion and other kinetic reactions involved in exocytosis. Voltage-dependent ionic channels involved in the sequence of events leading to secretion could be calcium, sodium and potassium channels [121]. They all exhibit some common kinetic properties that make them suitable for a common modeling approach. First, the activation of these channels usually increases as the cell becomes depolarized. Second, the channels deactivate when depolarization disappears. Third, a strong or a sustained depolarization induces channels inactivation (in some of them) i.e., the ionic flux through the channel diminishes even when depolarization continues. However, each ionic current exhibits its own dynamic behaviour, so it is necessary to propose a specific model for each ionic channel.

There are two common approaches to model channel gating that produce ionic currents: the Hodgkin-Huxley paradigm and the Markov state modeling [45]. The former is widespread because of its capability to be managed and its ability to model macroscopic phenomena so, there are different parameter estimation methods and software based on it [195, 196]. However, this approach is unable to model single-channel behaviour since it is based on continuous and deterministic principles [25, 82, 170]. Markov state models are an adequate methodology to combine experimental information and mathematical modeling of single-channel behaviour [139] as each state is trying to resemble the conformational changes suffered by the channel, in order to reproduce whole-cell measurements. In this work we develop Markov state models for channels (shown in Figure 1.1) towards: 1) Relating ionic channel properties to secretion, and 2) Simulating ionic currents actually measured in depolarization experiments. Notice that these channel models are suitable to be incorporated in microscopic schemes capable of simulating high-resolution temporal and spatial events related to exocytosis [61, 188].

On the assumption that transition rates could be interpreted as transition probabilities per time unit, we propose a minimal state model for each ionic channel and associate each transition rate between states (q_{ij}) to a channel property (Figure 1.1). Therefore, based on this minimal approach, each model contains just one Open (and active) state and one or more Closed and Inactive states, in order to reproduce the behaviour observed during depolarization experiments. The Open (active) state is the only conducting one, so open probability is calculated based on the number of channels that reach this state. Specifically, we understand *Activation* as those transitions going to the Open state, and *Deactivation* as those transitions going to Closed states. Activation and deactivation are both functions of membrane voltage in a symmetrical manner. Since some channels also present *Inactivation* (i.e., no response

under constant stimulation), we interpret it as transitions to Inactive states. There are two possible channel inactivations: one, due to extreme depolarization (known as voltage-dependent inactivation), and due to the accumulation of Ca^{2+} near the channel mouth (known as calcium-dependent inactivation) [199]. Our models include both cases, when appropriate, and the voltage or calcium dependence is included in the definition of the transition rates to Inactive states, as shown in the corresponding tables for model parameters. All transition rates follow the main idea of the Markov models, i.e., transitions only depend on the present state [25, 155]. The minimal state models proposed here are constrained to fit an experimental current-to-voltage (IV) function and, at the same time, to adequately reproduce dynamic currents; when possible, we also take into account other kinetic data such as steady-state inactivation curves, or time constants. Our models are based on previously reported models, but are simplified in order to have the minimum number of states to reproduce current dynamics suitable to facilitate the understanding of intrinsic channel properties.

Following the idea that activation/deactivation are symmetrical exponential functions of membrane potential difference [45], we define opening and closing rates as exponential functions. Inactivation rates are defined as sigmoidal functions of membrane potential difference, considering that experimental data commonly shows that currents inactivate in this manner. For N- and L-type Ca^{2+} channels, we also added calcium-dependent inactivation since these channels exhibit this particularity, as discussed in [199]. Finally, all other transition rates are fitted as time constants, as is the case in many state models. Although there are other methods to estimate current kinetic properties using the Hodgkin-Huxley approach [180], we favour the use of experimental data, obtained in voltage-clamp protocols, to estimate model parameters.

Parameter estimation for channel models

Parameter estimation for each model was done using a Monte Carlo algorithm which looks for a parameter set that fits an experimental IV curve with minimal error. Although we are not following a formal methodology to fit kinetic parameters since we have no numerical data for single currents, our algorithm considers the guidelines discussed in [124] to estimate parameters; they are: 1) To fit the model several times while randomly changing the parameters; 2) To fix some parameters to improve the identifiability of the model; 3) To make the number of trials large enough (proportional to parameter space) to improve confidence, and 4) To use a defined stimulation (like a depolarizing pulse). Our main algorithm follows these steps (see Figure 1.2): First, it determines the number of trials as a function of the number of parameters; second, it generates random parameter combinations for the parameter space; thirdly, it calculates the peak current at specific voltages by solving channel equations for each parameter set; finally, it computes the chi square deviation of the simulated peak currents to experimental ones, and finds out the set with minimal deviation. The main algorithm calls a program that solves the system of differential equations derived from each channel model, and shown at the right in Figure 1.1, at the steady state. Specifically, this program obtains the peak current for each model at one membrane voltage with the given parameter set. For example, for the two-state model (Figure 1.1(a)), the equations are

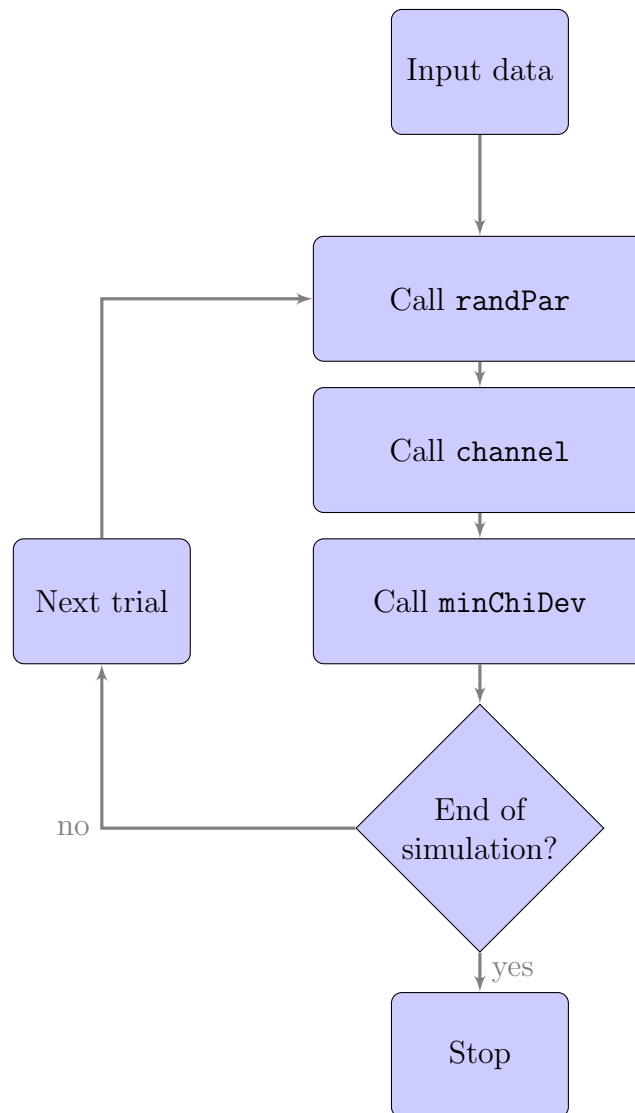


Figure 2.2: Flow diagram of the algorithm to find the parameter set that best fits experimental peak currents for each channel model. It was used for all channel models, just specifying the routine that solves the corresponding system of differential equations. Routines are described in Appendix B.1.

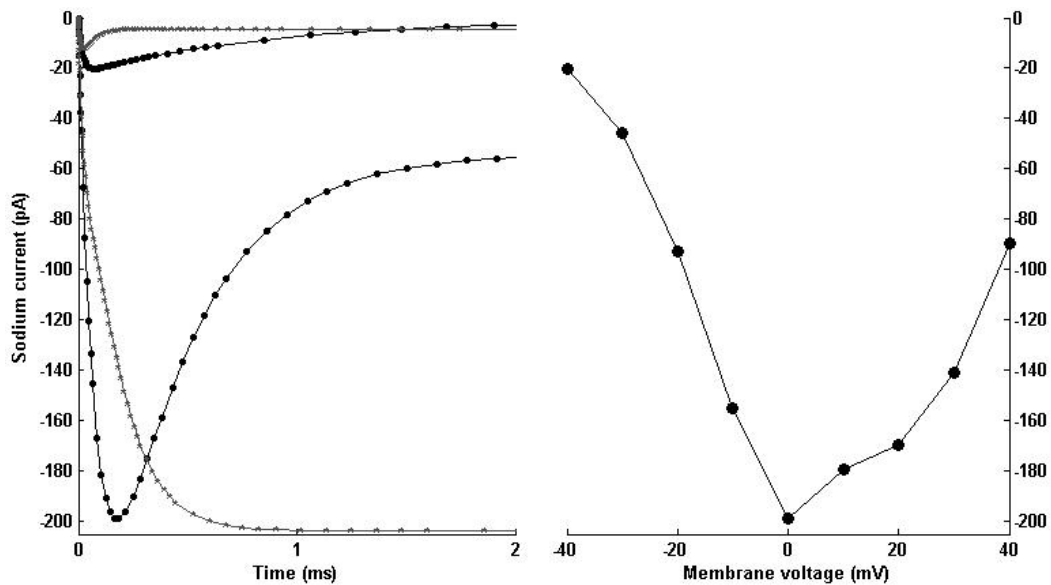


Figure 2.3: Example of the limitations of static parameter estimations to adequately reproduce dynamic behaviour. (Left) Comparison of alpha-cell sodium currents induced by two kind of depolarizations: strong (0 mV, large currents) and weak (-40 mV, small currents). Currents were simulated using: 1) The static parameter set obtained by fitting the IV curve (stars), and 2) The modified set (dots). As observed, parameter modifications improve dynamic simulations; in this case, new parameter values allow fast sodium current inactivation as found in alpha-cell experiments [9]. (Right) Comparison of IV curves: experimental read from [9] (triangles, error bars and line), static best-fit (stars) and modified (dots). Notice that parameter modifications do not significantly affect the IV curve fitting, since new values still follow steady-state behaviour.

$$\frac{dP_{e_0}}{dt} = q_{10}P_{e_1} - q_{01}P_{e_0}, \quad \frac{dP_{e_1}}{dt} = q_{01}P_{e_0} - q_{10}P_{e_1}, \quad (2.2)$$

where P_{e_i} represents the probability that a channel is in state e_i . An extra equation refers to probability conservation i.e., $\sum_n P_{e_n} = 1$. The solution to (Eq.1.2) for P_{e_0} and P_{e_1} at the steady-state (i.e., where each $\frac{dP_{e_i}}{dt} = 0$), would be

$$\begin{aligned} P_{e_0} &= \frac{q_{10}}{q_{01} + q_{10}}, \\ P_{e_1} &= \frac{q_{01}}{q_{01} + q_{10}}, \end{aligned} \quad (2.3)$$

which has two rates to be fitted, q_{10} and q_{01} . For this two-state model, these transition rates refer to the activation and deactivation of the channel, and as mentioned above, they are exponential functions of the membrane potential. Indeed, there are two parameters per exponential to be fitted (amplitude and time constant) so, for the two-state model the parameter space is made of five parameters in total: four for the rates, and one for the channel population. It is important to mention that the number of channels is always considered to be a free parameter ranging between 100 and 10,000; these limits are based on density values for the calyx (10 channels in $0.1 \mu m^2$) [158], and for neuroendocrine and pancreatic beta cells (5 to 15 channels in $1 \mu m^2$) [98, 123].

The solution for the Open state probability (P_{e_0} in Eq.(1.3)) allows estimation of the number of open channels. The total current is calculated multiplying the unitary current by the open channel population, as described for L-type calcium channels in [74]. Notice that the unitary current is specific to each channel, and it depends on the membrane voltage and the single-channel conductance; these values are given in the tables included in each chapter, as well as the fixed values used to estimate the free parameters and to simulate the electrical currents. The estimated values for the transition rates for each channel model, are also given in these tables.

Using an optimal set of parameters for each model, we simulate the dynamic behaviour of a current by solving the ordinary differential equations for each multi-state model. In this way, we try to reproduce the measured currents following experimental protocols in a cell type. These protocols usually consist of fixing a resting condition for the cell (at a very negative membrane potential), and then stimulating it with a depolarization pulse. For our simulations, all channels are assumed to be closed as initial condition, and then, they increment their opening probability as depolarization increases. We compute the total current as the product of the number of channels in the Open state by the unitary current, per each time step. To achieve this, we use an adaptive time-step ordinary differential equation solver for stiff problems (*ode15s*) implemented in Matlab (<http://www.mathworks.com>).

It is important to mention that there is a strong compromise between fitting an IV curve, and correctly reproducing the current dynamic behaviour. On the one hand, the IV curve is built from peak currents (as in experimental reports) which corresponds to the maximal conductance of a channel population i.e., the maximum number of channels that could be open due to the electrostatic force of the applied membrane potential difference. This is calculated on the basis that Open probability rapidly increases for membrane depolarizations, so peak current value is mainly due to steady-state Open probability. On the other hand, the dynamic behaviour of the current

exhibits the rapid and transitory changes of the channel i.e., the transitions to/from one state to another, including the Open state. These transitions are attributable not only to membrane potential variations but also to stochastic transitions over time. Using this approach, the set of parameters found for peak currents is a static approximation of this behaviour. Therefore, it does not necessarily reproduce current dynamics, although it provides a good set of starting values to restrict the model and the channel populations.

To overcome this limitation and bearing in mind that our main goal is to simulate the real electrical activity observed in cells, we have taken the channel model parameter set obtained while fitting the IV curve, as described above, as a starting set of parameters to simulate the corresponding current dynamics. After the simulations, we observed that some dynamic properties, mainly deactivation and inactivation, were underestimated. We tested different options in order to correctly simulate experimental currents. The most suitable one was to fix deactivation parameters and to increase inactivation amplitudes. Then we checked that the new IV curve was not far off the expected values. Figure 1.3 shows an example of this methodology for sodium currents, measured in alpha cells, where comparisons between the IV curves and the underestimated vs. modified currents are demonstrated.

2.1.2 Modeling calcium diffusion

Diffusion (of ions or molecules) refers to the random spread of particles following the concentration gradient direction, i.e., from high to low concentration regions. Buffered diffusion refers to the case when the spread of particles is not free but it is modified by the presence of a *buffer* (a molecule that can bind particles). In our case, modeling calcium buffered diffusion means to calculate the quantity of free calcium ions that is present in each place of the cell at each time, considering that some ions are free, and some can be bound (or unbound) by a buffer. This calculation gives the dynamical description of the calcium quantity considering its temporal and spatial dependence, and this description is really complex since there are several intracellular mechanisms that can act as buffers or barriers affecting free calcium diffusion, such as the mitochondria, the endoplasmic reticulum, or the cytoskeleton, to cite some examples [14]. In this section, we just discuss possible approaches to model free diffusion that could be coupled to calcium buffering equations, which are discussed in Section 1.1.3.

As shown in Equation 1.1, the free diffusion term (neglecting other fluxes) is calculated based on the diffusion equation:

$$\frac{\partial C_a(\mathbf{r}, t)}{\partial t} = D_{Ca} \nabla^2 C(\mathbf{r}, t), \quad (2.4)$$

where $C_a(\mathbf{r}, t)$ now denotes the quantity of free Ca^{2+} in the position \mathbf{r} at time t . In the case of a spherical cell, the simplest approximation is to consider that ion diffusion occurs in a homogenous sphere of radius R , where D_{Ca} is assumed to be constant, and ions *mainly* travel in the radial direction (say x), so Equation 1.4 can be reduced to

$$\frac{\partial C_a(x, t)}{\partial t} = D_{Ca} \frac{\partial^2 C(x, t)}{\partial x^2}, \quad (2.5)$$

restricted by the boundary conditions $\frac{\partial c}{\partial x} = 0$ at $x = 0$ and $x = R$ i.e., no flux at the cell borders. This is a parabolic equation which can be solved by finite differences schemes, such as the Crank-Nicholson method [28].

Models describing buffered diffusion based on differential equations need drastic geometrical simplifications in order to be solved with ease. Depending on the geometrical assumptions considered, the differential models lie within two categories: Shell models, in which it is assumed that ions enter uniformly over the cell membrane, and that only the radial diffusion is of relevance for spherical cells or domains (for example [69, 153, 198]), and Microdomain models (for example [98]), which solve the reaction diffusion equations in the vicinity of a channel pore, assuming azimuthal symmetry around the pore; in this last case it is necessary to assume that all channel pores are equidistant. We have applied this deterministic approach to develop our spherical cell model described in Section 1.2.3, and called in this thesis, *Shell model*. This model was used to study exocytotic dynamics in chromaffin cells, as discussed in Chapter 4, and to estimate calcium distribution in alpha cells, as exposed in Chapter 6. However, it is well known that ions do not enter uniformly given that the Ca^{2+} channels are not regularly spaced. These departures from symmetry may have an important impact on the functionality of the cells. In [66] it was described how channel clustering gives rise to calcium profiles which cannot be obtained as a superposition of calcium concentrations developed by individual channels. Moreover, non-uniform calcium influx and distribution may have a crucial influence on cell activity, in particular, on exocytosis, as in the case of neurons where local calcium signals determine the quality of neurotransmitter release [7].

Over this basis, a second option emerges to solve Equation 1.4 without neglecting spatial dependence of diffusion, and taking into account the random nature of calcium distribution. This task can be accomplished using a random-walk algorithm inside a small domain that forms part of the cell. One possibility is to consider a cubic microdomain where one or a fixed array of channels are located near a vesicle [13, 163]. Another approximation is to take a conical or cylindrical domain and to divide it in small cubic compartments, where ions can randomly move in any direction of the cubes. This approach allow a more robust method to calculate ion diffusion in any cell geometry, but needs the implementation of stochastic methods which elevate the computational time of the numerical simulation. Despite their complexity, these stochastic schemes permit to study calcium dynamics with more flexible and more realistic geometric parameters, as clearly discussed and implemented in [66]. In the present thesis, the reported Monte Carlo scheme of Gil et al. has been extended to study secretion in the calyx of Held, as discussed in Chapter 3, and to study cytoskeleton influence on secretion in bovine chromaffin cells, as discussed in Chapter 4. Notice that the random-walk algorithm defines a relationship between the time step Δt (temporal resolution), and the associated spatial discretization Δx :

$$\Delta t = (\Delta x)^2 / 4D_{Ca}, \quad (2.6)$$

where $D_{Ca} = 220\mu m^2/s$ [2]. The implication of this equation is that if spatial resolution is increased, i.e., Δx is reduced, the time step will be also reduced in a quadratic manner, so it will take much more iterations to end a simulation, increasing the computational time.

2.1.3 Modeling biochemical reaction kinetics

Chemical or reaction kinetics studies explore the reaction's mechanism and transition states that describe a particular reaction. This information allows the researcher to build a mathematical model of the reaction as a sequence of steps governed by reaction rates which may depend on the concentration of reactants, the temperature, the presence or not of a catalyst, or any other parameter. Modeling biochemical reactions through kinetic schemes is a useful tool to obtain differential equations, as they relate main variables (usually, concentrations or quantity of matter) with time, and they can be solved in order to obtain the dynamic behaviour of these variables. This methodology has been widely used in biological problems, as reviewed in [95, 165]. Here, we present two specific sub-cellular phenomena described with kinetic schemes and differential equations, which are included in our models.

The calcium buffers

Calcium ions are importantly buffered in the cytoplasm since there are many intracellular proteins (enclosed as *endogenous buffers*) able to bind Ca^{2+} , such as parvalbumin, calbindin, amongst many others [48]. Moreover, in many experiments calcium dyes and exogenous buffers are added to record intracellular calcium dynamics, so they should be taken into account [173]. Therefore, a correct model of Ca^{2+} diffusion in the cytoplasm must include all the buffer molecules, endogenous and exogenous. A basic scheme of representing the Ca^{2+} binding to a buffer molecule is



where B represents the free buffer molecule, and BCa represents the buffer molecule bound to one Ca^{2+} . As represented in this kinetic or reaction scheme, the calcium ion can be bound or unbound depending on the value of the k_{on} and k_{off} rates. When several buffers are considered, the system of differential equations describing the corresponding kinetic reactions, based on Equation 1.7, would be:

$$\begin{aligned} \frac{d[Ca]}{dt} &= \sum_i (k_{off}^i [B_i Ca] - k_{on}^i [Ca] [B_i]), \\ \sum_i \frac{d[B_i]}{dt} &= \frac{d[Ca]}{dt}, \quad \frac{d[B_i Ca]}{dt} = -\frac{d[B_i]}{dt}, \end{aligned} \quad (2.8)$$

where $[Ca]$ is the concentration of free Ca^{2+} at time t , k_{on}^i and k_{off}^i are the binding and unbinding rates for buffer i , and $[B_i]$ is the concentration of buffer i at time t . These concentrations could be interpreted as continuous or discrete variables. As a continuous variable, concentration would be quantity of mass per volume, usually in Molar (mol per liter) units, as a function of time. This kind of formulation is called Continuous Deterministic or classical Kinetics [77]. In contrast, in a discrete interpretation, concentration is seen as the number of particles (ions or molecules) of every species per volume unit, at a given time. The set of all concentrations in a time is called a state, and the stochastic solution calculates the probability that the system is in a particular state [77]. These two interpretations are really different since they call for completely different methods to solve Equation 1.8, and more importantly,

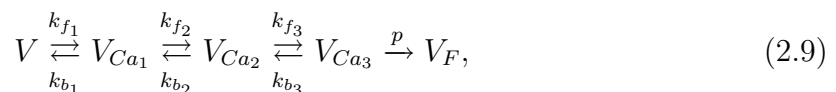
they are adequate for two unlike cases: many particles versus few particles. The stochastic interpretation is specially suitable for few particles in the medium, and it should converge to the continuous solution as the number of particles is increased [200]. However, the opposite is not always true; a continuous interpretation may not give an accurate solution for all cases, as discussed in [55].

If there are few calcium ions and buffer molecules in a volume, the dynamics of the variable $[Ca]$ is highly influenced by the probability that Ca^{2+} could be bound or not at each time interval (where this probability is in terms of k_{on} and k_{off} rates and the size of the time interval Δt), so its correct evaluation requires a stochastic numerical method, as Monte Carlo algorithms; the implementation of buffer kinetics along with calcium diffusion is clearly explained in [66]. These algorithms were extended and used, for the present thesis, to study calcium dynamics in the calyx of Held, as discussed in Chapter 3, and to study cytoskeleton influence on spatial calcium dynamics in chromaffin cells, as discussed in Chapter 4. On the other hand, if there are many calcium ions and buffer molecules in a volume, the dynamics of $[Ca]$ could be estimated as the average quantity of ions at each time interval. This evaluation can be directly coupled to a reaction-diffusion model, and solved by a numerical method, as explained in [73]. The algorithms developed in this thesis were adapted and extended to estimate calcium distribution in alpha cells, as exposed in Chapter 6, and to study calcium dynamics in human chromaffin cells. In the latter case, we have combined both interpretations, discrete and continuous, because secretion in human chromaffin cells may be explained with them for rapid and intermediate secretion, respectively, as discussed in Chapter 5.

The calcium sensor for vesicle fusion

Calcium ions trigger exocytosis thanks to the existence of a calcium-binding protein (*calcium sensor*) in the cytoplasm that activates the secretory machinery. *Synaptotagmins* are widely accepted calcium-sensor proteins involved in regulated exocytosis; some Synaptotagmin subtypes are attached to the vesicle and some other are attached to cell membrane, and each one exhibits a specific calcium affinity. It is known that 3 to 5 calcium ions could be bound to these proteins to activate them [171]. Calcium binding leads to vesicle fusion and finally, to release; both these processes are commonly described as biochemical reactions consisting of several steps [24].

The binding and unbinding of free calcium ions to the calcium sensor could be represented as a kinetic scheme, which can be written as a set of ordinary differential equations describing the temporal dependence of these cellular processes. For example, if three Ca^{2+} needs to be bound to the calcium sensor (i.e., a sensor with 3 binding sites) to trigger vesicle fusion and release, the kinetic scheme describing this process could be



where V represents a vesicle with an empty sensor, V_{Ca_i} are the states of the vesicle with i calcium ions, and V_F represents the fused vesicle. The transitions between states are managed by the rates p , k_{f_i} and k_{b_i} , that are the fusion, the forward

(activating) and the backward (deactivating) rates, respectively. Notice that some of these rates are calcium-dependent since vesicle fusion is activated by Ca^{2+} , whereas some other are just functions of time. Moreover, the forward and backward rates may show *cooperativity*, that is, rates are increased upon the binding of each calcium ion. Commonly, the vesicle states V_{Ca_i} are called *pools*, and the dynamics of these pools is what is understood as *secretion dynamics*.

Due to the Ca^{2+} -dependence of vesicle fusion, it is common to define the forward rate as $k_{f_i} = (N - i + 1)k_{on}[Ca]$, where N is the number of binding sites of the calcium sensor i.e., the number of calcium ions needed to trigger vesicle fusion, k_{on} is the Ca^{2+} -binding rate of the sensor, and $[Ca]$ is the Ca^{2+} concentration felt by the sensor. The backward rate is defined in a similar manner: $k_{b_i} = ik_{off}$, where k_{off} is the Ca^{2+} -unbinding rate of the calcium sensor. The rates k_{off} and k_{on} are related with the dissociation constant K_D of the sensor by the equation $K_D = k_{off}/k_{on}$, where K_D is a measure of the Ca^{2+} affinity for Ca^{2+} of exocytosis [171]. The above-mentioned definitions for k_f and k_b assume that the calcium sensor involved in exocytosis does not exhibit cooperativity with Ca^{2+} , so the states of the vesicle are sequential steps that only depend on the quantity of Ca^{2+} near the sensor. These kind of kinetic models are called *non-cooperative* schemes, and have been proposed to model the final stage before vesicle fusion and release in synapses, with five binding sites ($N=5$) [20], and in neuroendocrine cells with three binding sites ($N=3$) [85]. An alternative kinetic model consider that the sensor has more affinity for Ca^{2+} at low concentrations, so the backward rate includes a parameter $b^{(i-1)}$ that stands for cooperativity; it was proposed for the calyx of Held with $N=5$ [159]. There are other models intended to explain asynchronous release observed in neurotransmitter release [109, 172]. In this Project, we have mainly used the non-cooperative scheme for modeling secretion in the calyx of Held (with $N=5$), and also in chromaffin and alpha cells (with $N=3$), although we have done a comparison of release predictions of the non-cooperative and *cooperative* models for the calyx of Held.

As noted before, to trigger vesicle fusion the sensor depends on the quantity of Ca^{2+} in its vicinity. The limits for this vicinity are an important item to accurately simulate Ca^{2+} -triggering of release. Indeed, fast secretion (as occurring in the calyx of Held), is triggered by the very local Ca^{2+} concentration, so the implementation of the kinetic model can affect the precision of simulations. In a homogenous media, the Ca^{2+} dependence of the vesicle sensor could be seen as deterministic if the calcium concentration near this sensor is almost stable in a time span. However, this dependence needs a stochastic interpretation if the number of calcium ions near the sensor is unstable, changes very fast, or is very low. In any of these cases, Ca^{2+} quantities might be different for neighboring vesicles, and the simulation should take into account these differences. These two different circumstances lead to completely distinct cellular phenomena, then the kinetic model should be solved and implemented in a distinct manner. Implementations may be deterministic or stochastic, as the solution methods, similar to what happened with buffers.

In the case of an active zone, Ca^{2+} channels and vesicles are few and have specific locations and organizations (clusters); these features require a stochastic implementation of the kinetic models for vesicle fusion, as we have done with the calyx of Held and with fast secretion in chromaffin cells. In both cell types we used a statistical

approximation for simulations: in order to have a significant number of fused vesicles per time step, we consider that the whole sub-membrane region is full of vesicles. We have done several tests comparing simulations with excessive vesicle population (M vesicles) versus detailed simulations (k simulations with M/k vesicles each), and the results show no statistically significant deviation. From a kinetic point of view, this approximation is justified given that the kinetics of exocytosis is much slower than the kinetics of buffers, as well as there are fewer vesicles than buffers. However, it is important to mention that this approximation is valid only for high Ca^{2+} influx (as the one induced with pulse depolarization experiments in the calyx), or for a non-very small spatial resolution (as in neuroendocrine cells). This is not the case for the Ca^{2+} influx induced by an action potential in a presynaptic terminal, for which it is necessary to run a large number of simulations with few vesicles to obtain a correct estimation of secretion dynamics [65].

2.1.4 Modeling calcium extrusion

Calcium extrusion is mainly done by pumps and transporters located at the cell membrane, and they all help in keeping the adequate intracellular calcium concentration, in particular, after stimulation periods. Pumps are active mechanisms (i.e., mechanisms that require ATP energy to function) that take calcium ions out of the cell, no matter the calcium gradient. Transporters, on the other hand, are passive mechanisms that follow the calcium gradient, so they expel calcium ions depending on the electrochemical gradient. The most common pumps found in cells are the family of Ca^{2+} -ATPases [201], and the most common transporters are the family of sodium-calcium exchangers [177]. For the present thesis, these calcium-extrusion mechanisms were included in the Shell model, used to study human chromaffin cells and alpha cells. In both cases, we include the differential equation used in [138] to describe the rate of calcium extrusion along time assuming that it exhibits Michaelis-Menten (sigmoidal) kinetics, that is,

$$\frac{d[Ca]}{dt} = -\mathcal{V}_{max} \frac{A}{V} \frac{[Ca]}{[Ca] + K_m}, \quad (2.10)$$

where $[Ca]$ is the intracellular calcium concentration at time t , \mathcal{V}_{max} is the maximal speed of the pump, A is the whole-cell area, V is the volume of the outermost shell, close to the pump, and K_m is the half-maximal activating calcium concentration. This equation was coupled to diffusion, calcium buffering, and the vesicle calcium-sensor, in the Shell model.

2.2 Developed models

2.2.1 Active-zone model

The Active-zone model (AZ model) was intended to simulate Ca^{2+} -triggered exocytosis, with high spatial and temporal resolution, in an active zone where calcium channels and the secretory machinery could be located in specific positions. The AZ model includes submodels for the Ca^{2+} channels, the buffered diffusion of Ca^{2+} , and the

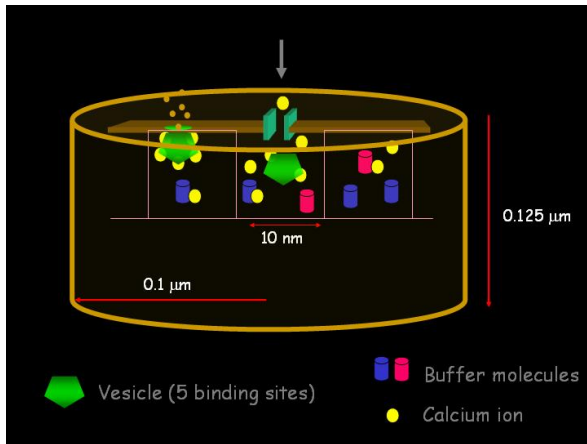


Figure 2.4: The Active-zone model represents an active zone where secretion occurs. The cylindrical domain is mapped into a 3-D grid made of cubic compartments where Ca^{2+} ions, buffers and vesicles may be found. Ca^{2+} channels and vesicles are placed only in the first layer of the domain. The included sub-cellular mechanisms are Ca^{2+} influx, buffered diffusion, and vesicle fusion.

kinetics for vesicle fusion. All these mechanisms are considered as stochastic processes taking place in a domain (conical or cylindrical volume) that represents the active zone, as shown in Figure 1.4. The base of the domain represents a cell membrane patch that is embedded inside a larger portion of the membrane where Ca^{2+} channels are, on average, uniformly distributed, so we can assume that the flux of ions and buffer molecules through the lateral sides of the domain is zero. This simplification imposes a simple boundary condition in the walls of the membrane: ions bounce back when they encounter a wall. At the domain base, this condition is interpreted as reflection while, on the domain lateral sides, reflection is equivalent to consider that the outgoing flux equals the incoming flux, due to the symmetry of the geometry.

An orthogonal 3-D regular grid maps the domain of simulation with a distance between grid points chosen by the user, as the spatial discretization (Δx). Each point of the grid is associated with a cubic compartment of volume $(\Delta x)^3$. Therefore, grid points or cubic compartments are equivalent concepts. Calcium ions and buffer molecules may move from one compartment to another due to diffusion, which is modeled as a random walk process. The time scale for the random walk is calculated from the spatial discretization, and the fastest diffusion coefficient of the system, following Equation (1.6). Commonly, the Ca^{2+} diffusion coefficient imposes the limit for the time step Δt . Ions will be moved every time step, Δt , using a random walk algorithm, in which each ion will have 50 % chance to remain in its initial position, and 25 % chance to move either in the positive or negative direction, for each spatial dimension. In the first slice of the domain, that represents the cell submembrane region, Ca^{2+} channels and vesicles are distributed. Different distributions for both can be chosen: cluster, correlated cluster or random. All equations representing sub-cellular mechanisms in the active zone (shown in Figure 1.4) are solved using Monte Carlo methods, i.e., differential equations are interpreted in a stochastic manner, then the AZ model is suitable to simulate short timescale Ca^{2+} and secretion dynamics (first milliseconds) in presynaptic and neuroendocrine cells. The implemented algorithm to solve the model is shown in Figure 1.8. This model does not consider main calcium-extrusion mechanisms found in presynaptic terminals, such as the $Na^+ - Ca^{2+}$ exchanger and the Ca^{2+} pump, since the former is not colocalized with release sites, and the latter has a slow extrusion rate that is out of the simulation timescale [93]. Other phenomena not considered in the AZ model are the effect of diffusion barriers, such as release granules or mitochondria,

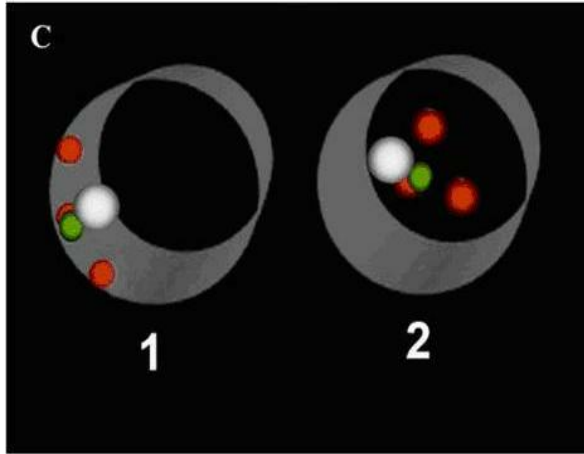


Figure 2.5: The Cytoskeleton-cage model reproduces a prototypical cytoskeleton cage found in bovine chromaffin cells. The cylindrical domain ($0.3 \mu\text{m}$ of radius per $1 \mu\text{m}$ of height) contains 3 clusters of Ca^{2+} channels (medium spheres), colocalized to one vesicle (big sphere) and its secretory machinery (small sphere). The figure shows the two studied configurations: in the borders (1) and in the center (2).

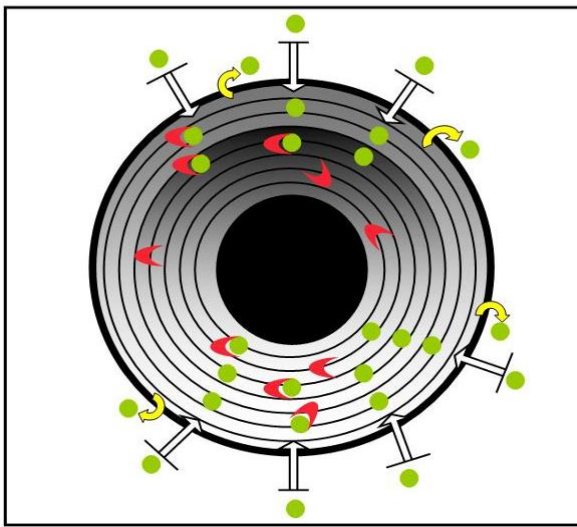


Figure 2.6: The Shell model represents a spherical cell divided in concentric layers, where the most internal one is the nucleus, and the most external one is the cell membrane. Ca^{2+} channels (entering arrows) and the Ca^{2+} pump (outgoing arrows) are localized in the cell membrane, whereas buffers (u-shaped figures) are distributed in the cytosol.

which were studied by A.Gil and collaborators in [160].

2.2.2 Cytoskeleton-cage model

The Cytoskeleton-cage model (CC model) was designed to study the cytoskeleton influence on Ca^{2+} -triggered exocytosis in bovine chromaffin cells, as will be detailed in Chapter 4. This model is a particular case of the AZ model, then, it includes the same mechanisms (Ca^{2+} channels, buffers, diffusion, and vesicle fusion) acting in a cylindrical domain, as shown in Figure 1.5. However, the CC model accounts for the participation of L- and P-type calcium channels in each channel cluster. The implemented algorithm to solve the CC model is the one shown in Figure 1.8, with the addition of a state model for the L-type calcium channel, as a Monte Carlo algorithm, in program `chanmod`.

2.2.3 Shell model

The Shell model (S model) is intended to calculate the intracellular calcium concentration ($[\text{Ca}^{2+}]_i$) over time, considering Ca^{2+} influx through voltage-dependent Ca^{2+} channels, buffered diffusion, and extrusion. It is assumed that the starting stimulus is a depolarization pulse applied at the cell membrane, as in voltage-clamp

experiments. This model is a modified version of our previously developed Ca^{2+} -regulation model [73]. The algorithm assumes that the cell can be approximated as a homogeneous sphere divided in concentric layers, where the most internal one represents the nucleus, and the most external one corresponds to the cell membrane, and diffusion only occurs in the radial direction. The boundary conditions to solve this system are: there is no calcium flux between the nucleus and the cytosol, and the external concentration of calcium is infinite. Ca^{2+} channels and the Ca^{2+} pump are localized in the most external layer, whereas the endogenous buffer is distributed in all the cytosol. The algorithm calculates $[Ca^{2+}]_i$ in time and space by solving Equations 1.5, 1.8, and 1.10, as well as a constant leak flux added to keep basal conditions in the steady-state, using the Crank-Nicholson method (see Section 1.3.2).

2.3 Mathematical and numerical methods

When solving reaction-diffusion equations, several time scales get involved, such as the diffusion time for each species, reaction rates, and buffering rates. In order to accurately solve the set of differential equations, an appropriate time scale should be taken considering that it is defined by the fastest process. This point imposes a restriction that may bring out a multiscale problem. The main aspect involved in the solution of a model for studying Ca^{2+} dynamics is the buffered Ca^{2+} diffusion problem. In the present thesis, we have used stochastic and deterministic approaches to solve this problem. A description of these approaches is given in the next two sections.

2.3.1 Stochastic methods

Monte Carlo methods

Monte Carlo methods are a class of mathematical methods, and its computational algorithms, that rely on repeated random sampling to compute their results. They usually make use of computers since they need a lot of calculations [112]. The name is related to the city of Monte Carlo in Monaco, famous for its casinos and where the roulette, the gambling game, is a *random number* (a number that is never predictable) generator. These methods, which were originally developed by J. von Neumann and S. Ulam [122], are specially useful: 1) To solve models of phenomena with uncertainty in its inputs, reflected in the use of random numbers to calculate the solution, or 2) To solve microscopic models where the main variables, acting as particles (ions or molecules), may follow random movements (such as random walk [46] and *Brownian motion* [135]).

Monte Carlo methods have proven to be very valuable to simulate the diffusion of particles in a non-homogeneous media i.e., a media that presents spatial or temporal dependence of the diffusion coefficient such as degradation or barriers, or in non-symmetrical spaces [46]. In these cases, the random walk method is highly accurate, since it evaluates the probability that each particle can move to any of its possible trajectories (in one, two or three dimensions) in each time step, as depicted in Figure 1.7. Moreover, Monte Carlo methods find a solution in any geometrical domain, being appropriate when particles are few and are non-homogeneously distributed in the do-

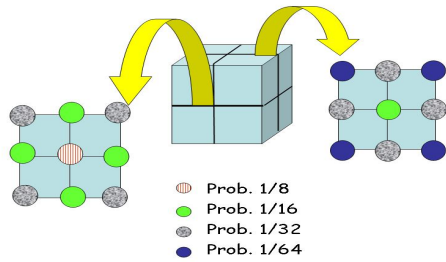


Figure 2.7: A drawing about how the Random-walk algorithm works in three dimensions: Each time step, a particle located inside the cube may move to one of the twenty-six neighbouring positions with the indicated probabilities, or may stay in its current position.

main. However, the main restriction of these methods is that they are computationally expensive and time consuming, so they are suitable for short to median timescale simulations, which in turn, implies small spatial domains.

In neurotransmitter secretion, exocytosis is started by few calcium ions [53, 60, 72], and in neuroendocrine cells, the secretory machinery appears clustered in specific zones [160]. These characteristics impose severe restrictions to the spatial dependence of calcium diffusion and binding. To accurately estimate these two processes, stochastic methods are the best option. Therefore, for the present thesis, the Monte Carlo method was employed to solve the Active-zone and the Cytoskeleton-cage models that allow us to simulate fast secretion in the calyx of Held and in bovine chromaffin cells. For both models, the random walk algorithm was implemented to estimate calcium diffusion in a three-dimension space, as shown in Figure 1.7.

Our random walk algorithm estimates the probability that a particle (a calcium ion or a mobile buffer) may move or not at each time step. The whole domain (cylinder or cone) is divided in cubes, each one identified by its three-dimension position. Inside a cube, there may be one or more particles, and each particle may move to one of the twenty-six neighbouring positions with the probabilities indicated in Figure 1.7, or may stay in its current position. If the cube is located in the boundaries of the domain, it is assumed that it will be reflected. Calcium ions diffuse faster than mobile buffers, i.e., buffers have smaller diffusion times than calcium ions, then the algorithm moves buffer particles less frequently than calcium particles.

In order to estimate the stochastic binding and unbinding of calcium ions due to buffers and the vesicle sensor, a Monte Carlo algorithm was used. This algorithm evaluates, each time step, the probability that a calcium ion may be bound or unbound by a buffer or by the sensor. The corresponding probabilities are calculated based on the binding and unbinding rates, k_{on} and k_{off} , as well as the time step, assuming that binding process follows a binomial distribution, as clearly described in [63]. The flow diagram of the computer programs developed to solve the AZ and the CC models (Stochastic models) is shown in Figure 1.8, and the main steps are briefly described below. All programs were implemented in Fortran 77 language for Linux Operating System.

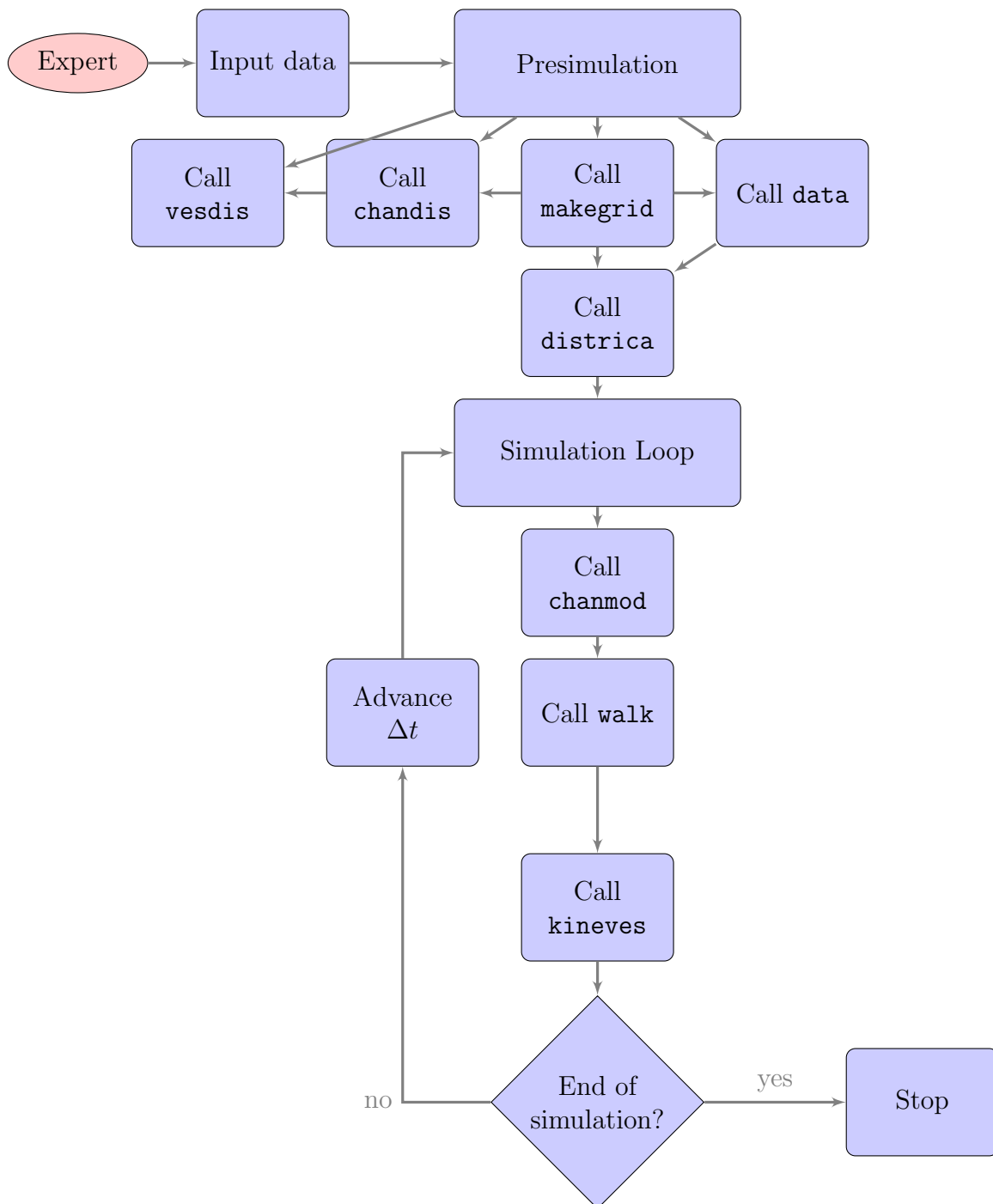


Figure 2.8: Flow diagram of programs that solve the Active-zone and the Cytoskeleton-cage (Stochastic) models. Routines are described in Appendix B.2.

Main input data:

- Domain type (cylindrical/conical)
- Channel distribution (random/cluster/correlated-cluster)
- Initial Ca^{2+} and buffer concentrations
- Depolarization pulse (voltage, duration)
- Simulation time

Presimulation stage:

- Transform the macroscopic input variables into microscopic quantities (call Program `data`)
- Map the simulation domain into a 3-D orthogonal grid (call Program `makegrid`)
- Distribute calcium channels over the upper layer of the domain (call Program `chandis`)
- Distribute vesicles over the upper layer of the domain (call Program `vesdis`)
- Distribute uniformly the initial number of calcium ions and buffers over the whole domain (call Program `districa`)

Simulation stage: At each time step, Δt , calculate the following values:

- Number of incoming calcium ions (call Program `chanmod`)
- New position of calcium ions and mobile buffers due to diffusion, and increase one time step (call Program `walk`)
- Number of free and bound calcium ions due to kinetic reactions of the buffers and the vesicle calcium sensor, as well as the number of fused vesicles (call Program `kineves`)

Most programs shown in Figure 1.8 were written and tested by A. Gil and J. Segura [64]. New programs developed for this thesis are: `vesdis`, which distributes vesicles; `chanmod`, which calculates the number of calcium ions entering to the cell through P-type and L-type Ca^{2+} channels with a Monte Carlo algorithm; and `kineves`, which calculates the number of free and bound calcium ions resulting from the kinetic reactions associated with buffering and vesicle fusion. The latter program also calculates the number of fused vesicles (secretion) for non-cooperative and cooperative kinetic schemes. Program `chanmod` is a Monte Carlo algorithm that solves the state model of a calcium channel, as those models shown in Figure 1.1. Program `kineves` implements a Monte Carlo solution to the kinetic schemes described in Section 1.1.3. All routines are described in Appendix B.2.

2.3.2 Deterministic methods

A variety of deterministic numerical methods for solving differential equations, ordinary and partial, can be found in almost any standard textbook of numerical analysis (see for example [28]). The choice of a particular method will depend on: 1) The kind

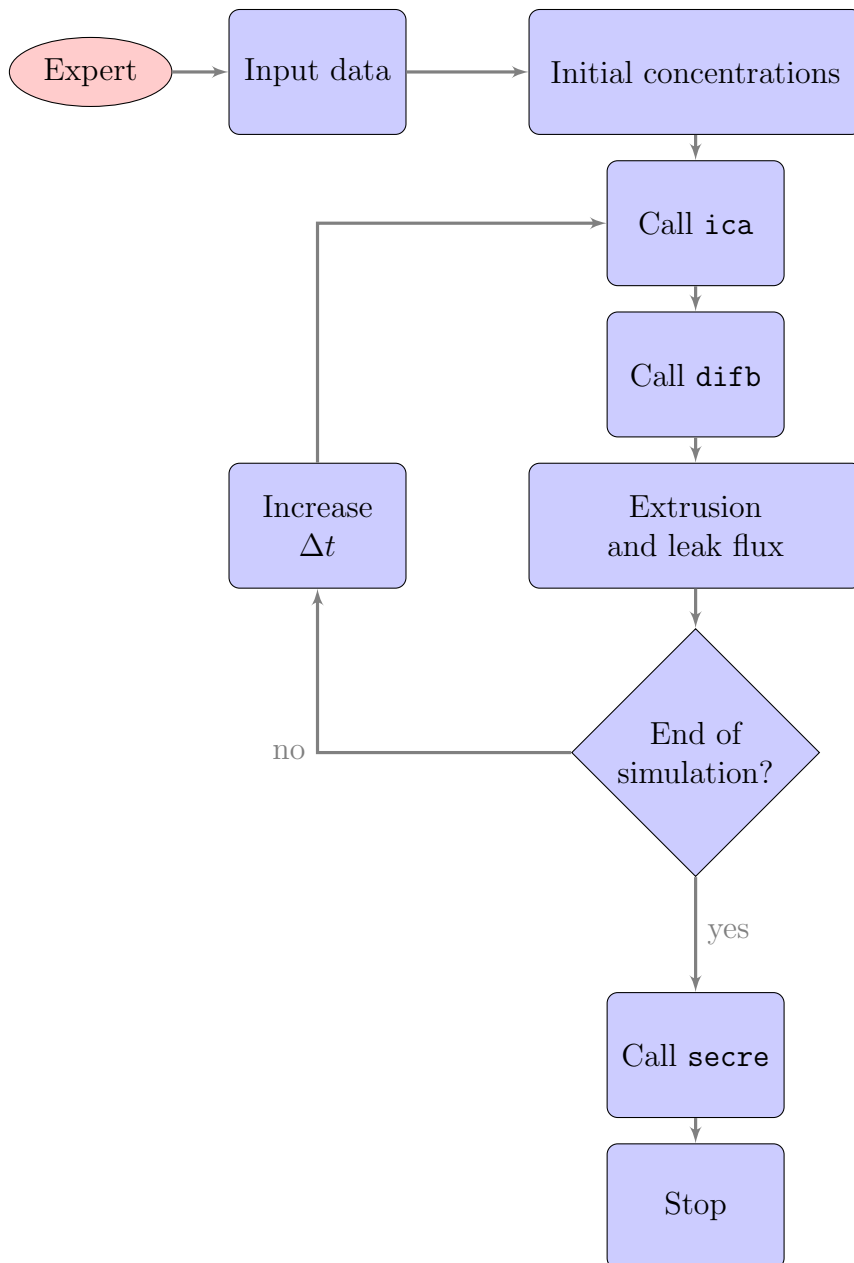


Figure 2.9: Flow diagram of the computer programs developed to solve the Shell (Deterministic) model. Routines are described in Appendix B.3.

of problem to be solved, that is, initial or boundary value problem; 2) The problem stiffness, i.e., is it a smooth or a stiff problem? and, 3) The compromise we have between accuracy and efficiency, which leads to choose simple or sophisticated methods. In the present thesis, to simulate Ca^{2+} and secretion dynamics using the Shell model, we have had to combine two deterministic methods: one for solving the reaction-diffusion partial differential equations (a parabolic equation), and one for solving the set of ordinary differential equations describing the kinetic scheme associated with vesicle fusion. Reaction-diffusion is a process mainly managed by the Ca^{2+} diffusion coefficient, whereas Ca^{2+} binding is governed by the kinetic rates associated with the Ca^{2+} sensor, which call for a multiscale solution. Then, as a first approximation, we decided to solve kinetic reactions separately from the reaction-diffusion process, assuming that the Ca^{2+} binding by the vesicle sensor does not considerably affect Ca^{2+} dynamics. This approximation is adequate for whole-cell Ca^{2+} concentrations as those used with the Shell model, but could fail when dealing with low Ca^{2+} quantities.

In order to solve the reaction-diffusion process, i.e., the parabolic equation, we have chosen the Crank-Nicholson method which consists of a convex combination of explicit (in time) and explicit (in space) schemes [28]. This finite-differences method has the advantage of being stable for any positive choice of discretization steps. Specifically, we solve Equations 1.5, 1.8, and 1.10, as well as a constant leak flux, assuming that diffusion occurs only in the radial direction of a homogenous sphere of radius R . This sphere, that represents the cell, is divided in concentric layers of thickness Δx . The calcium concentration in the most external layer is affected by calcium influx due to channels, calcium extrusion, leak flux and buffers, as well as diffusion. The most internal layer, representing the nucleus has no calcium influx or efflux. Ca^{2+} concentrations in all other layers are influenced only by buffered diffusion. Boundary conditions are $\frac{\partial C}{\partial x} = 0$ at $x = 0$ and $x = R$, i.e., there is no flux at the cell limits, the nucleus and the external medium, except through Ca^{2+} channels. These considerations are depicted in Figure 1.6. Initial conditions, for all cells, are $[Ca^{2+}]_i = 0.1\mu M$, $-80mV$ of resting potential, and a specific endogenous buffer concentration.

On the other hand, to solve the kinetic reactions that model vesicle fusion, described in Section 1.1.3, we have used an adaptive time-step numerical method of integration, namely `ode15s`, as implemented in the Matlab software. Function `ode15s` belongs to the set of algorithms that solves initial value problems for ordinary differential equations, in particular, it is intended to be efficient and accurate for stiff problems. This function integrates the coupled differential equations in a specified time span, using the given initial conditions. For our purposes, we call this function to obtain the number of vesicles present in each state, or pool, shown in the kinetic scheme 1.9, at each time; this makes up the vesicle pool dynamics along the simulation time. In order to get these dynamic values, we assume an initial vesicle distribution which represents the physiological basal organization of the vesicle pools. This organization is a particular characteristic of each cell type, which in turn, determines the exocytotic response.

Computer programs developed for the Shell model implement both numerical algorithms, the Crank-Nicholson and the adaptive integrator in routines `difb` and `secre`, respectively. The flow diagram of the whole main program is shown in Figure 1.9, and the main steps are briefly described below. All programs were implemented in Matlab

language for Windows and Linux Operating Systems.

Main input data:

- Cell radius
- Shell thickness
- Depolarization pulse (voltage, duration)
- Simulation time

Presimulation stage:

- Uniformly distribute the initial concentration of Ca^{2+} and endogenous buffer in each shell

Simulation stage:

At each time step, Δt , calculate the following values:

- Calcium influx (call Program `ica`)
- Free Ca^{2+} and buffer concentrations in each shell (call Program `difb`)
- Calcium efflux due to the extrusion pump
- Leak flux

Calculate the number of fused vesicles (call Program `secre`)

The main algorithm shown in Figure 1.9 was written and tested by V. González-Vélez [73]. For the present thesis, new routines were developed: An improved version of Program `difb` that computes the concentration of endogenous buffer and free Ca^{2+} in each shell; program `ica` that reads experimental data of Ca^{2+} current; and, program `secre` that solves the kinetic reactions describing Ca^{2+} binding for vesicle fusion. Routines are described in Appendix B.3.

The calyx of Held presynapsis: Studying fast secretion

3.1 Introduction

The calyx of Held is a U-shaped large synapse (Figure 3.1) widely used to study stimulus-secretion coupling in neurotransmitter release, due to the fact that its huge size allows experimentalists to simultaneously record the pre- and post-synaptic events. It is located in the trajectory of the mammalian auditory central nervous system and it has been related to high-frequency sound source localization [158]. The whole calyx membrane area is about 2,500 square microns, from which about 40%, i.e., 1,000 square microns are in contact with the principal (postsynaptic) neuron. The thickness of the calyx is mostly less than $1 \mu\text{m}$. In the contact area, which is the releasing area, there are approximately 554 active zones of $0.1 \mu\text{m}^2$ each, and the center of any of them is separated from the nearest one by a mean of $0.59 \mu\text{m}$ [150]. All these characteristics, along with the limited diffusion of calcium ions inside the cytosol [119], support that

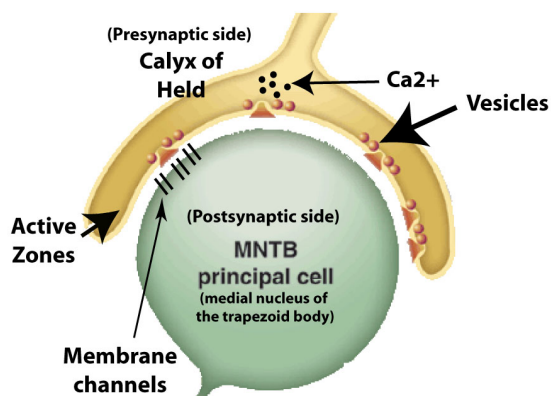


Figure 3.1: A simple diagram of the calyx of Held presynaptic terminal and the main postsynaptic neuron. The calyx is U-shaped and in its internal side the active zones are found. The diagram depicts that calcium ions near docked vesicles trigger glutamate release.

secretion dynamics may be studied based on single active-zone models.

At rest, the calyx has a potential difference between the inner side and the outside (named *resting potential*) around -75 mV [21]. Under stimulation, presynaptic action potentials are generated and depolarize the calyx forcing voltage-gated Ca^{2+} channels to open. Then, external calcium ions enter into the calyx forming calcium spots, named micro or nanodomains depending on the distance to the channel [131]. These domains can reach very high Ca^{2+} concentrations (up to tens or hundreds of micromolars) in the close vicinity of calcium channels, which is usually much larger than the average cytosolic calcium concentration [13, 32, 105].

Rapid and high elevations of $[Ca^{2+}]_i$ partially explain the very efficient coupling between the action potential stimulation and the initiation of glutamate release, delayed about one millisecond [19]. Indeed, the incoming ions trigger fusion and release of those docked and ready-to-be-fused vesicles (named *RRP*, *Readily Releasable Pool*, or *IRP*, *Immediately Releasable Pool* vesicles), by binding to their calcium sensor. It has been estimated that up to twenty calcium channels might open to trigger the two to five RRP vesicles found in an active zone, in the range of 10 to 20 nm from the contact area [150]. However, the fast and efficient secretion in the calyx is also due to the presence of non-uniform arrangements of calcium-channel clusters and vesicles, and to the Ca^{2+} affinity of the vesicle sensor [5].

Three subtypes of voltage-gated calcium channels have been described as the main gates of presynaptic calcium currents in response to depolarization: the P-, the N-, and the R-type [92, 100, 199]. Nevertheless, it had been observed that P-type channels participate more effectively in triggering release for mature cells than the other two types, probably because they are located closer to release sites [197] and/or because they remain after cell maturation [91]. Calcium channels are critical not only to allow Ca^{2+} influx that triggers secretion, but to physically interact with *Synaptotagmin-1* protein that acts as the vesicle Ca^{2+} sensor. In fact, it has been argued that this physical interaction is required to tether, dock and fuse vesicles, all steps required for fast secretion [26].

An important and extensively used parameter for the study of calcium dependence of release is the biochemical or kinetic cooperativity, which is the exponent of the non-linear relationship between release and calcium influx [35]. Cooperativity refers to the requirement for the binding of multiple Ca^{2+} ions to trigger fusion of presynaptic vesicles. It is generally accepted that release is highly cooperative, and that cooperativity values in the calyx are between two and five. These values have been measured using flash Ca^{2+} photolysis [109, 172] and depolarization pulses [151, 152]. Experimental findings also show that calcium cooperativity depends on the $[Ca^{2+}]_i$ range: there is low cooperativity for low $[Ca^{2+}]_i$ (near basal values), and high cooperativity for high $[Ca^{2+}]_i$, usually reached after a stimulus. A low Ca^{2+} cooperativity seems to be functionally relevant because it prevents a large increase in asynchronous release activity, as commented in [109]. Notice that spatial coupling of channel-vesicles as well as cooperativity seem to suffer developmental transformations that affect release efficiency [47].

The behaviour of Ca^{2+} dynamics in the calyx is started by calcium influx through voltage-gated P-type calcium channels opening, and then to its buffered diffusion. The latter behaviour is due to the action of efficient Ca^{2+} -reducing mechanisms such as the

sodium-calcium exchanger, the calcium pump and the mitochondria [96]. All entering calcium ions tend to diffuse into the cytosol along time, but free diffusion is also affected by the calcium buffers present in the calyx [32, 49, 151]. Then, the time course and the amplitude of local $[Ca^{2+}]_i$ transients are the result of all these mechanisms working simultaneously in the first few milliseconds after the appearing of the stimulus.

Some modeling works on exocytosis in the calyx and in other synapses have been reported. They range from those studying synaptic transmission (depression/facilitation) [78, 86, 117, 181], through those describing transmitter release [13, 15, 198], up to those theoretical studies of neurotransmitter modulation at the calyx of Held [119, 120]. There are also works on kinetic models of release [20, 159] which fail, however, in predicting the low cooperativity observed at low $[Ca^{2+}]_i$; then, alternative and more sophisticated models have been proposed [109, 172]. Some other works have studied the influence of the dynamics of Ca^{2+} influx and the geometry of the active zones in neurotransmitter release [13, 163]. However, the study of several relevant factors in neurotransmitter release at a microscopic level (such as vesicle population, channel-vesicle localization, calcium influx, and mobile buffers) has not been done, prompting the work developed for the present thesis.

The two standard experimental protocols for studying Ca^{2+} cooperativity in the calyx of Held are flash Ca^{2+} photolysis and pulse/action potential depolarization; in both cases, the technique induces a $[Ca^{2+}]_i$ increase which triggers neurotransmitter release. Both methods commonly estimate the release rate by deconvolution of the postsynaptic current, and evaluate the cooperativity by obtaining the slope of the best Hill fit (n) for the curve of peak release rate versus $[Ca^{2+}]_i$ (as in [20, 159]). Applying depolarization pulses follows a more physiological approach since release is triggered by presynaptic calcium currents, as when action potentials appear [151, 152], whereas the Ca^{2+} uncaging technique avoids participation of calcium channels. Using calcium uncaging cooperativity of release seems to be very high ($\sim 4-5$) for $[Ca^{2+}]_i > 1\mu M$, and to be much lower (2 or even less) below this value [109, 172]. Similarly, using depolarization pulses, the estimated values of the kinetic cooperativity are also high ($\sim 3-4$) and the effect of exogenous buffers (commonly used in experiments, such as BAPTA, EGTA or FURA) can also be studied [151, 152]. Based on the reported data obtained in the calyx of Held about Ca^{2+} -triggered secretion, for the present work we have simulated the presynaptic calcium currents induced by pulse depolarization, and the corresponding secretion rates of glutamate.

3.2 Modeling

Neurotransmitter secretion in a presynapsis is a very fast process that takes place in a few milliseconds after the appearance of the stimulus. The calcium ions that trigger this process are those localized close to ready vesicles. Therefore, an adequate model should be able to estimate calcium influx and vesicle fusion in a few milliseconds with high spatial resolution. This can be achieved by proposing a small-sized model containing the main features involved in secretion (channels, vesicles, buffers). Moreover, since the simulation periods we are interested in fall in the range of milliseconds and an active zone can be approximated as a cylinder of $0.1\mu m$ of radius, as found in microscope data [150], it is feasible to use a microscopic model and to choose high spatial and

temporal resolution. Therefore, in order to simulate presynaptic secretion occurring in the calyx, the Active-zone model was chosen, and it was solved with Monte Carlo methods explained in section 1.3.1. Inside the active zone, we include models for calcium buffered diffusion, non-cooperative or cooperative calcium-binding schemes for vesicle fusion, and P-type voltage-gated calcium channels. To model vesicle fusion, we compare two different five binding-sites schemes, one assuming cooperativity [159], and another one assuming there is no cooperativity [20], as will be discussed later. For the P-type calcium channels, we have developed a three-state Markov model, following the methodology detailed in Section 1.1.1, which allows us to simulate the calcium influx observed during experimental protocols. Since this channel model was fitted to reproduce the characteristics of calcium influx in the calyx, it is a specific model. Then, particular details about this model are given in the following section. The whole set of parameter values used to simulate calcium influx and secretion in the calyx are given in Table 3.1.

3.2.1 P-type Ca^{2+} channel model

Following a previous three-state Markov model for L-type voltage-gated channels [74], we propose a P-type channel model which includes voltage activation and deactivation, as well as voltage- and Ca^{2+} -dependent inactivation, as reported for these channels [199]. L- and P- type channels exhibit similar high-voltage activation, showing a fast activation for depolarizations above -40 mV; additionally P-type channels exhibit a steep voltage-dependent inactivation that follows the inward current profile, even though internal calcium elevation can trigger some level of Ca^{2+} -dependent inactivation [27]. The current to voltage curve and the 3-states model for our P-type channel model are shown in Figure 3.2. Expressions and values of the transition rates are given in table 3.1. In contrast to our previous L- channel model, the P- model considers inactivation as a non-linear function of the membrane voltage, as well as the internal and external Ca^{2+} concentrations. The latter is included in the model because it has been shown that the external Ca^{2+} concentration affects the number of open calcium channels [59]. Also, the implementation of this model in our Monte Carlo simulation scheme has the additional feature of considering the calcium concentrations in the compartments located just below the channels which allows, in this way, for a correct evaluation of the Ca^{2+} -dependent inactivation. For all simulations, we assume that the external calcium remains constant at the common value for mammals (2 mM) [197].

3.3 Simulations

Our simulations calculate presynaptic calcium currents induced by pulse depolarization. In order to activate this calcium influx, we simulate the application of a depolarizing pulse lasting 4 ms, and with different amplitudes. For all simulations we assume resting conditions of $0.1\mu M$ as internal calcium concentration, and -80 mV of cell voltage, as in experimental protocols [21, 152]. All parameters used in the Monte Carlo scheme for these simulations are given in Table 3.1.

To study Ca^{2+} -triggered secretion in the Calyx, we pose two main questions: 1) How is the exogenous buffer kinetics affecting the fast release of glutamate?, and 2)

Table 3.1: Parameter values used to simulate secretion in the calyx of Held, using the Active-zone model

Parameter	Value	Reference
INPUT DATA		
Domain type	Cylindrical	Experimental
Base radius (μm)	0.1	[120, 150]
Height (μm)	0.125	Proposed†
Number of vesicles	300	See Section 1.1.3
Number of channels	10	[120, 150]
Channel distribution	Random/Cluster	To test
Ca^{2+} concentration (μM)	0.1	[21]
SPATIAL AND TEMPORAL DATA		Chosen
Spatial resolution (nm)	10	†
Temporal resolution (μs)	0.11	
Simulation time (ms)	10	
VESICLE FUSION SCHEMES		
Number of binding sites	5	
<u>Non-cooperative</u>		[20]
Forward binding rate ($M^{-1}s^{-1}$)	$k_{on} = 3.10^8$	
Backward binding rate (s^{-1})	$k_{off} = 3000$	
Fusion rate (s^{-1})	$p = 40000$	
<u>Cooperative</u>		[159]
Cooperativity factor, b	0.25, 0.5	
Forward binding rate ($M^{-1}s^{-1}$)	$k_{on} = 9.10^7$	
Backward binding rate (s^{-1})	$k_{off} = 9500$	
Fusion rate (s^{-1})	$p = 6000$	
P-TYPE Ca^{2+} CHANNEL		
Unitary conductance (pS)	9	[38, 121]
Transition rates (ms^{-1})		Fitted
α	$5 \exp(0.06(V - 20))$	
β	$0.02 \exp(-0.07(V - 20))$	
ω	0.5	
γ	$0.15[Ca]_i / \cosh((V - 40)/10)$	

†Similar to the distance taken by [150] to count docked vesicles in an active zone (200 nm).

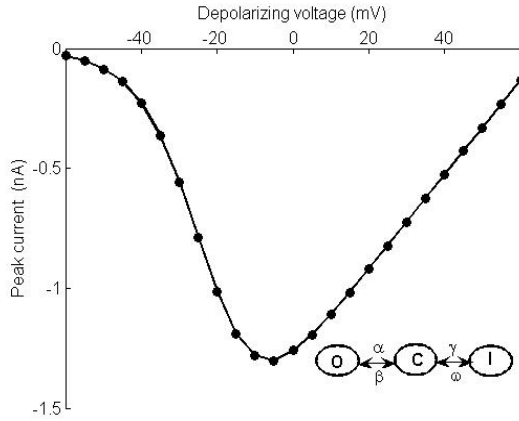


Figure 3.2: Current-to-voltage relationship of our model for the P-type calcium channel found in the calyx of Held. The activation threshold is near -40 mV, and the peak current is reached for membrane voltages between 0 to 20 mV , as reviewed in [158]. In the inset, we show the proposed model, a three-state (**O**pen, **C**losed and **I**nactive) Markov chain. Values of the transition rates are given in Table 3.1.

Table 3.2: Continue from Table 3.1.

Parameter	Value	Reference
ENDOGENOUS BUFFER		[98]
Concentration (μM)	500	
Forward binding rate ($M^{-1}s^{-1}$)	$5 \cdot 10^8$	
Dissociation constant (μM)	10	
EXOGENOUS BUFFERS		
<u>EGTA</u>		
Concentration (mM)	0.5, 0.05	[151, 152]
Forward binding rate ($M^{-1}s^{-1}$)	$1 \cdot 10^7$	[128]
Dissociation constant	$K_D = 0.15 \mu M$	[128]
<u>BAPTA</u>		
Concentration (mM)	0.5	[151, 152]
Forward binding rate ($M^{-1}s^{-1}$)	$5 \cdot 10^8$	[42]
Dissociation constant (μM)	$K_D = 0.2$	[81]

How do the vesicle-fusion kinetic scheme and the spatial channel organization influence the estimation of Ca^{2+} cooperativity of release?. These questions are important since fast release in the calyx is crucial to have an adequate transmission in the auditory pathway, as explained in the Introduction. A deeper knowledge of those elements affecting presynaptic stimulus-secretion coupling in any pathway of the nervous system is still a matter of research [33]. Then, in the next three sections, we figure out these two questions through the analysis of our dynamic simulations.

3.3.1 Influence of exogenous buffers on fast release

To study the influence of exogenous buffers on fast release, we consider that an exogenous buffer (EGTA or BAPTA) is present at a time, in the active zone, when a depolarizing pulse appears to stimulate secretion, following experimental protocols as described in [151, 152]. In this section, results were obtained using the Active-zone model described in Section 1.2.1, and considering the non-cooperative kinetic scheme for vesicle fusion, and a random distribution of calcium channels.

Figure 3.3 shows four simulations of the calcium influx (panels in first row) and secretion profiles (lower panels) obtained with four different depolarizing pulses, and including 0.5 mM of EGTA or BAPTA. The amplitudes of the pulses were thought to explore strong to weak stimulations that evoke release, as tried in experiments [152]. Our simulations reproduce shape and magnitude of the experimentally measured calcium influx through P-type channels in the calyx, and their corresponding release profiles, as reported in [151, 152]. Our results for BAPTA, a fast Ca^{2+} chelator, show that this exogenous buffer highly affects fast release as discussed in [21], increasing the delay of the peak release rate. The delay, as can be seen in figure 3.4, is particularly noticeable for extreme voltage pulses (weak -20 mV and 40 mV) that allow scarce calcium influx. In this case, there is no local buffer saturation and the delay is reflecting the faster binding rate of BAPTA in comparison to EGTA. Indeed, for these extreme pulses the delay differences between the two buffers would be even bigger if we took the EGTA binding rate used in [152] ($2.7 \times 10^6\text{ M}^{-1}\text{ s}^{-1}$), which is about four times smaller than the value we are using for our simulations (see Table 3.1). Notice that delay divergences between both Ca^{2+} chelators are very small for pulses in the range of $[-5\text{ mV}, 20\text{ mV}]$, that is, for high calcium influx.

In figure (3.5) we show a comparison of accumulated secretion without exogenous buffer and with 0.5 mM BAPTA, for two depolarizing pulses: from -80 mV to 0 mV (to induce high influx) and from -80 mV to -20 mV (to induce low influx). In the case of low influx, there is a considerable difference between the secretory responses with and without exogenous buffering; this is not the case for high calcium entry. Then, large calcium currents provoke fast local buffer saturation which reduces, in turn, the effectiveness of BAPTA in blocking secretion.

From an experimental point of view, the effect of exogenous buffers on the exocytotic response seems also to vary depending on the stage of maturation of the calyx, as discussed and analyzed in detail in [99], being the probability of local buffer saturation greater in mature terminals. This fact also supports a higher degree of organization in older calyces which, as we will point out in the next section, could have a measurable influence on estimations of the kinetic cooperativity for secretion.

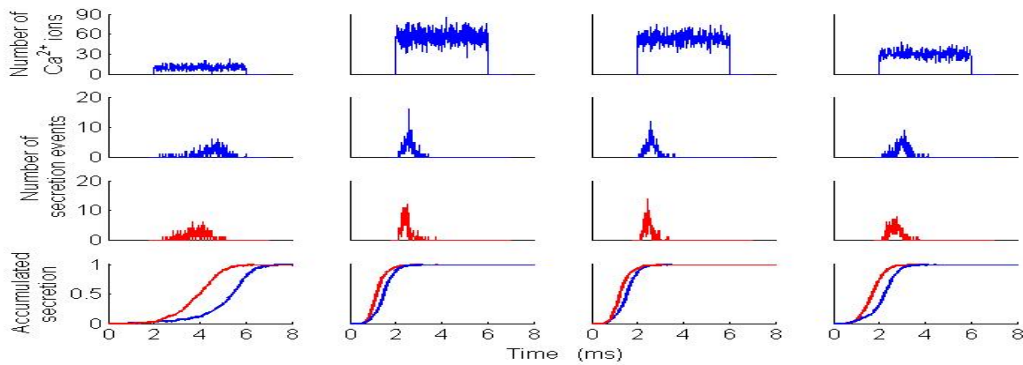


Figure 3.3: Influence of exogenous buffers (BAPTA and EGTA) on fast release. Simulations show Ca^{2+} influx in number of Ca^{2+} ions (first row), secretion rates with BAPTA (second row) and EGTA (third row), and the corresponding accumulated secretion (fourth row), in response to four depolarizing pulses to -20 mV (first column), 0 mV (second column), 20 mV (third column) and 40 mV (last column), respectively. The results were obtained using the Active-zone model (described in Section 1.2.1), and considering the non-cooperative scheme for vesicle fusion as well as a random distribution of Ca^{2+} channels.

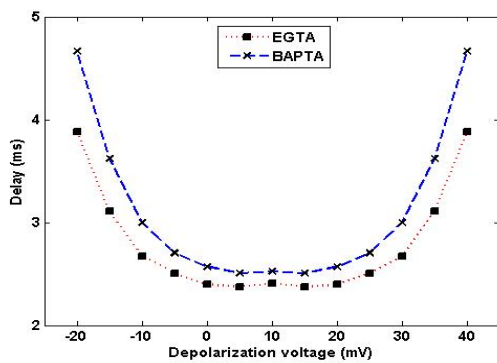


Figure 3.4: Delay of peak release rates obtained with EGTA (\bullet) or BAPTA (\times). Delays were computed based on statistical peak release rates. As expected, delay is greater with BAPTA specially for very low calcium influx, at -20 mV and 40 mV , corresponding to the first and fourth columns of Figure 3.3.

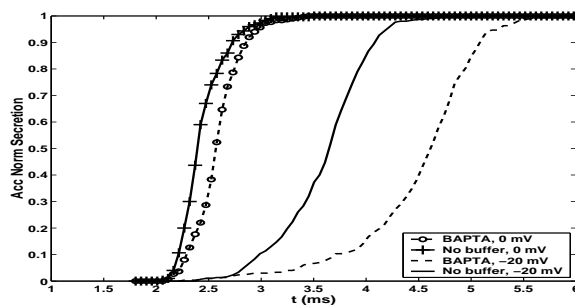


Figure 3.5: Accumulated secretion without exogenous buffer (lines), and with 0.5 mM BAPTA (dotted lines) for two depolarizing pulses: to 0 mV (high Ca^{2+} influx), and to -20 mV (low Ca^{2+} influx).

In all previous simulations, we have used a non-cooperative vesicle fusion scheme with the parameters given in Table 3.1. However, under the same buffering conditions, it is interesting to compare the influence of the kinetic scheme for the secretory vesicles on the secretion time course. Figure 3.6 shows the comparison of the normalized accumulated secretion for three kinetic schemes: the non-cooperative scheme (Scheme 1) suggested in [20], the cooperative scheme (Scheme 2) given in [159] and the same cooperative scheme but with $b = 0.5$ (Scheme 3). The last scheme is considered a control, since it has a higher cooperativity factor that should decrease the unbinding probability. As can be observed in figure (3.6), the non-cooperative scheme provides a slightly faster secretory response than the cooperative scheme due to its faster binding rate. This results in a higher sensitivity to Ca^{2+} in comparison to the cooperative model. Nevertheless, scheme 3 provides a faster secretory response than scheme 1 due to the cooperativity factor, which decreases the probability of unbinding. Additional information on the implications of the vesicle fusion kinetic scheme is provided in figure (3.7). In this figure we show and compare the calcium thresholds for triggering secretion using Scheme 1 and Scheme 2, in response to high calcium influx with 0.5 mM EGTA. We compute a calcium threshold, when an exocytotic event takes place, by averaging the calcium concentration reached over those sub-membrane compartments sharing a similar relative position with respect to the calcium channels. Note that since the spatial resolution considered in the simulations is 10 nm , thresholds were evaluated using calcium concentrations between 0 to 10 nm from the membrane surface. Results obtained for Ca^{2+} thresholds are statistically summarized in figure (3.7) using boxplots. These boxes have lines at the lower quartile, median, and upper quartile values of each data sample. As a first comment, we observe that Ca^{2+} thresholds strongly depend on Ca^{2+} influx (top versus bottom plots): the median values obtained for high influx are in the interval $[100\text{ }\mu\text{M}, 150\text{ }\mu\text{M}]$, while for a low influx, median values are about $20\text{ }\mu\text{M}$. On the other hand, comparing data obtained with both kinetic schemes we find that 25% of total vesicle population depletes for a significantly lower Ca^{2+} threshold than the median value, when the non-cooperative kinetic scheme is considered. This lower threshold, in comparison to other presynaptic terminals, seems to be consistent with experimental data in calyx of Held, as discussed for instance in [20]. It is also noticeable that vesicle fusion occurs at similar thresholds for both kinetic schemes (left versus right plots).

3.3.2 Vesicle-fusion models and cooperativity of release

Within our simulation scheme, we now try to simulate an experimental study (based on the application of depolarizing voltage pulses) for estimating the kinetic cooperativity for secretion. Specifically, we calculate the number of vesicles released during the first millisecond after the calcium current is switched on. The results obtained have been normalized in order to obtain the release rate per vesicle (f_{pv}). We then plot these values as a function of the average number of ions per unit of diffusional time step entering in the microdomain during this first millisecond. The data have been fitted to a Hill function:

$$f_{pv} = \frac{N_{Ca}^n}{N_{Ca}^n + K^n} \quad (3.1)$$

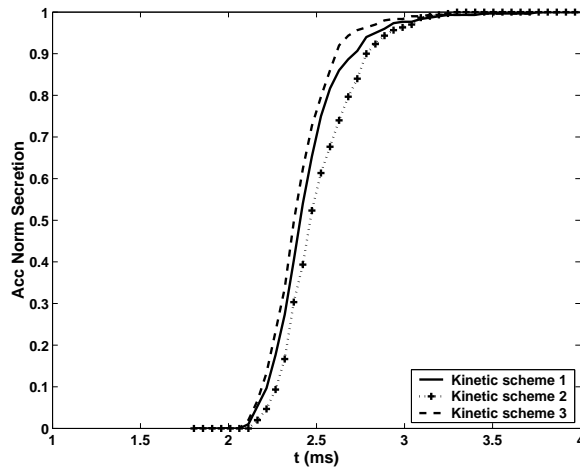


Figure 3.6: Accumulated secretion with three different vesicle-fusion kinetic schemes: a non-cooperative (Scheme 1) [20], a cooperative (Scheme 2) [159], and the cooperative scheme but with an increased cooperativity factor ($b = 0.5$) (Scheme 3). Values for all kinetic parameters are given in Table 3.1.

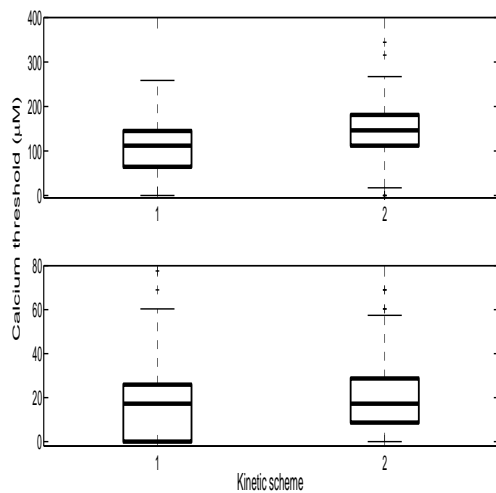


Figure 3.7: Estimated Ca^{2+} thresholds of secretion, considering a non-cooperative (1, left) and a cooperative (2, right) kinetic scheme for vesicle fusion. Secretion is triggered by a depolarization pulse that induces low (bottom plots), and high (top plots) Ca^{2+} influx. Boxes have three horizontal lines to mark lower quartile, median, and upper quartile values of each data sample.

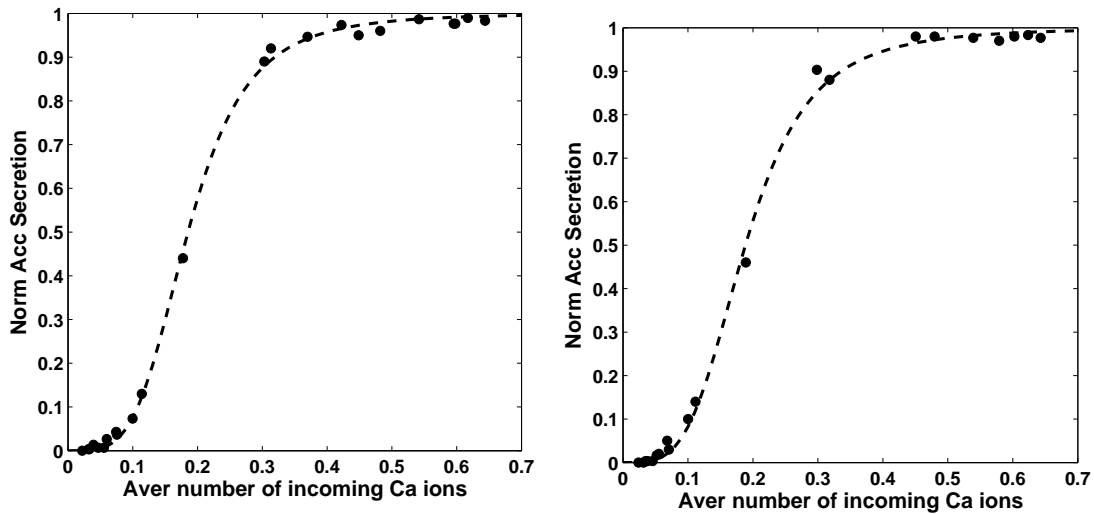


Figure 3.8: Release rates under 0.5 mM EGTA buffering and considering a random spatial arrangement of calcium channels. (Left) Release rate computed using the non-cooperative scheme for secretion. The parameters of the Hill fit are $n = 4.04$ (95 % confidence interval [3.82, 4.27]) and $K = 0.19$. (Right) Release rate computed using the cooperative scheme for secretion. The parameters of the Hill fit are $n = 3.81$ (95 % confidence interval [3.47, 4.14]) and $K = 0.19$. Hill fit follows equation 3.1.

where N_{Ca} represents the average number of ions entering in the active zone during the first millisecond, K is the average number of ions producing half maximum release, and n is the exponent of the function. The fitted value of the parameter n can be interpreted as the *kinetic cooperativity for secretion*. In order to test the influence on the estimated cooperativity values of the kinetic scheme used for vesicle fusion, we have run simulations for both kinetic schemes, the cooperative and the non-cooperative (described in Section 1.1.3), using the parameters given in Table 3.1.

Figure (3.8) shows the results obtained for the non-cooperative (left) and the cooperative (right) kinetic schemes, using 0.5 mM EGTA as exogenous buffer. For the non-cooperative scheme, we obtain a fitted value for the kinetic cooperativity of $n = 4.04 \pm 0.23$, while for the cooperative scheme the fitted value is $n = 3.81 \pm 0.33$. The width of the 95% confidence intervals is similar in both cases and the estimated value for the average number of ions producing half maximum release (K) is the same. Note also that there are no apparent significant deviations of the fitted curve to the data in the lower range of the abscissas axis.

3.3.3 Spatial channel organization and kinetic cooperativity

Previous results were obtained considering a random distribution of channels in the first layer of the simulation domain, which represents the cell membrane. This should be understood as an average configuration compatible, somehow, with whole cell recordings in the calyx. However, calcium channels seem to be organized in clusters associated with vesicles [120]. On the other hand, the possibility of considering non-uniform spatial distributions of calcium channels with ease is one of the key features of our

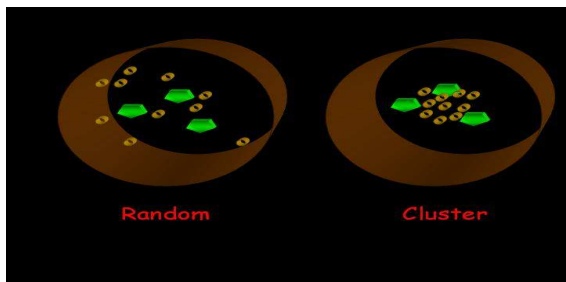


Figure 3.9: Depiction of tested spatial distributions of Ca^{2+} channels (circles) and vesicles (pentagons) in an active zone of the calyx of Held. A random (left) and a clustered (right) organization of channels are shown.

Monte Carlo simulation scheme [66]. Then, we have determined the cooperativity value for a non-uniform distribution of calcium channels, that is, when channels are grouped forming a cluster. Figure (3.9) shows an example of a random spatial configuration versus a clustered configuration just to emphasize how different their spatial distribution is. What we try to elucidate is if there could be any influence of this distribution on the estimated value of n , in a hypothetical experiment based on the application of depolarizing pulses at a microdomain level.

Figure (3.10) shows the results considering a cluster of channels and 0.5 mM EGTA as exogenous buffer, to be comparable to figure 3.8. In this case, the estimated value of the parameter n of the Hill fit is $n = 3.43 \pm 0.30$. The mean value for the estimated kinetic cooperativity is also in the range of $3 - 4$, which is admissible according to the experiments based on the application of depolarizing pulses, but the fitted curve shows deviations in the lower range. In order to get a closer look at these results, figure (3.11) shows a zoom of the release rate at very low calcium for the three different configurations considered so far with 0.5 mM EGTA: 1) A cluster configuration of channels and a non-cooperative scheme for secretion (shown in figure 3.10), 2) A random spatial distribution of channels and a non-cooperative scheme (shown in figure 3.8A), and 3) A random distribution of channels and a cooperative kinetic scheme for secretion (shown in figure 3.8B). As observed in figure (3.11), the highest release rate is obtained for the cluster configuration; this behavior can be fitted with a Hill curve with $n = 2.5$, which represents a reduction of the previously estimated cooperativity value of 27%. This apparent reduction of the kinetic cooperativity can be explained in terms of calcium gradients, which become steeper near a cluster of calcium channels than for dispersed channels. This observation suggests that a possible experiment using depolarizing pulses for estimating the kinetic cooperativity of the calcium sensor could also be used to extract information regarding the geometry of the system. In fact, the possibility of a high degree of clustering in mature calyces, whose kinetic cooperativity is smaller than the one estimated in young calyces, is suggested in the experimental study of [47].

3.4 Discussion of results

The calyx of Held is a widely used system in the study of neurotransmitter release, due to the fact that its size allows researchers to measure pre- and post-synaptic responses, as well as presynaptic $[Ca^{2+}]_i$. Here, we have presented a study of the exocytotic dynamics for a pool of readily releasable vesicles located in a model of one active zone

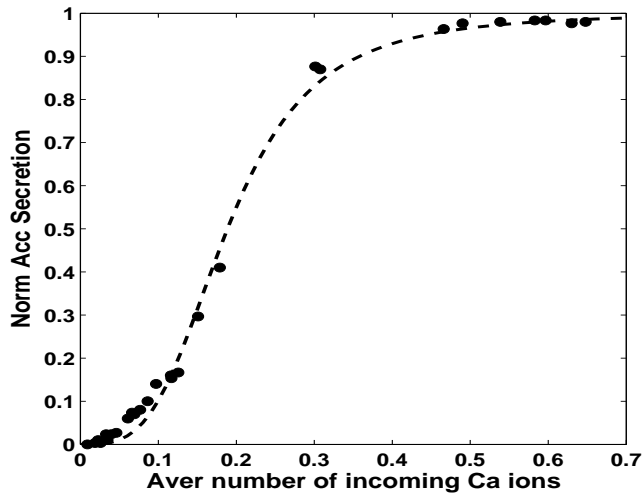


Figure 3.10: Release rate under EGTA buffering. A cluster of calcium channels and a non-cooperative kinetic scheme for secretion are considered in the simulations. The parameters of the Hill fit (equation 3.1) are $n = 4.12$ (95% confidence interval [3.67, 4.57]) and $K = 0.18$. Notice deviations of the curve in the lower range.

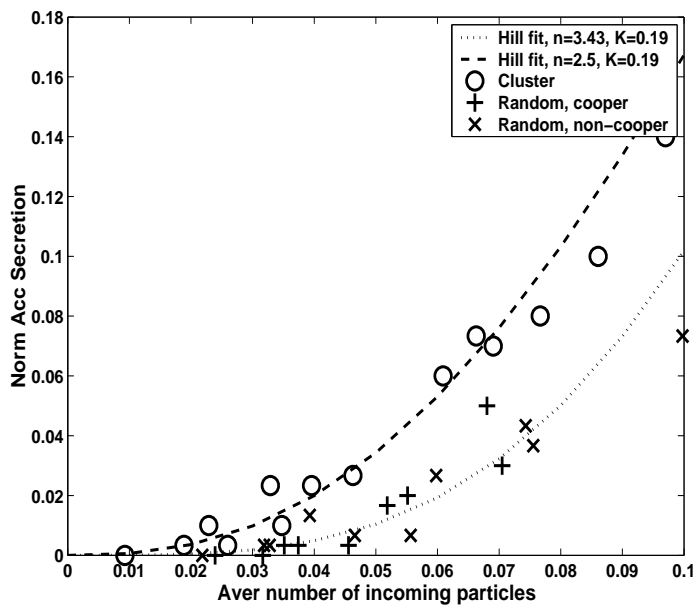


Figure 3.11: Kinetic cooperativity at low Ca^{2+} influx for a random (+,x), and a clustered (o) distribution of Ca^{2+} channels. Results with the non-cooperative (x) and the cooperative (+) scheme, and a random channel distribution, are also shown. Two Hill fits are also drawn (dotted lines): one with $n = 3.43$, which fits the random channel distribution, and another one with $n = 2.5$, which fits the clustered channel distribution.

of the calyx. This model includes P-type calcium channels, endogenous and exogenous (mobile) buffers, secretory vesicles, as well as the microscopic diffusion of mobile buffers and calcium ions. As detailed in Chapter 1, the Active-zone model is suitable to be solved with Monte Carlo methods. Neurotransmitter secretion is accurately simulated with this method, on the one hand, because it takes into account the inherent noise associated with the stochastic nature of voltage-gated calcium channels, buffered diffusion and Ca^{2+} binding [66, 120, 199]. On the other hand, because the calyx of Held can illustrate that, macroscopic descriptions obtained with differential methods in homogeneous geometries, are not always valid or accurate. As shown in our simulations, calcium concentrations at the low regime (low influx) are so small that, for the spatial resolutions considered, just few calcium ions enter into the active zone. Then, microscopic models, such as those based on Monte Carlo methods, are more accurate and useful. Thus, the Active-zone model has been able to reproduce the release triggered by calcium influx through voltage-gated P-type Ca^{2+} channels opened by a brief pulse depolarization, as well as the release delays due to the presence of exogenous buffers, such as EGTA or BAPTA. The effect on the secretory time course of the kinetic vesicle-fusion model has also been illustrated, as well as its influence on the average calcium thresholds to trigger secretion.

Kinetic cooperativity of secretion reflects the need that multiple Ca^{2+} ions be bound to the vesicle Ca^{2+} sensor, in order to trigger vesicle fusion. We have found that when channels are non-uniformly distributed, i.e. they are grouped in a cluster, and stimulation induces low Ca^{2+} influx in an active zone of the calyx, there is a reduction of the apparent value of the kinetic cooperativity. Our results suggest that future experimental studies, based on depolarizing pulses to study secretion kinetics but at a microdomain level, could reveal information about the spatial organization of the subcellular mechanisms, such as Ca^{2+} channels and vesicles. Knowing this microscopic organization, disposed by nature, will allow us to understand developing changes suffered during maturation of the calyx of Held, and the whole auditory pathway in mammals.

Bovine chromaffin cells: Studying spatiotemporal features

4.1 Introduction

The medulla inside the adrenal glands, which are situated over the kidneys, is composed of chromaffin cells (figure 4.1). These cells have the very important role of releasing *adrenaline* (also called *epinephrine*) and noradrenaline in response to fear, stress or conflicts (usually named "*fight or flight*" body response). In chromaffin cells, as in other neuroendocrine cells, the exocytotic process is started by cell depolarization that allows Ca^{2+} influx through high-voltage-activated (*HVA*) calcium channels. Then, vesicle fusion is triggered by calcium ions and, finally, the release of hormones takes place [58]. Chromaffin cells have been widely used to study neurosecretion since they exhibit similar calcium dependence of several exocytotic steps as synaptic terminals do, but having the enormous advantage of being neither as small or fast as neurons, nor as slow as endocrine cells. Apparently, Ca^{2+} control of secretion is common for neurons and neuroendocrine systems, but their differences are contrasted in detail in [130]. These differences allow the simultaneous study of exocytosis and $[Ca^{2+}]_i$ dynamics that is impossible in neurons, as well as other sub-cellular aspects of the stimulus-secretion

Adrenal Gland

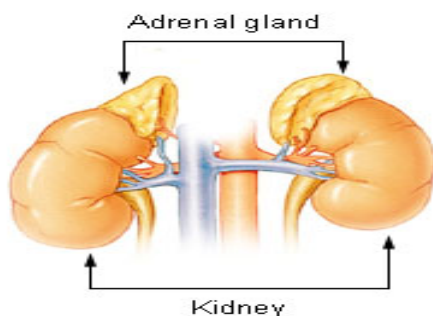


Figure 4.1: Adrenal glands are located over the kidneys, and they secrete hormones that control heart rate, blood pressure, and metabolism in response to stress. These glands have two distinct structures: the cortex and the medulla. Medulla is made of chromaffin cells.

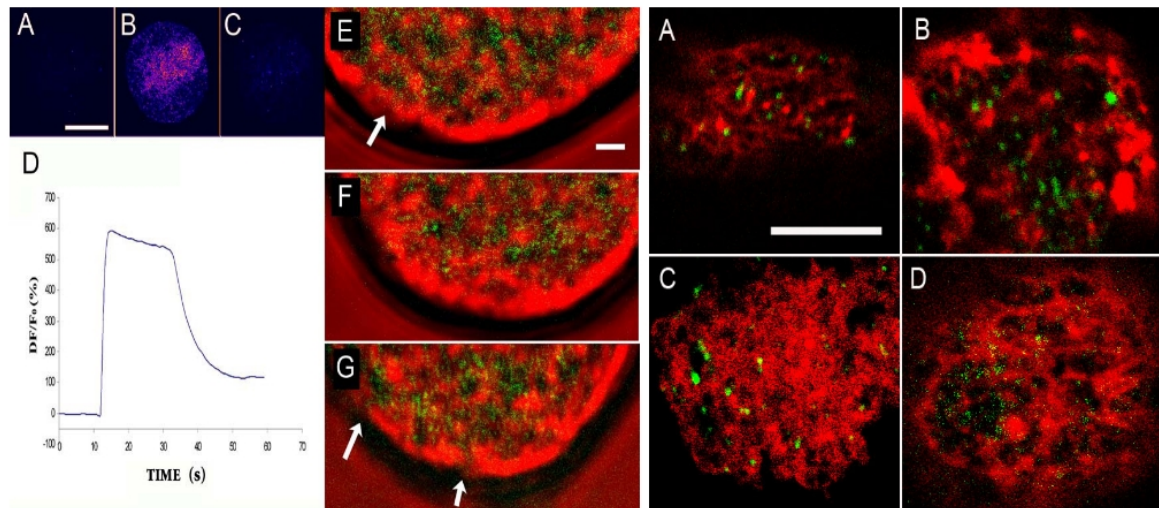


Figure 4.2: Spatial heterogeneity of the cytosolic Ca^{2+} elevation, and localization of Ca^{2+} channel clusters in bovine chromaffin cells. (Left) Fluo-3 images of cytosolic Ca^{2+} distribution in a chromaffin cell in response to a depolarizing stimuli that open Ca^{2+} channels: (A) Resting level, (B) Peak level (maximum in pink), and (C) Sustained level. (D) Ca^{2+} dynamics along time in fluorescence units. (E,F,G) Fluorescent calcium ions (green dots) are found in the empty spaces of cytoskeleton. Arrows point out a "cytoskeleton cage" that we take as a prototype cage for modelling. Real scales: 10 m (in A) and 1 m (in E and G). (Right) Ca^{2+} channel clusters (green dots) are localized in the borders of the F-actin cytoskeleton (red) but not in the empty zones. (A,B) P/Q-type channels are marked, (C,D) L-type channels are marked. Real scale: 5 m. Images recorded, and kindly shared, by the research group of Dr. Luis Miguel Gutiérrez, Institute of Neuroscience, Universidad Miguel Hernández-CSIC, Alicante, Spain.

coupling [137]. One interesting aspect found in chromaffin cells, which is still under research, is the influence of cytoskeleton structure on Ca^{2+} spatial distribution and on secretion [62, 70]. Another relevant topic that is still under investigation is the influence on secretion of the localization of calcium channels, vesicles and regulating proteins (all together named *secretory machinery*) [67]. One other significant issue is the apparent spatial mobility of the secretory machinery that may influence secretion kinetics [108]. Although all these topics have been explored using experimental techniques, models are valuable to help understand the relevance of $[Ca^{2+}]_i$ dynamics on secretion, as well as the influence of the spatial localization of the secretory machinery in the efficiency of the exocytotic response in neuroendocrine cells. Moreover, models developed for chromaffin cells in an animal species may need to be modified to be applicable to other species, so those models considering real cellular mechanisms may be able to highlight specific differences between mammals.

4.2 Experimental data

Transmitted light has been proved a useful technique to visualize the organization of the F-actin cytoskeleton in chromaffin cells, as described in [70]. Once Ca^{2+} enters in the

cell, it has been observed using this technique, that calcium ions are heterogeneously distributed in different zones of the cytoplasm. Among several factors contributing to this non-homogeneous spatial distribution, the F-actin cytoskeletal network seems to play a crucial role in this dynamic behaviour [71]. Cytoskeleton is a dynamic supporting structure inside the cell that exhibits a very complex 3-D polygonal shape. It forms walls and empty spaces in the cytosol where cell mechanisms can place or move along. In chromaffin cells, it has been found that the highest levels of $[Ca^{2+}]_i$ are found in the interior of cytoskeletal cages, i.e. the empty spaces, whereas $[Ca^{2+}]_i$ is low in the cytoskeletal walls, as observed in experiments (Figure 4.2). Since cytoskeleton is not a static structure, its complex dynamics would affect the $[Ca^{2+}]_i$ spatial distribution along time and finally, it would also have an impact on exocytosis. Moreover, evidence indicating that Ca^{2+} channels are organized in clusters has been found. Likewise, it has also been observed that they are positioned in the border of cytoskeletal cages together with the secretory machinery, namely, secretory vesicles and SNARE proteins [179]. Then, active zones for secretion, where release occurs, may be placed near empty spaces of cytoskeletal cages, probably to improve exocytotic efficiency.

4.3 Modeling

In order to study the influence of cytoskeleton structure on the calcium signal, we based on experimental observations demonstrating that calcium channels and the secretory machinery are closely positioned, and that they both are localized in the borders of the cytoskeleton, as shown in Figure 4.2. Therefore, the goal for the modeling task was to propose an adequate model able to test the hypothesis that the cytoskeleton may act as a physical barrier, and then, may modify the spatiotemporal behaviour of $[Ca^{2+}]_i$ after calcium channels have opened. The experimental group¹ envision a model where calcium-channel clusters, vesicles and the secretory machinery are all located in the borders of a cytoskeleton cage, so that, calcium ions might diffuse only into the empty space of the cage (Figure 4.3A and B). Thus, we proposed a three-dimensional model of a prototype cage (the Cytoskeleton-cage model), assuming it is an empty cylinder whose boundaries are the cytoskeleton, i.e., the boundaries are the physical barrier against free Ca^{2+} diffusion. The model contained three clusters of calcium channels and vesicles on top of the cylinder (Figure 4.3C). This model allowed us to compare the secretory response obtained with two different spatial localizations of the cluster-vesicle arrangement.

In order to test the hypothesis about cytoskeleton could act as a physical barrier to improve exocytosis, the Cytoskeleton-cage model described in Section 1.2.2 was used with two different spatial locations of channel clusters and secretory machinery, at the center and at the border, as shown in Figure 4.3C. Each cluster-secretory machinery arrangement is composed of three clusters containing three calcium channels each, two P/Q- plus one L-type, next to one vesicle. The interesting periods to be simulated are in the range of tens of milliseconds (up to 50 ms), and the cage model has $0.3 \mu m$ of radius and $1 \mu m$ of height, as found in fluorescence images [70]. Then, it was feasible to

¹Research group led by Dr. Luis Miguel Gutiérrez, Institute of Neuroscience, Universidad Miguel Hernández-CSIC, Spain

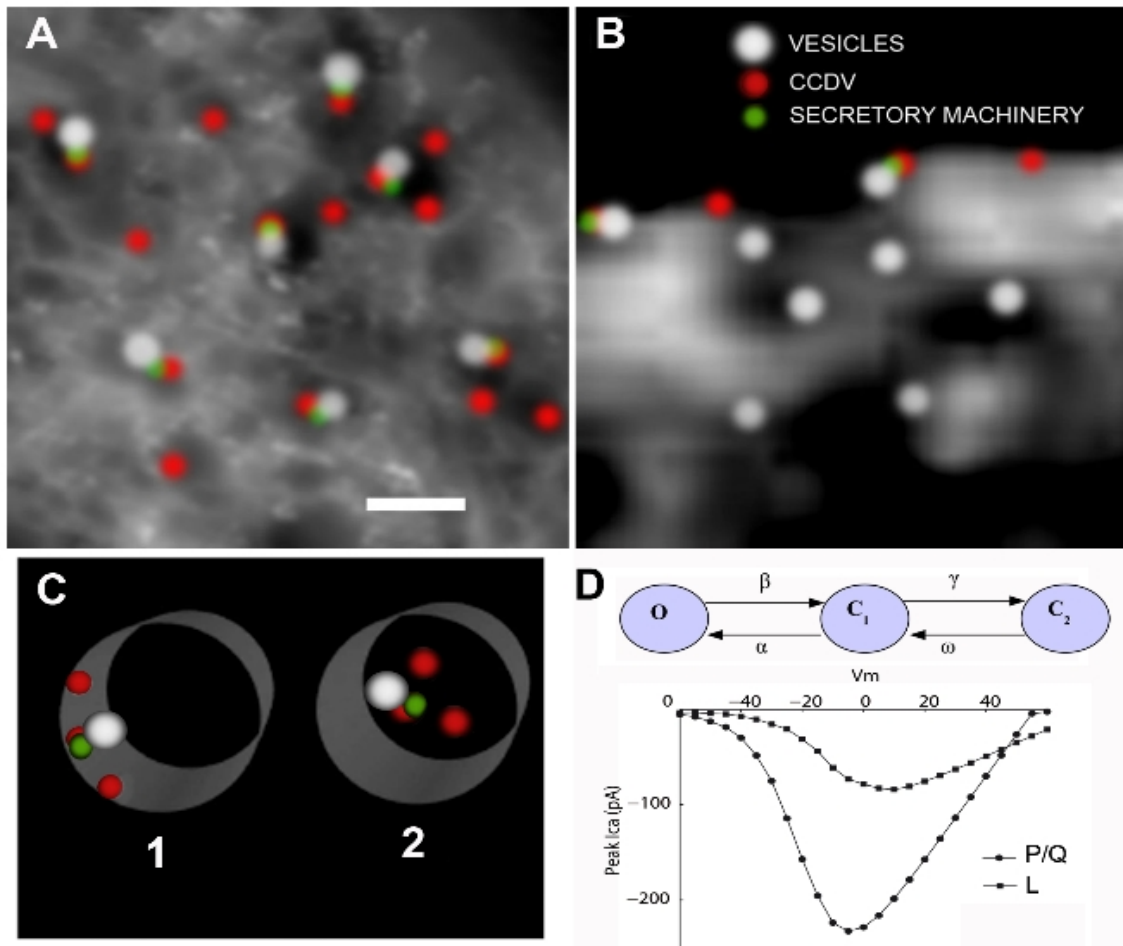


Figure 4.3: Model of spatial arrangements of channel clusters and the secretory machinery in chromaffin cells, proposed in [178]. (A,B) According to the experimental data, cytoskeleton is envisioned as a structure where calcium-channel clusters, vesicles and the secretory machinery are all located in association with its borders, so that, calcium ions might diffuse only into the empty space of the cage. (C) Implemented model of a cytoskeleton cage with two possible locations of channel clusters and the secretory machinery: (1) At the cage limits, and (2) In the cage centre. (D) Three-state model and current-to-voltage relationships of the P/Q- and L-type calcium channels, both included in the channel clusters.

solve the Cytoskeleton-cage model with Monte Carlo numerical methods explained in section 1.3.1. The simulation scheme allows us to choose the microscopic location of the arrangement, in order to simulate the local Ca^{2+} increases that may affect secretion. Vesicle fusion was modeled as a non-cooperative process (described in Section 1.1.3). The whole set of parameter values is given in Table 4.1.

4.3.1 L- and P/Q-type Ca^{2+} channel models

In bovine chromaffin cells, there are voltage-dependent P/Q-, L- and N-type calcium channels, accounting for 50%, 20-38%, and 12-30% of the whole calcium current, respectively [58, 110]. Since the first two types are preferentially localized in secretory sites [67], we propose a specific model for each one. Both calcium channels (L and P/Q) are high voltage activated channels (named HVA) but in bovine chromaffin cells, the P/Q voltage threshold is slightly lower than L threshold. L-type channels exhibit strong calcium inactivation, and have a peak current about 30 pA/pF for $\sim 10 - 20$ mV and half maximal activation about -8 mV. On the other hand, P/Q-type channels show almost no inactivation and a peak current near 200 pA between -5 and +5 mV. With regard to conductances, L channels have been reported to have a higher unitary conductance than P/Q ones.

Both calcium channel subtypes were modeled as three-state Markov processes, with different transition rates to fit the particular current-to-voltage functions (shown in Figure 4.3D), following the methodology explained in Section 1.1.1. Fixed values defined to fit transition rates of the state models were: the threshold voltage (-30 mV for the P/Q and -40 mV for the L), and the unitary conductance (2.5 pS for the P/Q and 8.4 pS for the L). Estimated transition rates are given in Table 4.1.

4.4 Simulations

4.4.1 Spatio-temporal distribution of $[Ca^{2+}]_i$

In order to study the influence of cytoskeleton structure on the spatial distribution of calcium elevations along time, we simulate a depolarizing pulse from -80 mV to 20 mV, to induce calcium-channel opening. On the hypothesis that cytoskeleton act as a physical barrier to $[Ca^{2+}]_i$ distribution, we run dynamic simulations using both cluster localizations shown in Figure 4.3C. Figure 4.4 show the resulting spatial distribution of $[Ca^{2+}]_i$ at different times. For configuration 1, i.e. channel clusters at the cage border, the obtained Ca^{2+} signal reaches high concentration values near the clusters, and then diffuses into the empty space, to arrive at a heterogeneously distribution, 35 ms after. Indeed, this cluster location induces a more heterogeneous spatial distribution of the calcium signal than the corresponding one obtained for configuration 2. Then, simulated calcium dynamics seems to point out that channel clusters near the cage border reproduces a non-homogeneous $[Ca^{2+}]_i$ elevation, which is in better agreement with experimental observations, as those shown in Figure 4.2.

Table 4.1: Parameter values used to simulate secretion in bovine chromaffin cells, using the Cytoskeleton-cage model

Parameter	Value	Reference
INPUT DATA		
Domain type	Cylindrical	Experimental
Base radius (μm)	0.3	[70]
Height (μm)	1	Chosen
Number of vesicles	300	See Section 1.1.3
Number of channels	$3L + 6P/Q$	Experiments
Channel distribution	3 Clusters	To test
Ca^{2+} concentration (μM)	0.1	Experiments
SPATIOTEMPORAL DATA		
		Chosen
Spatial resolution (nm)	30	
Temporal resolution (μs)	1	
Simulation time (ms)	50	
VESICLE FUSION MODEL		
		[98]
Type	Non-cooperative	
Number of binding sites	3	
Forward binding rate ($M^{-1}s^{-1}$)	$k_{on} = 8.10^6$	
Dissociation constant (μM)	$K_D = 13$	
Fusion rate (s^{-1})	$p = 40000$	
CALCIUM CHANNEL MODELS		
P/Q type		
Unitary conductance (pS)	2.5	[156]
α (ms^{-1})	$10 \exp(0.05(V - 30))$	
β (ms^{-1})	$0.02 \exp(-0.08(V - 30))$	
ω (ms^{-1})	0.5	
γ (ms^{-1})	$0.05[Ca]_i / \cosh((V - 40)/10)$	
L type		
Unitary conductance (pS)	8.4	[22]
α (ms^{-1})	$10 \exp(0.05(V - 40))$	
β (ms^{-1})	$0.02 \exp(-0.08(V - 40))$	
ω (ms^{-1})	0.02	
γ (ms^{-1})	$4.4[Ca]_i$	
ENDOGENOUS BUFFER		
		[98]
Concentration (μM)	500	
Forward binding rate ($M^{-1}s^{-1}$)	5.10^8	
Dissociation constant (μM)	10	

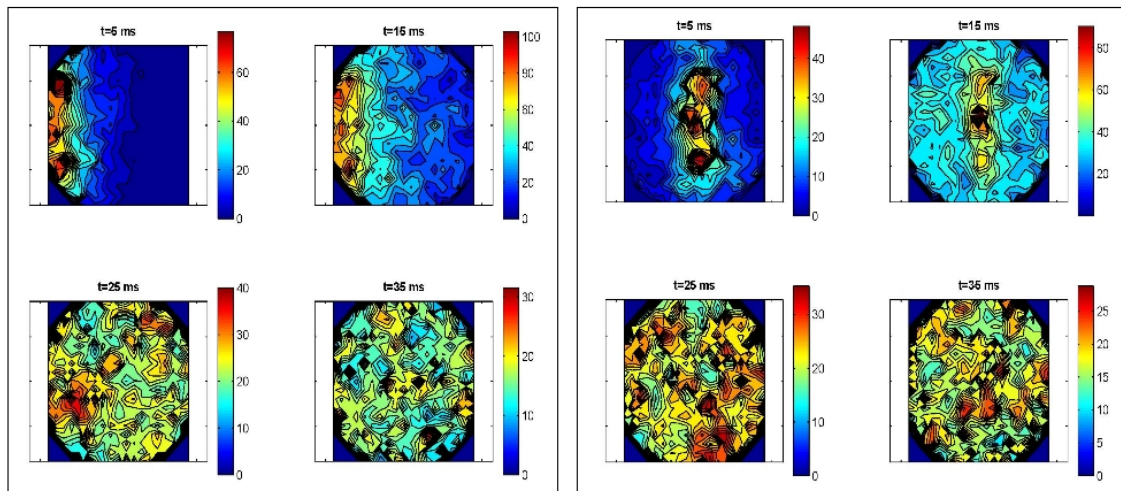


Figure 4.4: Simulations of the spatial Ca^{2+} distribution (in μM) along time using the Cytoskeleton-cage model. Each set of four maps shows $[Ca^{2+}]_i$ after 5, 15, 25 and 35 ms the depolarizing pulse appeared, i.e. after calcium channel opening. (Left) Spatial dynamics obtained when channel clusters are localized in the borders of the cage model (Figure 4.3C, configuration 1). (Right) Spatial dynamics when channel clusters are in the center of the cage (Figure 4.3C, configuration 1). Note concentration differences for each map, indicating that peak values are much higher when channels are in the cage border than in the center of it.

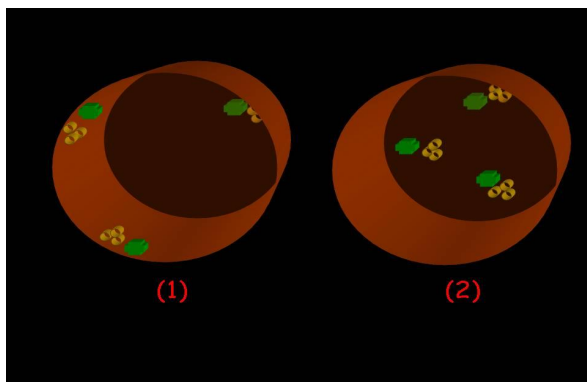


Figure 4.5: Tested cluster-vesicle positions used to investigate cytoskeleton influence on secretion. (1) Located at the borders of, and (2) Randomly distributed in, the cytoskeleton cage. Clusters are formed by three Ca^{2+} channels (circles), and are co-localized with the secretory machinery (crosses) in both arrangements.

4.4.2 Modeling cytoskeleton influence on exocytosis

What will be the influence on exocytosis of a heterogenous calcium distribution, which in turn corresponds to the role of cytoskeleton cages in secretion dynamics? To answer this question, we simulated along with calcium distribution, the secretion events occurring in the cytoskeleton cage for two different positions of the secretory machinery (Figure 4.5): (1) At the borders of the cytoskeleton cage, and (2) Randomly distributed inside the cage. The configurations also assume that three calcium-channels clusters, comprising three calcium channels each as before, are located next to vesicles as found in reported experiments [70]. To induce calcium influx and secretion, we simulated a depolarizing pulse from -80 mV to 20 mV, lasting 20 ms, and calculate calcium and secretion dynamics. Figure 4.6(a) shows the average calcium concentration in the first 30 nm from the cell membrane, for both configurations. Figure 4.6(b) shows the dynamics of the calcium ratio, defined as the calcium concentration close to a vesicle $[Ca^{2+}]_{local}$ over the average calcium concentration $[Ca^{2+}]_{aver}$ shown in (a). In our simulations, this ratio, which approximates the local calcium felt by the secretory sensor, has a mean value of 1.98 for configuration 1 whereas it has a mean value of 1.76 for configuration 2. This value difference means that local calcium effects are enhanced, in about 25%, when the secretory machinery is located in the borders of the cytoskeletal cage. In Figure 4.6(c), the triggered secretion is plotted, for both configurations, indicating that the higher local calcium concentration (corresponding to Configuration 1) triggers a faster exocytotic response.

4.5 Discussion

The organization of cytoplasm in excitable cells has been a factor largely ignored when mathematical models were developed to understand intracellular calcium and secretory behaviour. Based on experimental data, obtained with a combination of fluorescent evanescent and transmitted light microscopy [70], which explore the F-actin cytoskeletal organization in the vicinity of secretory sites in cultured bovine chromaffin cells, we applied the Cytoskeleton-cage model, solved by Monte Carlo methods, to study cytoskeleton influence on calcium and secretion dynamics. Our model allows us to test different spatial locations of calcium-channel clusters and the secretory machinery. The calcium level and the secretory response were simulated with high spatiotemporal resolution, able to perceive slight but important differences: 1) $[Ca^{2+}]_i$ distribution was calculated in a time scale below 35 ms, allowing to see concentration differences in the micromolar range; 2) The secretory machinery was put in specific locations with a resolution of 30 nm, about the size of a calcium channel; 3) Calcium concentration differences were noticed in the vicinity of ± 15 nm from the secretory machinery, which are local concentrations that experimental techniques can hardly measure.

Our results indicate that calcium concentration and distribution is highly influenced by the spatial position of the calcium channel clusters. Experimental data show that chromaffin vesicles are associated with the borders of cortical cytoskeletal cages, forming an intricate tridimensional network. In this sense, our results support the hypothesis that calcium signal and triggered secretion are both enhanced when clusters and secretory machinery are located in the borders of a cytoskeleton cage, improving the

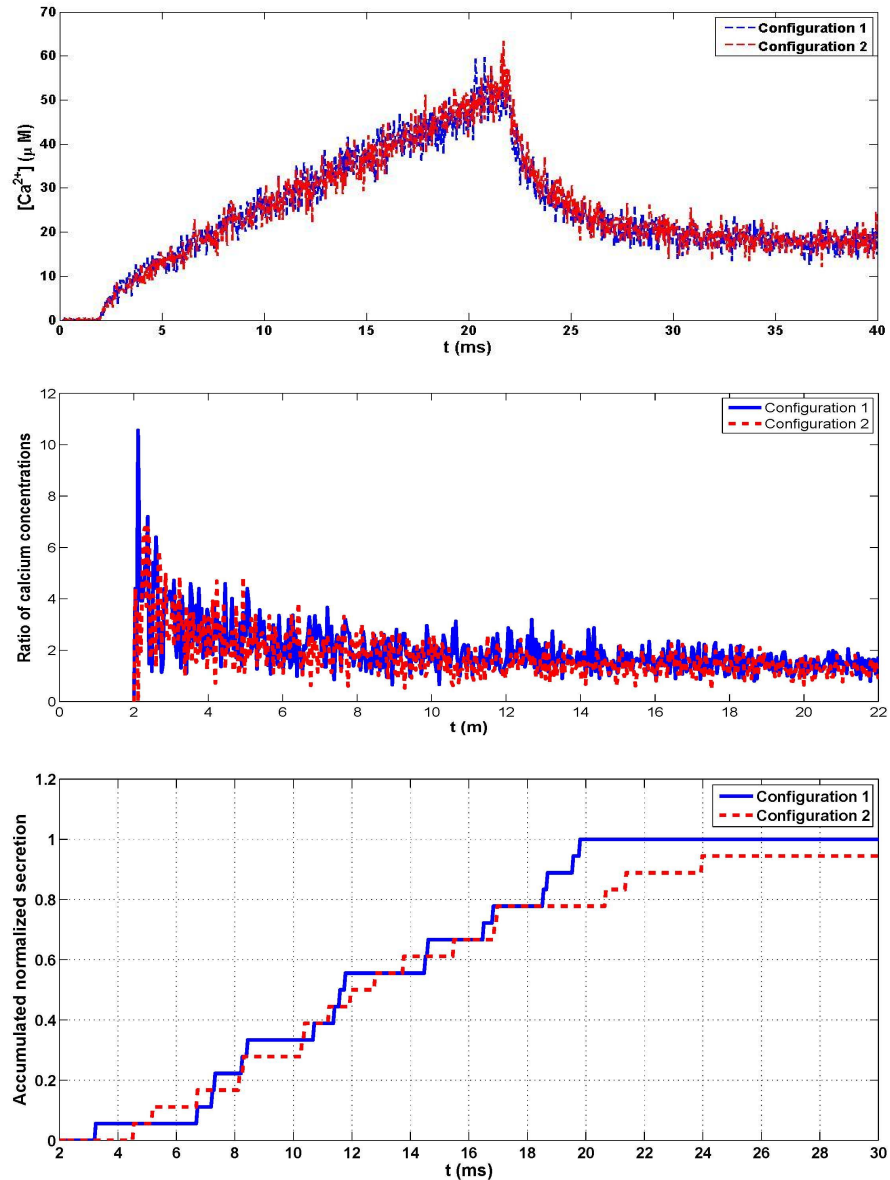


Figure 4.6: Ca^{2+} dynamics and secretion for the tested cluster-vesicle arrangements. (a) Intracellular Ca^{2+} concentrations, between 0 to 30 nm from the cell membrane, for configurations 1 and 2 shown in Figure 4.5. (b) Calcium concentration ratio ($[Ca^{2+}]_{local}/[Ca^{2+}]_{aver}$) for the same configurations. Mean value is 1.98 for configuration 1, and 1.76 for configuration 2. (c) Accumulated secretion events triggered by calcium concentrations shown in (a).

exocytotic response. The interface between the cytoskeleton wall and the cytoplasmic space could be a subject of interest in the field of neurotransmission. Moreover, vesicles seem to interact to, and remain associated with the cage walls during exocytosis [187]. Therefore, to consider the existence of such cytoskeletal organization appears as a relevant factor to model calcium-triggered exocytosis.

Human chromaffin cells: Studying intermediate secretion

5.1 Introduction

Ca^{2+} triggered secretion in chromaffin cells is a relatively slow process when compared to secretion of neurotransmitters in synapses [6, 104]. This is related to the distance between calcium channels and vesicles: when this distance is small (10 to 20 nm) then fast secretion is reached, whereas when this distance is longer (100 to 300 nm), secretion occurs in a longer time scale [129]. In neuroendocrine cells, secretion starts with a delay from short stimulus and lasts for several seconds [97]. At least three phases of secretion have been recognized: one fast, one slow, and one sustained; the kinetics of each phase strongly depends on the animal species, and is related to vesicle pools present in the cell [58]. In general, it is accepted that the fast component of secretion is due to a small pool of vesicles just waiting for Ca^{2+} to fuse and release (named rapidly or immediately releasable pool [3]); the slow component seems to be another pool of vesicles that can mature to become ready, or that follow a slower kinetic pathway; and the sustained phase is related to a depot or reserve pool with much more vesicles that need Ca^{2+} and time to be primed and to move towards the membrane [85, 97]. Vesicle pools in chromaffin cells can explain the experimental observation of different exocytotic phases, and they are also a useful concept to propose secretion models. There are some modeling works on secretion that cover different aspects of exocytosis in diverse animal species of chromaffin cells. In bovine cells, some works relate $[Ca^{2+}]_i$ gradients along time with secretion using a shell model in order to explore the importance of the various vesicle pools [98, 115], and some others study the relevance of channel-vesicle localization in exocytosis using a microscopic model [160]. In mouse cells, kinetic models that explicitly include various vesicle pools and Ca^{2+} participation have been used to study exocytotic steps [189]. One simulation study on the stimulus-secretion coupling in rat chromaffin cells, using public software environments, has also been reported [192].

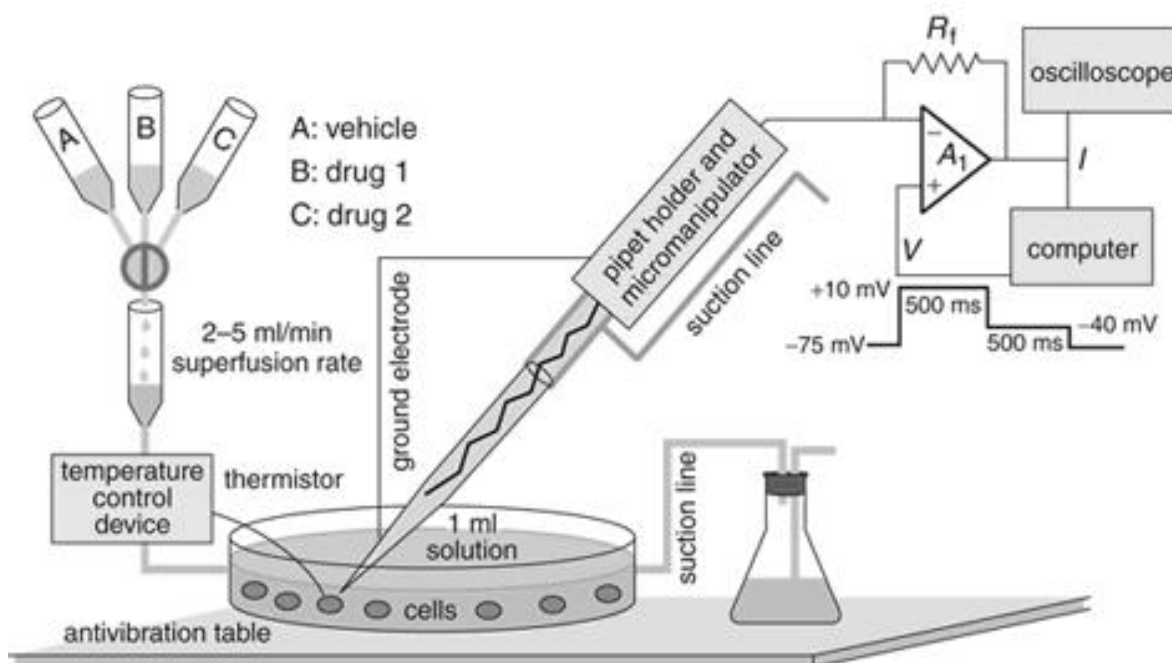


Figure 5.1: Experimental equipment used for the "patch-clamp" technique. This technique, conceived to study ion channel functioning, uses a single electrode to record ionic currents in response to a depolarization pulse and/or in response to a particular drug.

5.2 Experimental data

The patch-clamp technique is commonly used by experimentalists to measure cell secretion evoked by depolarizing pulses. This technique uses the equipment shown in Figure 5.1 which allows researchers to stimulate cells with depolarizing pulses and, simultaneously, to record evoked ionic currents and capacitance increments, as clearly described in [130]. Experimental data shown in this chapter have been recorded by the collaborating group¹ using this technique, and according to the method previously reported by them [137]. It is important to emphasize that experimental studies on human chromaffin cells are scarce since these cells come from adrenal glands of people who died from cerebral haemorrhage, and therefore, relatives need to approve their donation. In addition, glands must be immediately processed.

Figure 5.2 summarizes the measurements of Ca^{2+} currents and capacitance increments recorded in several human chromaffin cells. Cells were stimulated by depolarization pulses lasting from 10 to 200 ms, and the evoked calcium influx and secretion were recorded. The aim of our modeling work, described in the rest of this chapter, was to help in understanding how Ca^{2+} is controlling exocytosis over time and space. The main objective was to study the factors influencing the different secretion stages or bursts. The study of these stages allows one to dissect the intracellular mechanisms governing calcium-triggered exocytosis. Moreover, this study favors the discussion of

¹Research group led by Dra. Almudena Albillos from the Faculty of Medicine, Universidad Autónoma de Madrid, Spain.

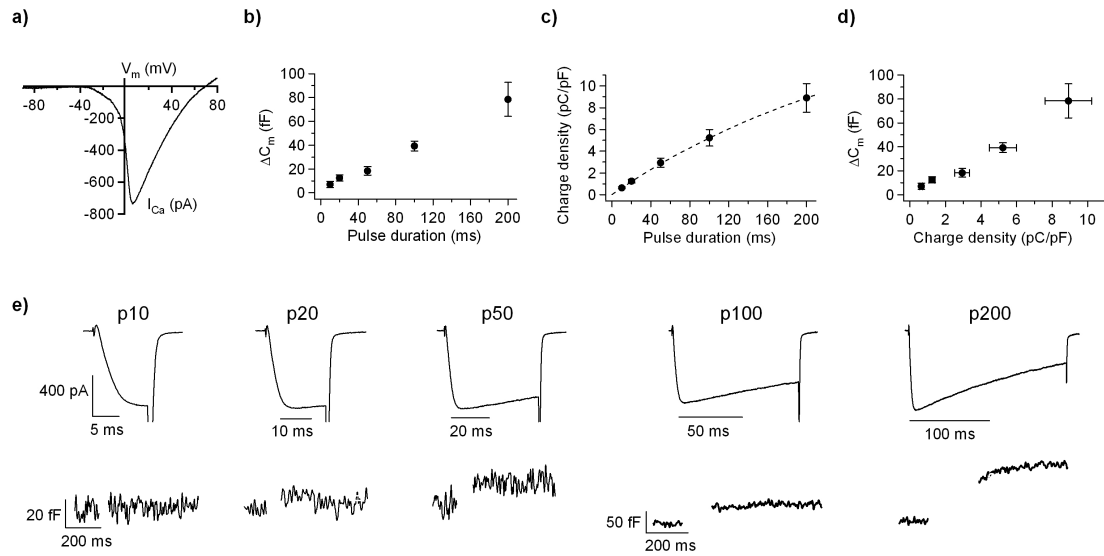


Figure 5.2: Experimental measurements of secretion and Ca^{2+} currents in response to depolarization pulses, in human chromaffin cells. (a) Current-to-voltage relationship of the calcium current (I_{Ca}). (b) Capacitance increments and (c) charge density, as functions of pulse duration. (d) Capacitance increments plotted against the evoked charge density. (e) Calcium currents and capacitance increments for pulses between 10 and 200 ms. Recorded, and kindly shared, by the research group of Dra. Almudena Albillos from the Faculty of Medicine, Universidad Aut3noma de Madrid, Spain.

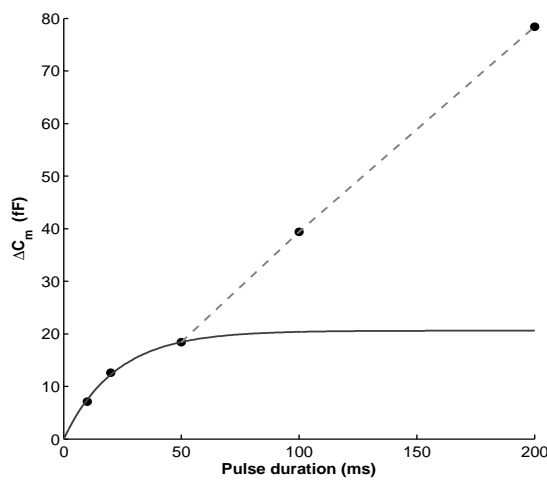


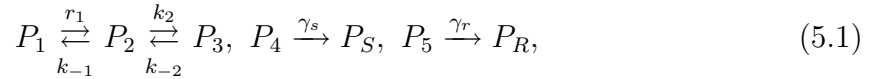
Figure 5.3: Relationship between cell secretion and pulse duration. Two exocytotic components are observed: an exponential component for pulses up to 50 ms that reaches a plateau of ~ 20.6 fF, and an increasing secretion for longer pulses.

species features by comparing results to similar studies carried out in mouse [190] and bovine [98, 115] chromaffin cells.

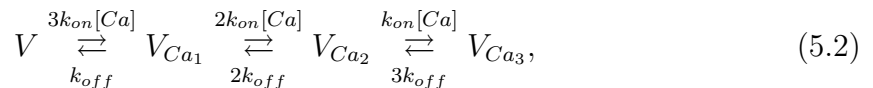
5.3 Modeling

To initiate the study of exocytotic dynamics in human chromaffin cells, we looked for a model able to reproduce the experimental capacitance increments measured for different depolarization pulses. We firstly observed that exocytotic responses in human chromaffin cells are larger than those reported for other species, although the rate of capacitance increments is slower than those recorded in rat [87], bovine [68], and mouse chromaffin cells [126]. However, secretion occurs in the same timescale, that is, from milliseconds up to seconds [130]. Therefore, our first modeling approximation was based on the coupling of the Shell model (described in Section 1.2.3), and a secretion model similar to those proposed for other chromaffin cells [160, 98, 189]. Our aims were to find the main differences between secretion in humans and other species, and to analyze particular parameter values and spatiotemporal features that explain the experimental data.

Experiments provide whole-cell Ca^{2+} currents and capacitance measurements in response to depolarizing pulses of 10 to 200 *ms*. Each cell exhibits different secretion and current dynamics, and each one has its own cell size and vesicle population. Then, in order to propose a secretion model able to reproduce our experimental recordings and to explore exocytotic dynamics, we averaged and normalized cell sizes and capacitance increments. The "average cell" was related to the "average capacitance increment" for all depolarizing pulses, as shown in Table 5.1. Plotting the experimental secretion versus pulse duration (Figure 5.3), we find two exocytotic components: an exponential component for pulses up to 50 ms that reaches a plateau of ~ 20.6 fF, and a linearly increasing secretion for longer pulses. We assumed that the first component is due to the depletion of a small rapidly releasable pool (RRP), and that the second component represents the participation of a slowly releasable pool (SRP) replenished by a depot pool along time, as proposed for mouse chromaffin cells [190, 189]. This analysis was implemented in the kinetic model of Figure 5.4, and it can be translated into the following kinetic scheme:



where pools P_4 and P_5 , which are the number of slowly and rapidly fused vesicles over time, respectively, are calculated considering 3 Ca^{2+} -binding sites for the vesicle sensor, that is:



where V represents a vesicle with an empty sensor, and V_{Ca_i} are the states of the vesicle with i calcium ions. The transitions between states are managed by rates k_{on} and k_{off} that are the binding and the unbinding rates, respectively, as well as the local Ca^{2+} concentration ($[Ca]$).

Table 5.1: Average data from experiments in human chromaffin cells

PARAMETER	VALUES
Cell size	8.86 pF , 8.39 μm (radius)
<i>Pulse duration</i>	<i>Secretion (fF)</i>
200ms pulse	78.4
100ms pulse	39.4
50ms pulse	18.38
20ms pulse	12.6
10ms pulse	7.1

Based on this three-pool kinetic scheme, we analyzed the exocytotic dynamics. Notice that there are two ready-releasable pools that have distinct kinetic properties to become fused. Transitions from the Docked to the SRP (r_1) and from the SRP and RRP to fusion k_{ons}, k_{onr} , are Ca^{2+} dependent processes, but going from the SRP to the RRP pool and viceversa k_2, k_{-2} , do not have Ca^{2+} dependence. In our implementation, we consider that resupply rate r_1 is constant (as discussed further), whereas Ca^{2+} binding rates k_{ons}, k_{onr} are functions of local calcium. This fact is a clue factor that allows us to introduce the influence of spatial localization of vesicles on secretion rates. Based on this view, we are assuming that releasable pools are triggered by the local $[Ca^{2+}]_i$ estimated by the models.

Increasing pulse duration commonly induce capacitance increments that seem to reach a plateau for short pulses. In other species, this behaviour has been related to fast secretion due to a small pool of releasable vesicles, named the Immediately Releasable Pool (IRP), who are tightly coupled to Ca^{2+} channels [3]. Therefore, and as done in other works [115, 190], we consider that the IRP size would correspond to the asymptotic value of the best-fitted exponential function of the form $f(t) = A(1 - e^{-Bt})$ for secretion evoked by short pulses (Figure 5.3). In our case, this maximum is $20.6 \pm 13 fF$ which represents $\sim 25\%$ of the exocytotic response evoked by the 200-ms pulse (see Table 5.1). To be consistent with the secretory model, and assuming that the IRP vesicles form part of the rapidly releasable pool, we will call RRP instead of IRP for modeling purposes.

After fitting the rapid pool size, we tried to theoretically infer if all releasable vesicles participating in the experimental secretory response are equally competent for fusion; i.e., if releasable vesicle pools only differ in their proximity to Ca^{2+} channels, but not in their kinetics. In other species this topic has been addressed experimentally by using flash photolysis experiments [189], but this information is not yet available in human cells. Simulations obtained on this basis indicate that if all vesicles followed the rapid pathway, they would have to be triggered by very low Ca^{2+} levels, similar to average cytoplasmic concentrations, to produce the second exocytotic component. This finding could have different interpretations: a) the second pool of vesicles is located “far away” from the cell membrane (about 800 nm from Ca^{2+} channels); b) there are cell features that act as physical barriers for diffusion of Ca^{2+} influx, so the calcium signal

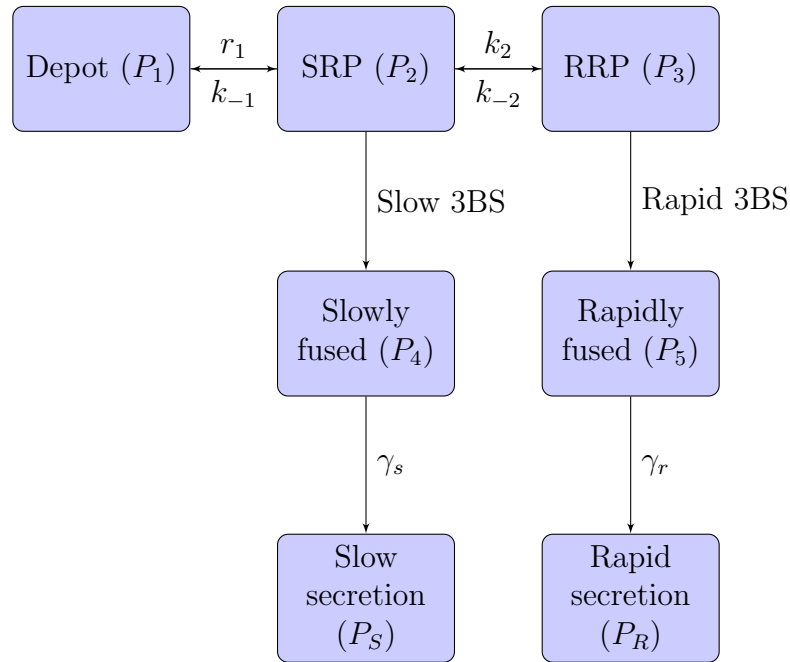


Figure 5.4: Depiction of the secretion model originally proposed for mouse chromaffin cells [189].

around these vesicles is significantly weakened; c) these vesicles are kinetically different from rapid vesicles. Possibility a) was excluded because it seems difficult to accept that releasable vesicles in human cells are located so far away from the cell membrane, when common distances in other species are about 300 nm [97]. Moreover, due to the fact that there are no available data about cellular spatial characteristics in human cells (as, for example in bovine, see Chapter 4), we take interpretation c) as modeling hypothesis, although other possibilities cannot be excluded.

5.3.1 Intermediate secretion

Using the experimental Ca^{2+} current evoked by each pulse as the input to the Shell model, we simulate how Ca^{2+} influx is distributed in the cytoplasm taking into account buffered diffusion and calcium extrusion. Parameter values used with the Shell model, in order to simulate $[Ca^{2+}]_i$ dynamics in human chromaffin cells, are detailed in Table 5.3. Extrusion pump and endogenous buffer equations and parameters are based on a previous model for chromaffin cells [98]. We added a leak flux to maintain basal $[Ca^{2+}]_i$ at the steady-state. Two dynamic $[Ca^{2+}]_i$ values are estimated by the model: $[Ca^{2+}]_i$ at the sub-membrane region, i.e., the first layer in the Shell model (0-100nm), and $[Ca^{2+}]_i$ at the third layer (200-300nm). These Ca^{2+} dynamic values are used to study pools dynamics, considering that rapid vesicles are triggered by sub-membrane $[Ca^{2+}]_i$ whereas slow vesicles are triggered by third-layer $[Ca^{2+}]_i$. This separation comes from the discussion above.

Figure 5.5 shows an example of a dynamic simulation obtained with the Shell model coupled to the secretion model: the experimental Ca^{2+} current (top panel) is used as the input; then, the model estimates dynamic Ca^{2+} concentrations at several distances

from the cell membrane (middle panel), as well as the corresponding secretion (bottom panel). Parameter values used with the secretion model, are given in Table 5.2. These models adequately estimate secretion for pulses between 50 and 200 ms, but they underestimate fast secretion evoked by short pulses. Decreasing shell thickness to 50 nm or 25 nm does not improve results, indicating that vesicle fusion and release are controlled by a non-homogeneous Ca^{2+} signal. This problem was also reported in bovine chromaffin cells [115], where it was related to a non-uniform Ca^{2+} distribution and to a co-localization of channels and vesicles, both influencing the fast secretion component. Thus, fast secretion was studied with the Active-zone stochastic model, as described following.

5.3.2 Fast secretion

We analyze the spatiotemporal features modulating fast secretion with the Active-zone model. In order to achieve this microscopic study of the rapid pool, including Ca^{2+} channels and rapid releasable vesicles, the Active-zone model is solved by Monte Carlo methods to accurately evaluate local $[Ca^{2+}]_i$ and secretion. However, this solution method imposes computational restrictions (discussed in Section 1.3.1), so we chose the 50-ms pulse as the point of convergence for results coming from both, the Shell model and the Active-zone model. The spatial relationship between both models is shown in Figure 5.7.

The relevance of local spatial factors in rapid secretion was firstly studied by testing different vesicle-channel arrangements in the active zone. The involved geometrical parameters are the calcium-channel density (ρ), and the relative distribution of vesicles and channels. In regard of the former, we assume a similar topography of calcium channels as in other species [51] (5 to 15 channels per μm^2), and then test the associated secretory responses. In the same way as with the Shell model we use the experimental whole-cell current as the input to the model, thus, the algorithm calculated the unitary current per channel for each density. Notice that a low channel density means that there is some degree of channel clustering. This condition leads to pronounced Ca^{2+} gradients in the vicinity of the clusters, as shown in Figure 5.8. The $[Ca^{2+}]_i$ maps of this figure emphasize that the presence of channel clusters induces heterogeneous spatial distribution of $[Ca^{2+}]_i$, even though the number of channels and the total current is the same in both cases. These irregular spatial $[Ca^{2+}]_i$ distributions trigger very different secretion dynamics since some vesicles would experience low calcium levels, while others not. We have tested different levels of co-localization between channels and vesicles, and concluded that a good agreement between theoretical and experimental data for fast secretion is found if 75% of rapidly releasable vesicles are fully correlated to calcium channels. This configuration accurately reproduces secretion for the 50-ms pulse, and matches well with Shell-model results as shown in Figure 5.9.

5.4 Results

Figure 5.6 shows the results obtained for fast and intermediate secretion, using the Shell and the Active-zone model, respectively. The experimental secretion is also shown to emphasize the reliability of the models to reproduce experimental results. Notice that

Table 5.2: Parameter values of the secretion model for human chromaffin cells.

Parameter	Value	Reference
POOLS SIZE		
Depot	4000 vesicles	[190]
<i>IRP</i>	~14 vesicles (30 fF)	See text
KINETIC CONSTANTS		
Resupply rate	$r_1=0.25s^{-1}$	Fitted
Reversal resupply rate	$k_{-1}=0.05s^{-1}$	
Transitions SRP-RRP-SRP	$k_2 = k_{-2}=0.1s^{-1}$	
SRP fusion rate	$\gamma_s=20s^{-1}$	
RRP fusion rate	$\gamma_r=1450s^{-1}$	
Number of binding sites	$N=3$	
Slow Ca^{2+} binding rate	$k_{ons}=0.5\mu M^{-1}s^{-1}$	
Rapid Ca^{2+} binding rate	$k_{onr}=4.4\mu M^{-1}s^{-1}$	
Slow Ca^{2+} unbinding rate	$k_{off_s}=4s^{-1}$	
Rapid Ca^{2+} unbinding rate	$k_{off_r}=56s^{-1}$	

for pulses lasting 10, 20 and 50 *ms*, the secretion values are 7.1 *fF*, 12.6 *fF* and 18.38 *fF*, respectively (Table 5.1), which means that the secretory response for the 20-*ms* and 10-*ms* pulses are 68.5% and 38.6% of the secretion for the 50-*ms* pulse. Stochastic simulations show that a spatial resolution (Δx) of 100 nm gives theoretical values below the experimental ones, especially for the 10-*ms* pulse, although in better than deterministic predictions. Superior results for short pulses are obtained by reducing the spatial resolution of the Active-zone model to 25 nm; in this case, secretion percentages are 69% for the 20-*ms* pulse and 38% for the 10-*ms* pulse. It is well worth noting that the need for increasing the spatial resolution means that vesicle calcium sensors are very sensitive to local calcium quantities, which becomes crucial as calcium influx gets smaller. Another interesting finding is that local calcium elevations, corresponding to a correlated arrangement of channels and vesicles, are enough for reproducing the experimental secretion for short pulses, and there is no evidence that other cellular features could be incrementing the Ca^{2+} signal, such as calcium barriers found in mouse cells [160], or such as cytoskeleton cages in bovine cells [187].

5.4.1 Multiscale aspects

Experimental data on Ca^{2+} currents and capacitance increments used in the present study come from five human chromaffin cells, using the technique described in Section 5.2. From the individual data, we calculated the average values presented in Table 5.1, and formulate two models that adequately predict secretion for short and prolonged stimulation, that is, for fast and slow secretion. Therefore, it is interesting to discuss the apparent stochastic and deterministic behaviour exhibited by secretion in these cells, which may involve multiscale aspects. This study is consistent since we have

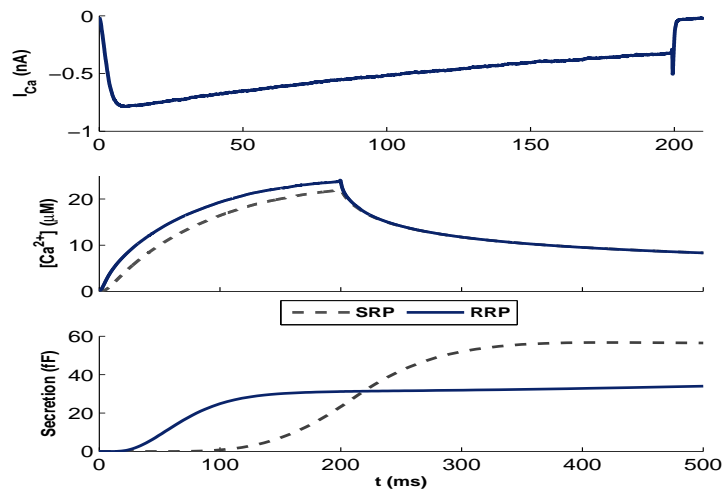


Figure 5.5: Example of a dynamic simulation performed by the Shell model coupled to the secretion model. The simulation corresponds to the average-cell response evoked by the 200-ms pulse. (Top) Experimental Ca^{2+} current used as input to the model. (Middle) Simulated $[Ca^{2+}]_i$ concentration at the first and third layers, as well as cytoplasmic concentration. (Bottom) Simulated secretion: rapid, slow, and total. Total secretion matches the experimental measurement.

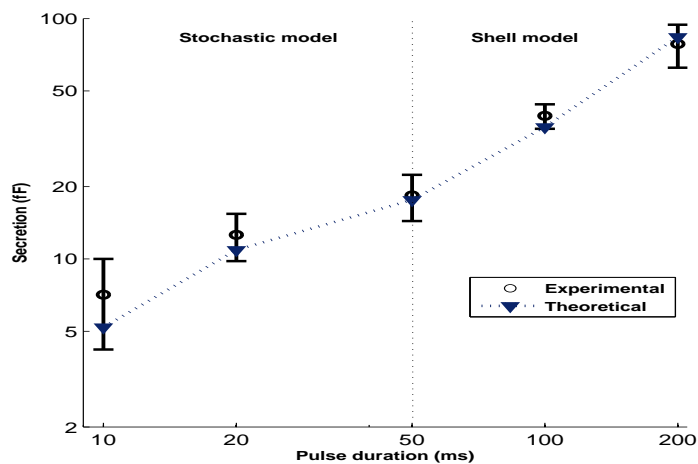


Figure 5.6: Secretion predicted by our models for the average cell, and for pulses between 10 and 2000 ms. Theoretical values are compared to experimental measures (circles), in logarithmic scale, to emphasize that best predictions of our Shell-secretion model are given for pulses above 50 ms (squares). The final model (triangles) complements theoretical predictions, for pulses below 50 ms, with results coming from the Active-zone model.

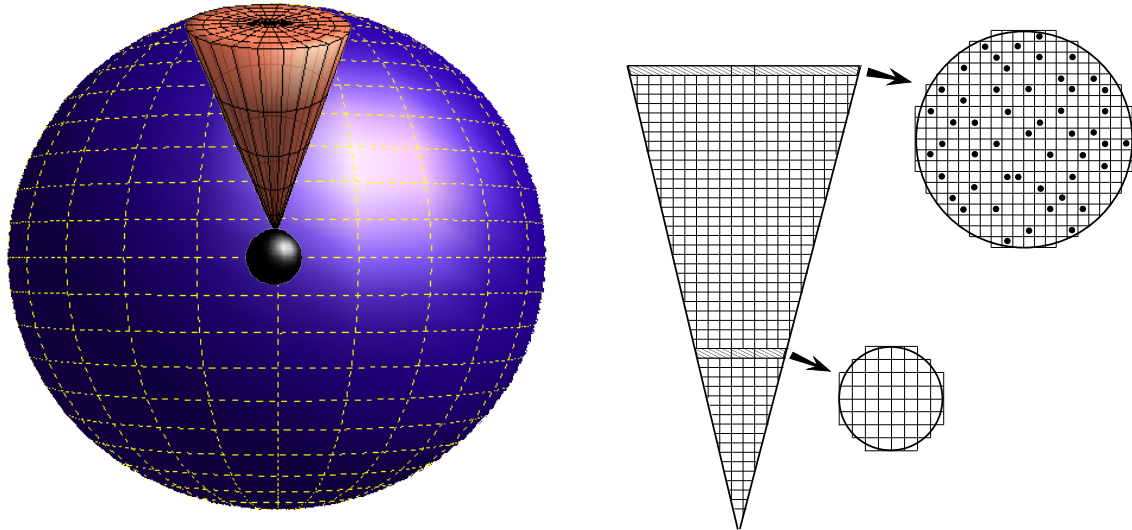


Figure 5.7: Spatial relationship between the Shell (S) and the Active-zone (AZ) model in human chromaffin cells. (Left) The S model is an homogeneous sphere representing the whole chromaffin cell, which has about 225 active zones. The AZ model is a 3-D cone representing a minimal cell patch where exocytosis takes place (active zone). (Right) 2-D schematic representation of the AZ model. The 3-D cone is divided in cubic compartments with side length of $\Delta x = 100nm$. On top of the domain, i.e., the first slice, Ca^{2+} channels and vesicles (dots) are located.

found that secretion evoked by short pulses cannot be predicted assuming the same spatial considerations than we have taken to predict secretion evoked by longer pulses, i.e., homogeneity. Different behaviour becomes evident for those time scales where the Shell-secretion model was unable to reproduce the experimental release, but secretion can be accurately predicted by the Active-zone model. Thus, for short pulses, it was necessary to build a non-uniform vesicle distribution, and to assume some degree of Ca^{2+} channel clustering, to be able to reproduce experimental secretion. However, a uniform distribution of channels and vesicles, as implicitly defined in the Shell-secretion model, was enough to explain secretion for longer pulses.

Figure 5.9 shows a comparison of the dynamic secretion (in percentage of released vesicles) simulated with the stochastic (lines) and the deterministic (dashed lines) models, for the 20-ms pulse and for five different cells (simulation time equal to 100 ms). As we can see, for the total simulation time (100 ms), both methods give very similar results; the largest error is seen for one cell, whose secretion is slightly overestimated by the deterministic model. However, it is well worth noting that for smaller times, secretion predicted by both models may have relevant differences since they are based

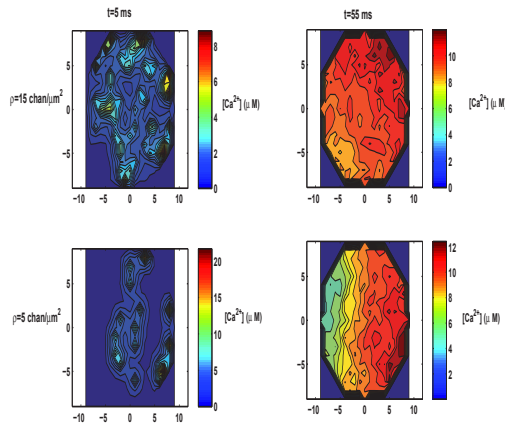


Figure 5.8: Maps of spatial $[Ca^{2+}]_i$ distribution at two time points, $t = 5\text{ ms}$ (left panels) and $t = 55\text{ ms}$ (right panels). Ca^{2+} influx was induced by the 50-ms pulse. Notice differences in concentration (color) scales. First row of maps was simulated with high channel density ($\rho = 15$), and second row, with low channel density ($\rho = 5$).

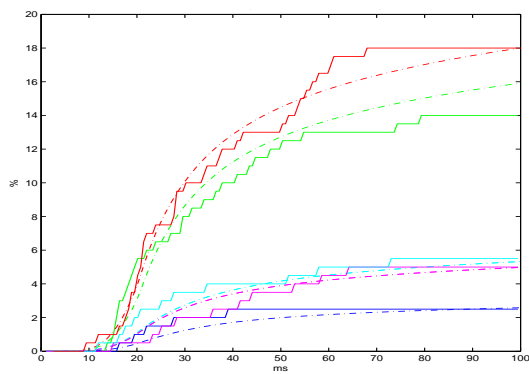


Figure 5.9: Comparison of accumulated secretion predicted by the stochastic (continuous lines) and the deterministic (dashed lines) models for human chromaffin cells. Secretion values are calculated as the percentage of released vesicles over the total RRP. Secretion was evoked with a 20-ms pulse, for 100-ms simulation time.

Table 5.3: Parameter values used to simulate $[Ca^{2+}]_i$ dynamics, in human chromaffin cells, using the Shell (S) and the Active-zone (AZ) model

Parameter	S value	AZ value	Reference
INPUT DATA			
Cell radius (μm)	8.39	–	From Table 5.1
Shell thickness (nm)	100	–	According to Δx
Ca^{2+} concentration (μM)	0.1	0.1	Experiments
Domain type	–	Conical	AZ of a spherical cell
Cone-base radius (μm)	–	1	[70]
Height (μm)	–	8.39	Average cell radius
Channel density (per μm^2)	–	5 or 15	[51]
Channel distribution	–	Random	
SPATIO TEMPORAL DATA			Chosen
Spatial resolution (nm), Δx	100	100 and 25	
Temporal resolution (μs), Δt	11	11 and 0.71	
Simulation time (ms)	500	≤ 100	Experiments
ENDOGENOUS BUFFER			[98]
Concentration (μM)	500	idem	
Forward binding rate ($M^{-1}s^{-1}$)	$5 \cdot 10^8$	idem	
Dissociation constant (μM)	10	idem	
CALCIUM-EXTRUSION PUMP			
Maximal speed ($pmolcm^{-2}s^{-1}$)	5	–	Fitted
Half-maximal constant (μM)	0.83	–	[153]
LEAK FLUX			
Rate (μMs^{-1})	0.054	–	Fitted

on discrete and continuous approximations to secretory events, which may not coincide for very few events. Then, the stochastic model allows us to look into fast releasing events occurring in the first milliseconds, and triggered by local $[Ca^{2+}]_i$ that increases as Ca^{2+} channels open. With the deterministic model, we lost these events since it assumes homogeneity. Complementing both model predictions enables us to adequately reproduce experimental responses, and to analyze the particular characteristics of the subcellular mechanisms involved in exocytotic dynamics of human chromaffin cells.

5.5 Discussion

Experimental measurements of the exocytotic dynamics in human chromaffin cells using the perforated-patch configuration of the patch-clamp technique, and theoretical predictions of both, the Active-zone and the Shell model, were done. Cell capacitance increments evoked by depolarizing pulses of different durations, as well as

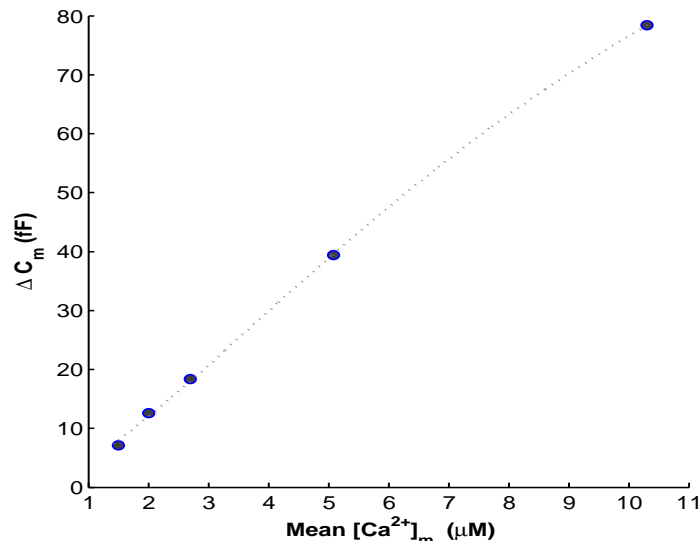


Figure 5.10: Capacitance increments as a function of mean membrane Ca^{2+} . Mean membrane Ca^{2+} is the average calcium concentration in the first 100 nm below the membrane during the whole simulation time. Data was fitted with a Hill equation ($n=1.49$, $K_D=10.9\mu M$).

Ca^{2+} currents, were the experimental data for the modeling study. Our results point out that secretion in human chromaffin cells could be predicted by a secretion model constituted by three pools: one depot, one slowly releasable (SRP) and one rapidly releasable (RRP). Rates connecting the pools and affinities for fusion, seem to be the same to those proposed for mice [189] although some important differences appeared: the resupply speed was smaller than those found in mice [189], and the estimated size and spatial characteristics of the rapidly releasable pool are in closer agreement to an immediately releasable pool, as defined in [3].

Based on average experimental values for cell size and secretion, we were able to simulate the $[Ca^{2+}]_i$ dynamics during and after the depolarizing pulse, up to 500 ms. Most simulations were obtained with the Shell model, which estimates cytoplasmic and local Ca^{2+} at different radial distances from the membrane (multiples of 100 nm), assuming homogeneity and uniform distribution of channels and vesicles. Based on calcium dynamic concentrations, the secretion model define the dynamics of vesicle pools for intermediate pulses (50-200 ms). Our simulations of $[Ca^{2+}]_i$ dynamics support that calcium gradients in human chromaffin cells do not have important participation of Ca^{2+} depleting nor Ca^{2+} -releasing mechanisms in the first 500 ms, as found for bovine chromaffin cells [116]. In regard of secretion, the Shell model was able to accurately predict capacitance increments for intermediate pulses, but not for short pulses below 50 ms. Therefore, the study was complemented with the Active-zone model to reveal the spatial features associated with fast secretion.

The secretion model was formed by three pools, but only two kinetic pathways for secretion, the rapid and the slow. The rapid pathway would be followed by those

vesicles tightly docked to the membrane, which would be the main responsible for the secretion evoked by short pulses. In contrast, the slow pathway would be responsible for the slower exocytotic component. Since flash photolysis experiments have not yet been performed in human chromaffin cells, we cannot exclude the contribution of vesicles kinetically equivalent to those forming the rapid pool but in an early maturation state. For both kinetic pathways, we are assuming low Ca^{2+} affinity for vesicle fusion, as proposed for other chromaffin cells [98, 189]. This assumption was based on the finding that our secretion data exhibit a dependence on sub-membrane Ca^{2+} levels that can be fitted with a low-affinity Hill function (see Figure 5.10). We noticed that the value for K_D does not change considerably if shell thickness is reduced to 50 or 25 nm, or if we take either the theoretical or experimental secretion values. Then, it seems that exocytosis in human chromaffin cells is mainly managed by a low-affinity Ca^{2+} sensor, for pulses up to 200 ms, as considered for other species [98, 189].

Pool contribution to secretion was also analyzed on the basis of model predictions (Figure 5.11). We found that for the shortest pulses (10 and 20 ms), the pool of rapid vesicles completely manages fast secretion, so local effects play a key role. As pulse duration is incremented, the rapid pool is becoming depleted and slow vesicles participate more substantially on the secretory response. Our data indicates an immediately releasable pool of 20.613 fF which follows the rapid kinetic pathway; this pool size is in good agreement with pools estimated in bovine and rat [3]. Moreover, our simulations indicate a close proximity of this pool of vesicles to Ca^{2+} channels, suggesting that human chromaffin cells have a tight control of releasable vesicles following a rapid kinetic pathway. Indeed, the best fitting for short pulses was obtained when 75% of the rapid vesicles are co-localized to the calcium channels, at a maximum distance of 25 nm. On the other hand, the resupply does not have a relevant participation for pulses below 100 ms.

Modeling the whole-cell calcium and secretion dynamics, complemented with the microscopic study of a releasing area, allowed us to unveil the multiscale features that manage exocytosis in human chromaffin cells. Assuming homogeneity and uniform distribution of the main subcellular mechanisms, i.e., Ca^{2+} channels and vesicles, we find that the Shell model can predict the exocytotic response for an intermediate timescale (hundreds of milliseconds), but it underestimates the short timescale (tens of milliseconds) response. The spatiotemporal features responsible for this discrepancy were determined by the Active-zone model: there is some degree of Ca^{2+} channel clustering, and there is a small pool of vesicles in close proximity to channels which controls fast secretion.

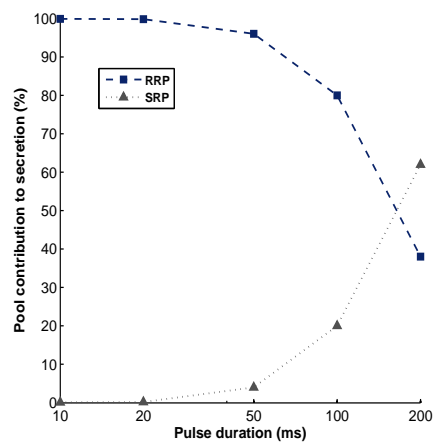


Figure 5.11: Contribution of the Slowly (SRP) and Rapidly (RRP) releasable pools to secretion evoked by depolarizing pulses.

Alpha cells: Studying slow secretion

6.1 Introduction

Pancreas, an organ of vertebrates that performs vital endocrine and exocrine functions, releases *glucagon*, *insulin* and somatostatin hormones through its exocytotic cells α , β and δ , respectively. These cells are grouped in areas called Islets of Langerhans, which constitute about 2% of the whole pancreas (1 million of islets per human adult pancreas). Glucagon secreted by the alpha cells of the pancreas induce mobilization of hepatic glucose; this capability avoids that the organism reaches a hypoglycemic state during long periods of glucose demand. Insulin, on the other hand, participates in nutrient metabolism, particularly carbohydrate metabolism, resulting in a reduction of glucose levels. The impaired secretion of glucagon hormone is related to type 2 Diabetes which is also combined with a deficient insulin secretion [141]. Alpha cells constitute 15-20% of total islet cells. They are commonly found in the periphery of the islets, especially in rodent, and are small-sized compared to beta cells. These characteristics impose a severe restriction to make experiments on glucose-induced glucagon secretion by α -cells, mainly in its isolated form [80]. Thus, research works are developed in intact

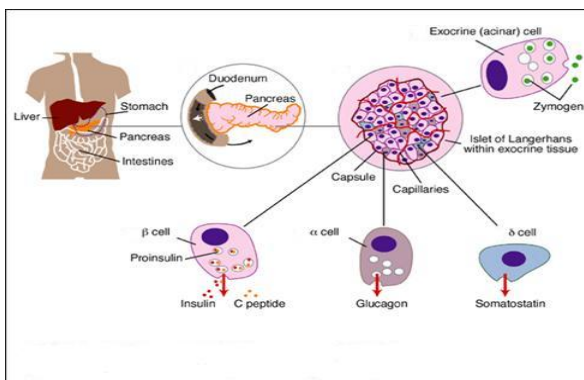


Figure 6.1: Location of pancreas within the human body, that performs vital endocrine and exocrine functions. Pancreas is made of Islets of Langerhans, which release hormones like glucagon, insulin and somatostatin through its exocytotic cells α , β and δ , respectively.

islets [83, 140], in isolated cells [143], or both [114, 142], or in cell lines [18].

From a physiological point of view, electrical activity exhibited by α -cells appears when they are exposed to low glucose levels (below the physiological concentration, i.e., 4 to 5 mM). In this situation, they generate action potentials simultaneously to glucagon secretion, in a similar manner to beta cells. This electrical activity is supposed to be triggered by a low ATP/ADP ratio, because of the absence of glucose [149]. In these conditions, the K_{ATP} channels found in the cell membrane are open, allowing K^+ to go out; these ions produce an ionic current that depolarizes the cell, so action potentials are generated. This electrical activity is possible thanks, on the one hand, to the Ca^{2+} and Na^+ channels that fire the depolarization stage, and on the other hand, to the K^+ channels that repolarize the cell [80, 141]. α -cell exocytosis in response to electrical stimulation has been well characterized through experiments where the secretory response is inferred from the associated increments in cell membrane capacitance due to granule fusion [9, 83, 75, 79, 111]. In these experimental works, the common protocol is to stimulate the cell with controlled depolarizing pulses from a fixed cell membrane potential, and then to measure the produced ionic currents and capacitance increments. Notice that data about Ca^{2+} currents involved in glucagon secretion and coming from the above-mentioned experiments cover a short timescale, namely, below one second. However, in physiological conditions, glucagon secretion could be maintained for minutes and hours to avoid hypoglycemia. Therefore, secretion evoked by depolarization reflects those control pathways mainly involved in the fast phase of glucagon secretion, which may not coincide with those triggered by glucose-induced secretion, which acts in a more physiological manner, and for a longer time scale. Unfortunately, works that induce glucagon secretion by low-glucose media, and that simultaneously record $[Ca^{2+}]_i$ dynamics for long timescales are scarce [114, 143, 185].

Experimentally, measurements of glucagon secretion are commonly obtained by incubating pancreatic islets in media with low glucose concentrations for several minutes. Under low-glucose levels (stimulated), the total amount of secreted glucagon in mice ranges from 30 to 60 picograms per islet (pg/islet) in one hour, and this amount is approximately twice the basal (non-stimulated) secretion that is seen at the high glucose concentrations typically used in these experiments [83, 111, 154, 182]. These quantities are inferred from measurements of the accumulated glucagon for a one hour period from a large number of islets, each mouse islet containing on average, 400 ± 200 α -cells [141]. Such an stimulated glucagon secretion could be produced by a constant rate of 0.5 to 1 pg/islet (or fF) per minute, as reported in one experimental work [83].

Glucagon secretion in alpha cells has been related to cytoplasmic calcium increases, although there is no clear idea about how it works to activate exocytosis. An elevation of Ca^{2+} , the messenger, is brought about by a low level of glucose in the extracellular medium and often appear in the form of sustained oscillations [140]. The signal transduction pathway leading to calcium increase appears to be rather complex, involving both voltage-gated channels and store-operated calcium entry [103]. Opposite to what happens in β -cells, that all of them undergo synchronized calcium oscillations upon stimulation with high glucose levels [140], only 30 to 50% of the total islet α -cells exhibit oscillations when exposed to low-glucose levels [114, 143]. These oscillations are asynchronous and highly irregular. Oscillation frequency can go from 0.1 to 0.7 per minute at 3mM glucose [16, 18, 140], up to 0.5 to 1 per minute at 0.5mM glucose [183].

The amplitude of these oscillations runs from basal Ca^{2+} levels (near 100 nM) up to two to five times this value [16, 44, 143]. Spontaneous Ca^{2+} oscillations are observed under low-glucose conditions in islets [140], in isolated alpha cells [143], and also in cell lines such as InR1-G9 glucagonoma cells [18] or α TC1-9 cells [183]. Nevertheless, oscillatory electrical activity and its implication in glucagon exocytosis remains to be documented. Moreover, a recent study shows that glucose inhibition of secretion may be associated with a depression of granule trafficking or a mechanism of the exocytotic machinery, and not to a $[Ca^{2+}]_i$ reduction [114].

One of the clue open questions about alpha cells is how glucose controls glucagon release. Elevations in extracellular glucose (up to 7 mM) seem to inhibit glucagon secretion; above 7mM, where inhibition reaches a maximum, glucose seems to stimulate glucagon release [154]. Moreover, α -cells, which are excitable cells, are not only sensitive to glucose but to other neural and hormonal factors, as well as to nearby cells (*paracrine* signaling) [80]. Indeed, insulin and/or zinc (cosecreted with insulin) appear to determine glucagon secretion in islets through a paracrine pathway [90]. In summary, there is no agreement about which are the main regulating factors involved in glucagon secretion, and if they are intrinsic to the cell [185] or external (as reviewed in [80]). Thus, and despite their physiological significance, the mechanisms that regulate α -cell exocytosis are still poorly understood. Besides the scientific interest of elucidating the molecular bases of the functional dynamics of glucagon release, this area of research represents an important therapeutic challenge since abnormalities in glucagon secretion are part of metabolic pathologies associated with type 2 Diabetes [141].

For the present thesis, we have accomplished a modeling study in α -cells, by dividing our work in two main tasks: one that developed minimal models for those ionic channels involved in glucagon secretion, and a second one that proposes a glucagon secretion model based on glucose-induced Ca^{2+} oscillations. Although these two activities are completely linked in the real α -cell, the mechanisms involved and the regulating pathways that allow this connection are still poorly understood. Moreover, there are few experimental data about Ca^{2+} dynamics recorded simultaneously to exocytosis, and few about secretion dynamics for a long timescale. Thus, although our modeling work was done separately, we are still in collaboration with the experimental research group, looking for new evidence that help unveiling regulation pathways of glucagon exocytosis.

6.2 Experimental data

Experimental data on glucose-induced Ca^{2+} oscillations and secretion were recorded by the collaborating group ¹ with the following protocol: Mouse intact islets of Langerhans are first exposed to low-glucose media (0.5 mM glucose, or 0.5G) at normal temperature for one hour, and then secretion is stopped by refrigerating the preparation. Glucagon is then quantified through RIA and then reported as the accumulated glucagon secreted per islet, depending on the quantity of islets in the preparation (pg/islet/hour). Figure 6.2 shows some alpha cells identified by immunofluorescence of glucagon hormone;

¹Research group led by Dr. Iván Quesada, at the Institute of Bioengineering, Universidad Miguel Hernández, Elche, Spain.

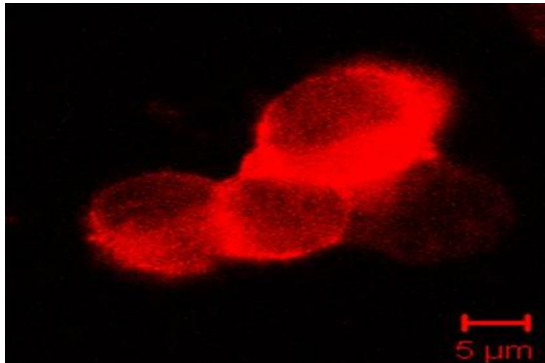


Figure 6.2: Immunofluorescence image of a mouse α -cell identified by labeling glucagon hormone in red. Image obtained, and kindly shared, by the research group of Dr. Iván Quesada from the Inst. Bioengineering, Universidad Miguel Hernández, Spain.

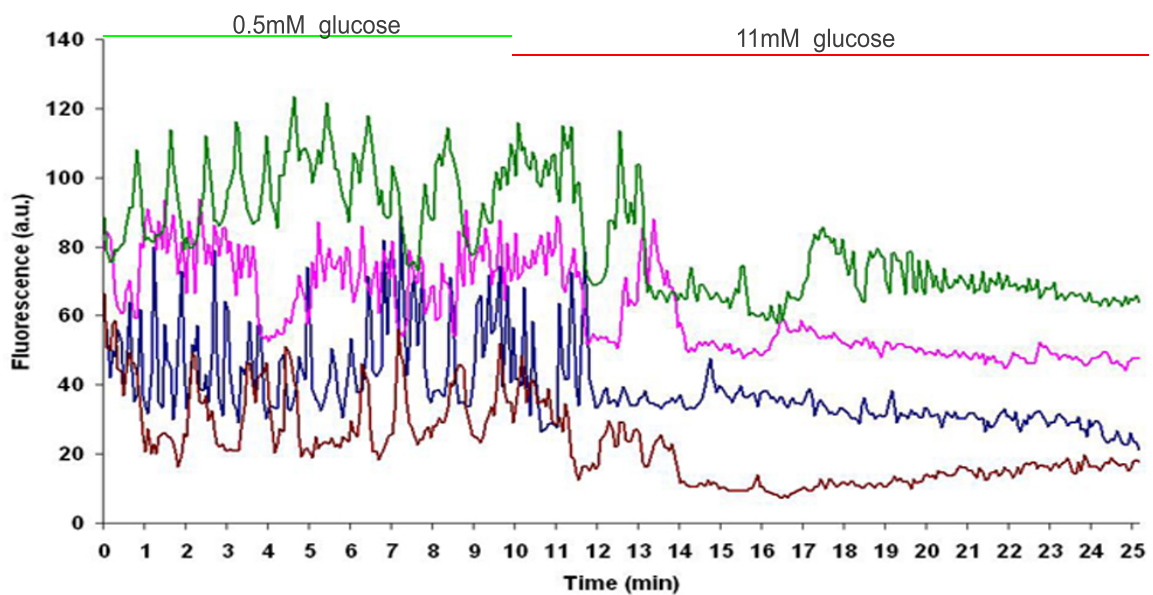


Figure 6.3: Some experimental Ca^{2+} oscillations recorded following the protocol described in Section 6.2: Islets are perfused with a solution containing 0.5 mM glucose for the first 10 minutes, and then, solution is changed to one containing 11 mM glucose for the following 15 minutes. Oscillations, triggered by low and high glucose concentrations, are highly irregular. The level of Ca^{2+} is indicated in arbitrary fluorescence units. Data kindly shared by the research group of Dr. Iván Quesada from the Inst. Bioengineering, Universidad Miguel Hernández, Spain.

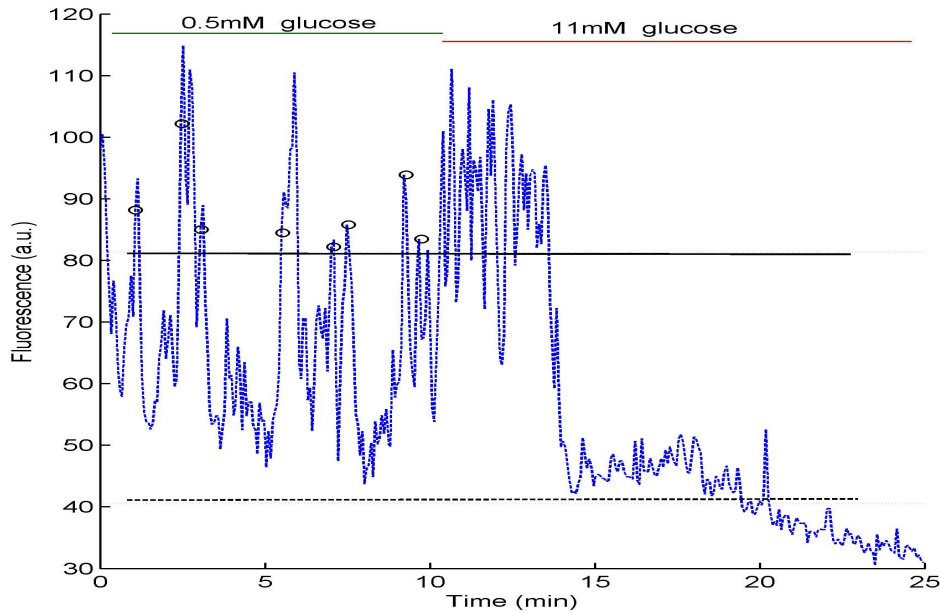


Figure 6.4: How the oscillation frequency in the first 10 min (low-glucose period) is computed: The threshold (continuous line) is taken as twice the mean basal level at high glucose, between minute 15 to 25 (dashed line). Peaks that overpass this threshold with positive slope (dots) are counted if they are separated by at least half a minute, in the stimulated period at 0.5mM glucose.

they are almost spherical, about $5\mu\text{m}$ of radius. For islets in low-glucose media and 2.5mM external Ca^{2+} , alpha-cell calcium oscillations are detected and recorded through confocal fluorescent microscopy. Oscillations appear spontaneously in these conditions, and are used to detect alpha cells in the islet, which are usually found in the peripheria. Oscillations evoked by alpha cells in perfused islets are recorded for 25 minutes, 10 minutes under a 0.5G solution, and 15 minutes under a 11G solution. Sampling rate is one data per 2 seconds, using FLUO4 marker that gives normalized variations in luminiscence (arbitrary units). Following these methods, a set of 14 calcium oscillation records lasting 25 minutes were obtained. Each record corresponds to a single alpha cell found in the fist layer of the islet. In figure 6.3 four Ca^{2+} oscillations are shown. Notice that the first five minutes at 11G (minute 10 to minute 15) seem to be a transition period in which glucose levels are changing in the bath, so they are not taken as valid data for the modeling work.

6.3 Modeling glucagon secretion based on calcium oscillations

6.3.1 Frequency of oscillations

First, we measure the oscillation frequency since it has been observed in experiments that, under high-glucose media, oscillations tend to be less frequent than under low-glucose media [140]. Our experimental method to measure frequency is to consider an

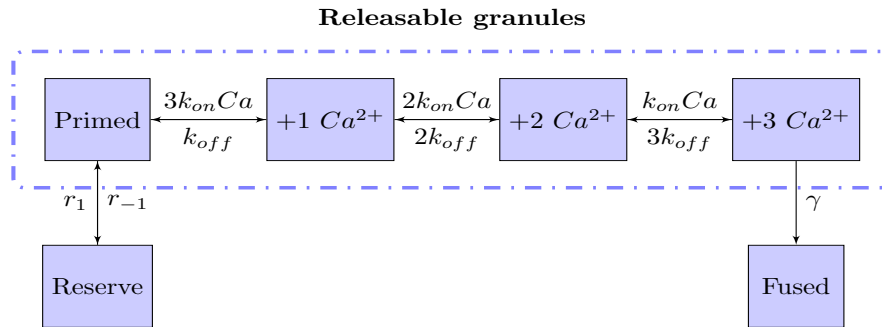


Figure 6.5: Stages proposed for glucagon secretion. Granules coming from the Reserve pool resupply the Primed pool and then, upon binding 3 Ca^{2+} ions, granules become Fused. The Releasable stage includes all primed granules with 0 to 3 bound Ca^{2+} . r_1 and r_{-1} are the forward and backward resupply rates, respectively. k_{on} and k_{off} are the binding and unbinding rates, respectively, associated with the Ca^{2+} -sensor for secretion. γ stands for the fusion rate that manages the last non-reversible step of exocytosis.

oscillation each peak that was at least two times higher than the background oscillatory noise in non-stimulated conditions. In order to systematize this procedure for 10-min low-glucose periods, we developed an algorithm consisting of the following steps:

1. Fix a threshold at 1.5 to 2 times the mean Ca^{2+} level at 11 mM extracellular glucose (11G).
2. Detect points crossing this threshold with positive slope if they are sufficiently separated from the last one (minimum half a minute).
3. Count peaks and divide by ten to compute an average frequency per minute.

A graphical example of how this algorithm works is shown in Figure 6.4. Computed frequencies will be shown in the Results section as they are related to secretion periods. Qualitatively, we observe that frequencies at low-glucose periods are higher than at high glucose.

6.3.2 Model description

Upon stimulation by low glucose, α -cells display two phases of glucagon release [83]: a first phase lasting 3min during which the rate of release increases very fast, followed by a sustained phase during which the rate of release remains elevated and unchanged. This situation is reminiscent of what happens in adrenal chromaffin cells, although the time scale is completely different, since the rapid and sustained phases in neuroendocrine cells occur in the milliseconds and the seconds timescales, respectively

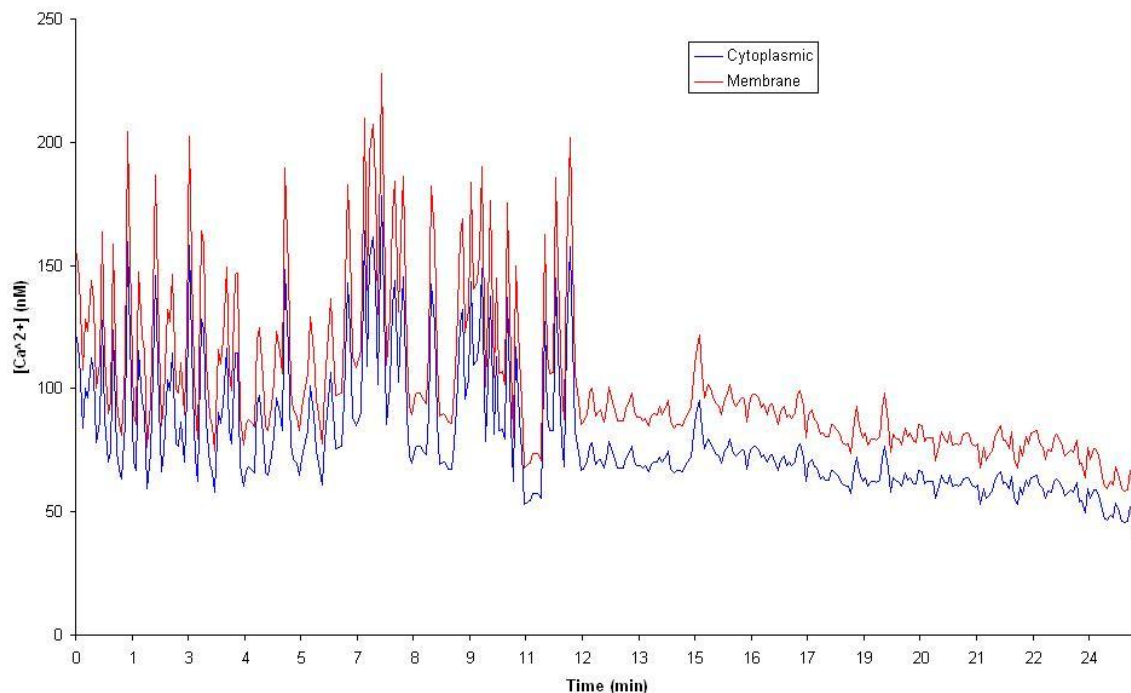


Figure 6.6: Example of cytoplasmic (experimental) and membrane (simulated) $[Ca^{2+}]_i$ in an alpha cell. Parameters for this simulation are given in Table 6.1.

[97, 160]. However, the time scales (but not the nature of the phases) observed in α -cells are similar to those characterizing secretion in pancreatic β -cells [134]. We thus hypothesized that glucagon secretion by α -cells can be described by a kinetic scheme resembling the one already proposed for chromaffin cells.

Following the neuroendocrine secretion process discussed in [97], which was implemented in a model proposed for mouse chromaffin cells [189], we hypothesize that glucose secretion evoked by low-glucose stimulation is due to a pool of releasable granules docked to the membrane, as well as to new granules coming from a reserve pool. In contrast to Voets model which considered the existence of two different types of pools characterized by different rates of fusion, we are just considering a minimal kinetic scheme containing one reserve pool and one readily releasable pool (RRP), ready to be triggered by Ca^{2+} , as shown in Figure 6.5. We consider that three Ca^{2+} ions are needed to trigger granule fusion, as the above mentioned modeling work, and as some models for β -cells [30, 136]. In our model, transition from the Reserve pool to the RRP (r_1) is defined as a function of cytoplasmic Ca^{2+} whereas Ca^{2+} -triggering steps are functions of membrane $[Ca^{2+}]_i$. This distinction in Ca^{2+} values is based on two observations for other exocytotic cells [8, 97]: 1) There are spatial differences on $[Ca^{2+}]_i$ (for example in beta cells local calcium quantities may be 10 times higher than in the cytosol); 2) Granule fusion occurs close to the voltage-gated channels, that are embedded in the plasma membrane and allow for Ca^{2+} entry. Another consideration, which will be discussed later, is that the rate of pool resupply is a linear function of glucose concentration. The rate of pool resupply is thus given by $r_1 = f(G) \cdot f(Ca_C)$, where $f(G)$ is a proposed function of the extracellular glucose concentration G (as

we discuss further below), $f(Ca_C)$ is a Michaelis-Menten function of cytosolic calcium concentration as proposed for other cells [30, 189]. Other kinetic steps schematized in Figure 6.5 are described by mass action law kinetics. The number of secreted granules in each time step (Δt) is then computed as the integral of γP_3 over this time interval, where P_3 stands for the granule population with three bound Ca^{2+} ions, and γ is the fusion rate.

The purpose of the secretion model is to quantitatively predict the level of secretion induced by real Ca^{2+} oscillations in α -cells at different glucose levels. The oscillations that will serve as an input to the secretion model are in arbitrary fluorescence units so, to fit parameters in molar units we seek for a reliable equivalence. Our data have not been calibrated but we simply compared them to those measured by other groups using similar techniques [18, 143]. We indeed mainly focus on the Ca^{2+} dynamics for which accurate calibration of the absolute Ca^{2+} levels are not necessary. We thus assume that one fluorescent unit approximately corresponds to two or three nanoMolar units of $[Ca^{2+}]_i$. On the basis of this empirical procedure, the values of cytoplasmic calcium range between 30 to 400 nM, in agreement with values reported in the above mentioned works.

Since oscillations reflect cytoplasmic Ca^{2+} concentration ($[Ca^{2+}]_c$), we estimated the corresponding dynamic values for the local Ca^{2+} concentration, just below the α -cell membrane ($[Ca^{2+}]_m$). In β -cells, it has been suggested that secretory granules are exposed to very high levels of local calcium (up to 10 times higher than in the cytosol) [8]. No data are available for α -cells probably due to the small size of these cells. Then, considering that granule diameter is between 260 and 290 nm [9], and that there are granules located below the plasma membrane [83], we performed simulations to estimate local $[Ca^{2+}]_i$ beneath plasma membrane and up to 300 nm. We used our previously published model that estimates $[Ca^{2+}]_i$ in concentric layers of specific thickness for a spheric cell considering buffered diffusion [73]; to this model, we added a Ca^{2+} -extrusion pump [138] and a compensating leak flux. Leak flux was adjusted to obtain a steady-state cytoplasmic $[Ca^{2+}]_i$ close to $0.1 \mu M$. Assuming that an α -cell could be approximated by a spherical cell of $5.3 \mu m$ of radius [9] with a large nucleus (60% of the cytoplasm), we obtained that $[Ca^{2+}]_m$ to $[Ca^{2+}]_c$ ratio ranges between 1.26 to 1.29 depending on the spatial extent considered for the layer beneath the membrane (from 10 to 300 nm). For all subsequent simulations we have taken 100 nm, where the ratio equals 1.282. Parameter values used to estimate membrane Ca^{2+} concentration ($[Ca^{2+}]_m$) are given in Table 6.1.

Parameter estimation

Using Ca^{2+} concentrations as inputs to the secretion model, we need to estimate the adequate values for its parameters r_1 , r_{-1} , k_{on} , k_{off} and γ (all shown in Figure 6.5). We assume that, as in chromaffin and beta cells [30, 136, 189], granule fusion is triggered by three calcium ions, so k_{on} and k_{off} are taken from [189]. Ca^{2+} oscillations data have been obtained on a limited number of α -cells located mainly in the periphery of intact islets, whereas accumulated glucagon secretion is measured per islet in one hour. Therefore, to make adequate comparisons we have repeated six times our 10-min data file of calcium concentrations to build a one-hour input file to the model. This was

Table 6.1: Parameter values to estimate membrane Ca^{2+} concentration using the Shell model.

Parameter	Value	Reference
INPUT DATA		
Cell radius (μm)	5.3	[9]
Shell thickness (nm)	100	According to Δx
Ca^{2+} concentration (μM)	0.1	Experiments
SPATIAL AND TEMPORAL DATA		Chosen
Spatial resolution (nm), Δx	100	
Temporal resolution (μs), Δt	45	
Simulation time (s)	10	
ENDOGENOUS BUFFER		[98]
Concentration (μM)	500	
Forward binding rate ($M^{-1}s^{-1}$)	$5 \cdot 10^8$	
Dissociation constant (μM)	10	
CALCIUM-EXTRUSION PUMP		[138]
Maximal speed ($pmolcm^{-2}s^{-1}$)	2	
Half-maximal concentration (μM)	0.83	
LEAK FLUX		
Rate (μMs^{-1})	21.9	Fitted

done for both sets of data (0.5G and 11G). Parameters were then fitted to reproduce the experimental one-hour secretion per islet under both conditions, considering that this secretion equals to the mean of the ensemble of individual secretions per hour multiplied by 200 α - cells per islet.

In a first approach, we tried to fit parameters values to reproduce experimental secretion levels with a resupply rate r_1 independently of the glucose level. With such a model, we could not find any set of parameter values that could correctly predict both stimulated and non-stimulated secretion. That is, using the same parameter values with our calcium data at 0.5 and 11G, we obtain at best a high glucose reduction in secretion of $\sim 75\%$, while the experimentally observed reduction lies in the 50 to 60% range. This also happens for a constant $[Ca^{2+}]_i$ level, equivalent to the mean of oscillation data. On the other hand, if we fit in a separate manner the model parameters to get appropriate secretion at 0.5G and at 11G, the two sets of parameter values lead to drastically different steady-state granule distributions for constant calcium levels equal to the corresponding average values. Indeed, we found that at low glucose 35% of total granules are releasable, and the rest (65%) are in the Reserve pool. In contrast, at high glucose, 66% are releasable granules whereas 34% are in the Reserve pool. Here, we are naming releasable granules to those belonging to the *Releasable* stage (marked with dashed line in the model of Figure 3), assuming that all of them are primed granules with 0 to 3 bound Ca^{2+} ions. Thus, the 35% at low glucose comes from 33% in the Primed pool plus 2% in the +1Ca pool; analogously, at high glucose, the 66% results from 63% in the Primed pool plus 3% in the +1Ca pool. These particular granule distributions are used as initial conditions, at both glucose levels, in order to solve the model.

The above mentioned preliminary results forced us to look for a different set of parameters (if possible) that could predict experimental secretion from Ca^{2+} oscillation data. Then, we analyze model response and sensitivity to all parameters, keeping in mind that the model should exhibit a reduction of 60% at most of stimulated secretion, when working at high glucose. A list of possible parameter modifications is below; we have tested all using a Monte Carlo algorithm that randomly generates values for the parameter, in a fixed range, and calculates the corresponding secretion. Results are plotted in Figure 6.7.

1. Smaller γ at 0.5G than at 11G.
2. Smaller resupply net rate at 0.5G than at 11G. This can be accomplished by:
 - (a) A higher r_{-1} at 0.5G.
 - (b) A reduced r_{max} at 0.5G.
 - (c) A reduced k_{off}/k_{on} of resupply at 11G.
3. A different apparent affinity K_D of the binding sites.
4. A dependence on glucose concentration of the resupply rate r_1 , so resupply could be smaller at 0.5G.

Results for tests of parameter estimations are shown in Figure 6.7. Notice that options 1, 2(a), 2(b) and 2(c) are counter-intuitive since they would mean that the

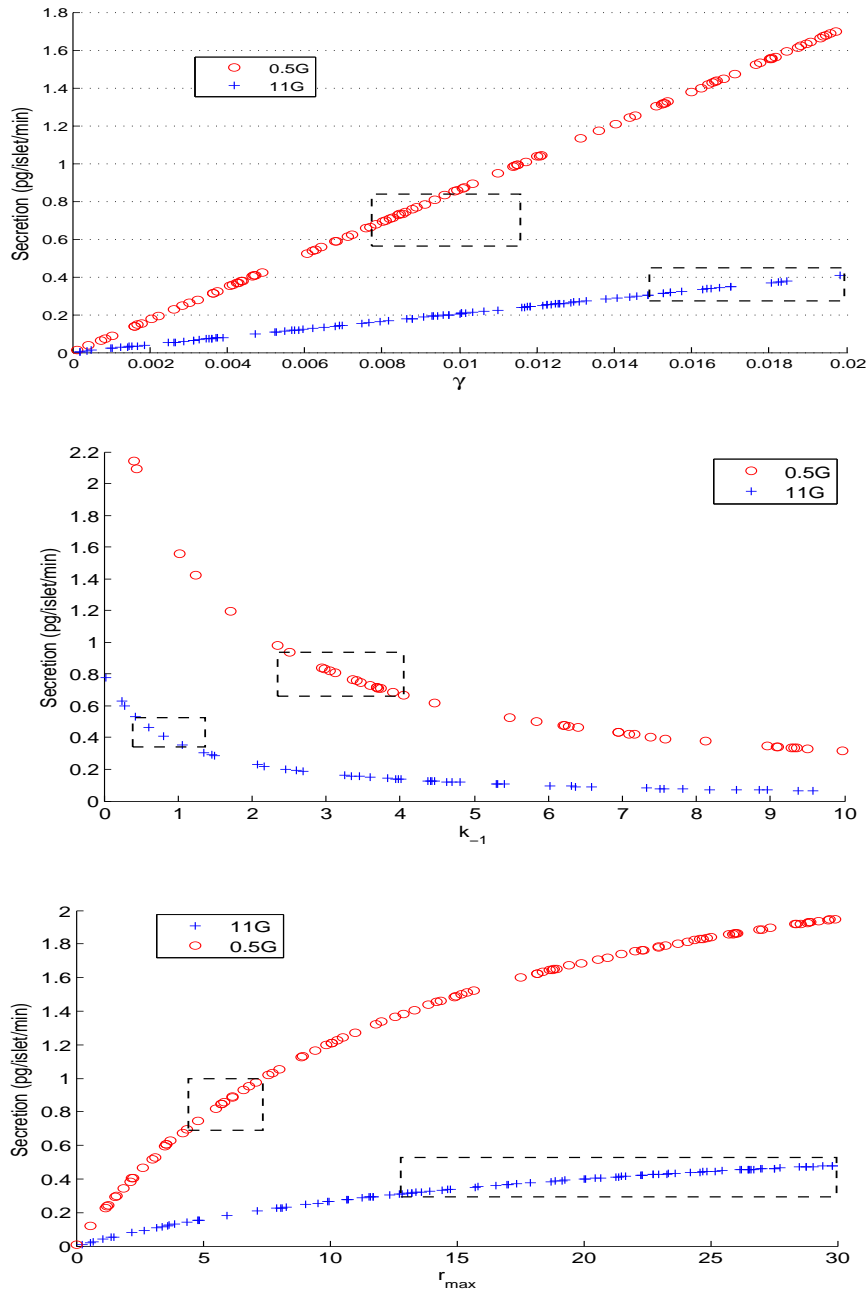


Figure 6.7: Tests done looking for the adequate parameter set that could predict experimental secretion, at 0.5G and 11G, from Ca^{2+} oscillation data. Expected predictions for both glucose levels are marked in dashed squares. Secretion predicted for different γ (top), k_{-1} (center), and r_{max} (bottom) values.

secretion machinery is "more active" at 11G than at 0.5G. Moreover, the mechanism responsible for providing new primed granules at 11G periods should be one different from the mechanism activated at 0.5G, and it should not be working at 0.5G. These ideas make it unfeasible to choose these options to explain experimental reduction on secretion. Option 3 was tested, moving the unbinding rate k_{off} . By decreasing its value from 4 to 3 s^{-1} at high-glucose, the model predictions were correct. However, this would mean that the Ca^{2+} -sensor responsible for high-glucose secretion is physically different from that for low-glucose secretion, and that the former should have higher affinity than the latter. This goes into unreal cellular conditions. Moreover, affinity differences in Ca^{2+} sensors are not enough to think they could be two different proteins; for example, two different subtypes of synaptotagmins, the most widely accepted Ca^{2+} sensors [171]. Although none of the tests allows us to find one parameter value that predicts the experimental high-glucose reduction, the plot at the right in Figure 6.7 indicates, interestingly, that the expected secretion could be obtained if the resupply would have different maximal rates, being higher at high glucose.

Therefore, we tested option 4 which expresses the possibility that glucagon secretion is influenced by glucose concentration through the resupply rate. This is the most plausible hypothesis due to the existence of experimental evidence, reported in a previous work [132], indicating that glucagon secretion is influenced by glucose concentration not only through changes in cytosolic Ca^{2+} but also through granule resupply, or granule mobilization. Hence, the equation for r_1 should also include a function of glucose concentration, that is $r_1 = f(G) \frac{Ca_c}{Ca_c + K_D}$, where Ca_c is the cytosolic Ca^{2+} concentration, and K_D is the half saturation constant of this process. Here, $f(G)$ is proposed as a linear function of glucose, $f(G) = 3G + 18.5$, since we only have two experimental glucose points to fit ($G = 0.5$ and $G = 11$); specifically, we estimate function parameters considering that $f(G = 0.5)$ should coincide with the estimated value of refilling rate in α -cells under stimulation (20 granules per second) [8]. We notice that this function can be tested experimentally in the future, and that our consideration does not discard the possibility that glucose dependence of resupply may behave differently for other glucose concentrations, as reported in [154]. Taking this glucose and Ca^{2+} dependence into account, the model now correctly predicts secretion values at low and high glucose by assuming that granule resupply increases from 20 granules per second at 0.5G up to 51.5 granules per second at 11G. In other words, our proposed glucose dependence predicts that granule mobilization is increased about 2.6-fold for high glucose, which is in good agreement with the experimental estimation of 3.3-fold reported in [132].

All parameters of the secretion model, used in simulations, are given in Table 6.2. The granule equivalence in femtograms (fg) was obtained considering that one islet contains about 2 nanograms of glucagon [90], and a minimum of 200 α -cells [141], so each cell contains, at most, 10 picograms of glucagon. Taking an average cell radius of $5.3 \mu m$ [9], the average α -cell volume is $623.6 \mu m^3$; then considering a granule density of $9.3 \text{ granules}/\mu m^3$ [9], each α -cell would have about 5800 granules. Assuming that each granule contributes with the same glucagon quantity, the granule content would be 1.72 fg of glucagon; for simulations, we are taking a round value of 2 fg per granule.

Table 6.2: Parameter values of the glucagon secretion model.

Parameter	Value	Reference
Glucose function $f(G)$	$3G + 18.5$	Fitted, see text
Glucose concentration G	0.5, 11 mM	Experiments
Ca^{2+} affinity of resupply K_D	$2.3 \mu\text{M}$	[189]
Backward resupply rate r_{-1}	2.1 s^{-1}	Fitted
Ca^{2+} -binding rate k_{on}	$0.5 \mu\text{M}^{-1}\text{s}^{-1}$	[189]
Ca^{2+} -unbinding rate k_{off}	4 s^{-1}	[189]
Fusion rate γ	0.011 s^{-1}	Fitted
<i>Other values</i>		
Cellular volume	$623.6 \mu\text{m}^3$	Computed
Granule density	$9.3 \text{ granules } \mu\text{m}^{-3}$	[9]
Granule equivalence	2 fg of glucagon	Computed

6.4 Results

6.4.1 Secretion induced at low and high glucose

Secretion dynamics in 20-minute periods for 14 different α -cells are shown in Figures 6.8 and 6.9. The Ca^{2+} time-series (top panels) are used as inputs to the Shell and the secretion model. The Shell model provides the values of $[Ca^{2+}]_i$ at the membrane and in the cytoplasm, which are used as inputs to the secretion model. The secretion model, finally, calculate the secretion rate along time, as well as the accumulated glucagon release. We notice high variability in individual secretory responses for low and high glucose periods. In Figure 6.10 we summarize individual secretion rates for 10 minutes at low, and then at high glucose, as well as the average rate. The cytoplasmic Ca^{2+} oscillation induces a secretion rate per minute that seems to have a delayed maximal response to low glucose. This delay corresponds to the time needed by granules to become releasable, as most granules are in the reserve pool at resting Ca^{2+} . Notice that steady-state secretion rate (after five minutes) at low-glucose is greater than at high-glucose, on average.

Individual secretion rates induced by each of the 14 experimentally obtained Ca^{2+} time-series were predicted using the one-hour files as inputs to the model, as explained in section 6.3.2, using the parameters of Table 6.2. Then, mean secretion of the ensemble in one hour was calculated to compare it to the measured experimental secretion. In figure 6.11 we show the resulting individual secretion rate per hour, as well as the average of all cells for low (0.241 pg/cell/hour) and high (0.103 pg/cell/hour) glucose. From these values, a high-glucose-induced reduction of 58% was obtained. Accumulated secretions predicted by the model would be 20.6 and 48.3 pg/islet in 1 hour at high and low glucose concentrations, respectively, considering 200 alpha cells per islet; these accumulated values are in the range of experimental measurements [182]. From this figure, we also elicit from predictions that eight cells from fourteen ($\sim 57\%$) clearly secrete more glucagon at 0.5G than at 11G, five cells ($\sim 36\%$) secrete almost equal at both levels, and one cell ($\sim 7\%$) secretes more glucagon at 11G than at 0.5G.

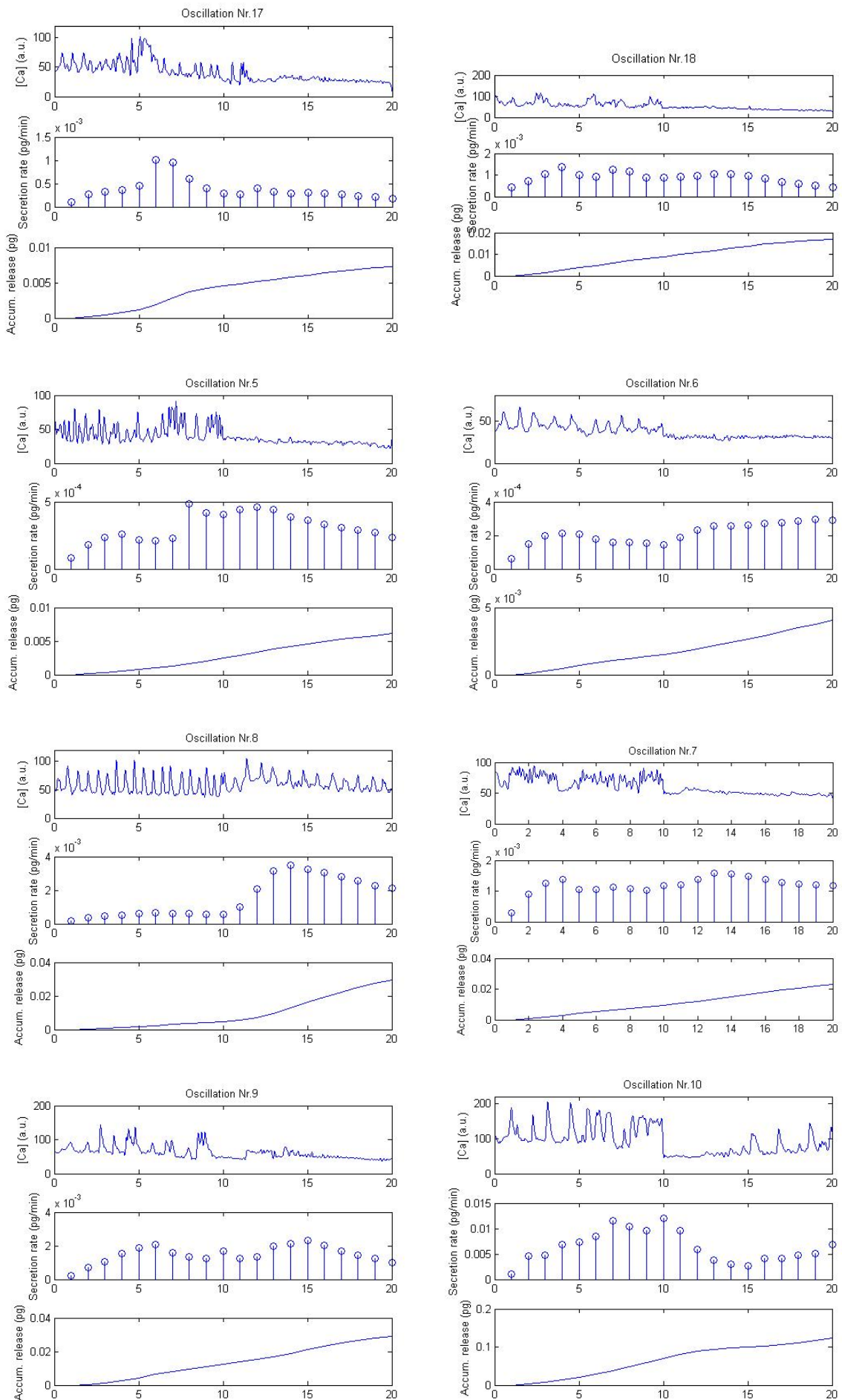


Figure 6.8: To be continued.

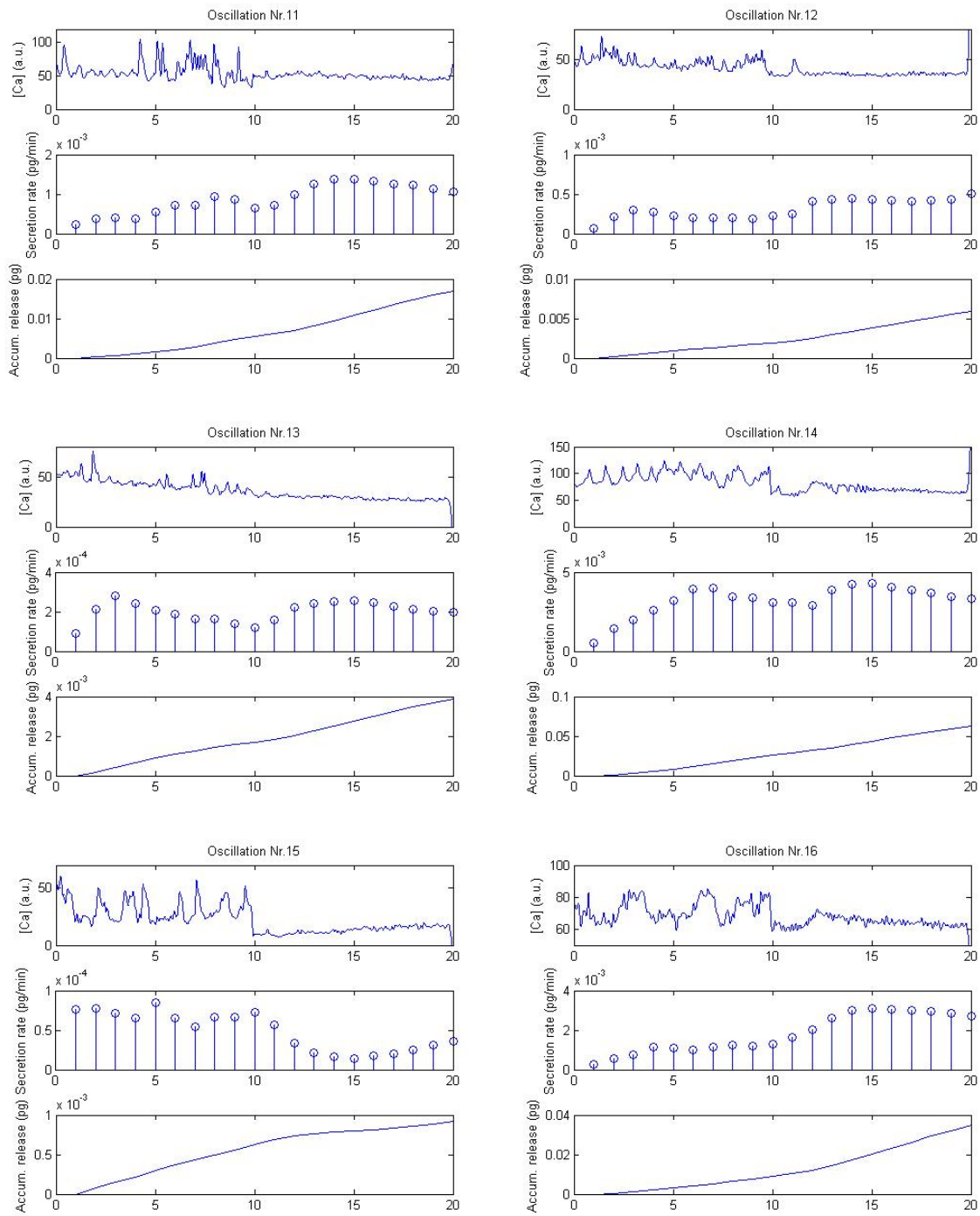


Figure 6.9: Individual secretion dynamics in 20-minute periods: from minute 0 to 10, cells were exposed to 0.5 mM glucose; from minute 11 to 20, cells were exposed to 11 mM glucose. Each figure corresponds to one α -cell and has three panels: The Ca^{2+} oscillation in a.u. (top panel), the individual secretion rate in pg per minute (middle panel), and the total accumulated glucagon release in pg (bottom panel). Notice the high variability in individual secretory responses.

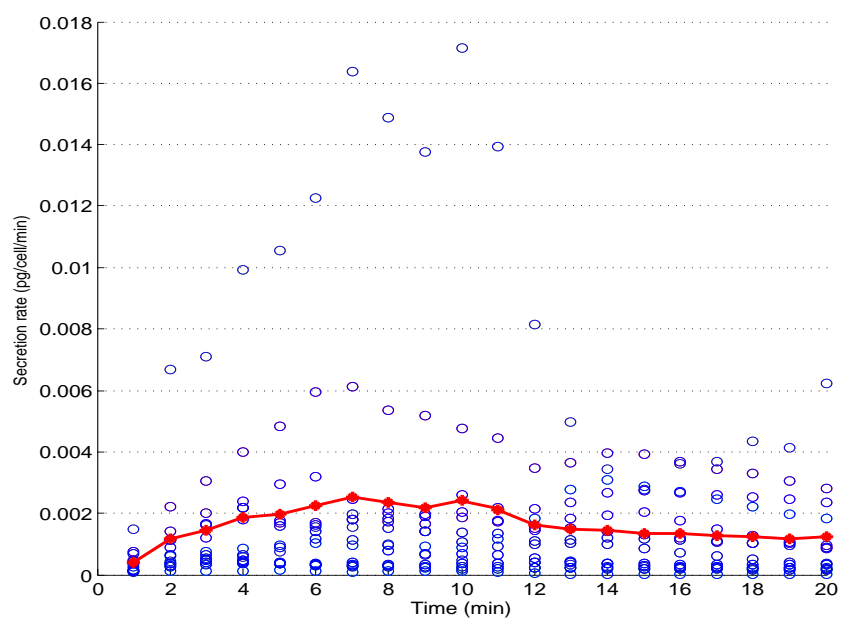


Figure 6.10: Summary of individual secretion rates (blue dots) in 20-minute periods: from minute 0 to 10, cells were exposed to 0.5 mM glucose; from minute 11 to 20, cells were exposed to 11 mM glucose. Average secretion rate in the whole period is also indicated (red line). Secretion in pg/islet was obtained considering 400 α -cells per islet.

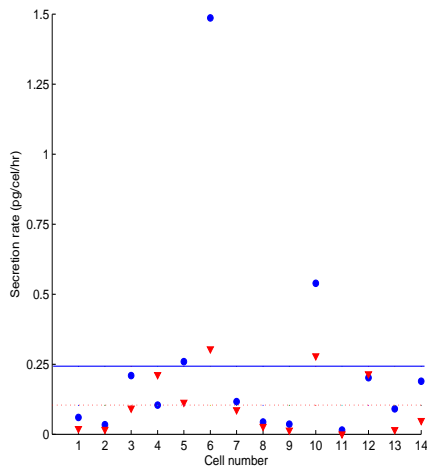


Figure 6.11: Secretion rates per hour induced by the experimental Ca^{2+} time-series at 0.5G (dots) and 11G (triangles). Lines show that mean secretion rate of the ensemble at low glucose (0.241 pg/cell/hour) is larger than at high glucose (0.103 pg/cell/hour). In agreement with experimental measurements, the model predicts that mean glucagon secretion is reduced 58% at high glucose.

These results agree with reported ideas that discuss α -cells work in an asynchronous manner, and about the unequal participation of each cell to whole-islet glucagon secretion [114, 127].

6.4.2 Secretion induced by constant $[Ca^{2+}]_i$ levels

In order to explore the impact of intracellular calcium oscillations on glucagon secretion from a theoretical viewpoint, we also tested the secretion predicted by our model for a constant $[Ca^{2+}]_i$ level equal to the mean value of each oscillation. This approach makes sense because it has been observed that only 30 to 50% of alpha cells exhibit oscillating calcium levels [114, 143]. The effect of oscillations on various cellular responses has indeed been modelled in other cell types. For example, it was predicted that calcium oscillations in liver cells can potentiate glycogenolysis in response to low levels of stimulation [56]. In other systems, where Ca^{2+} -calmodulin kinase II is involved, the level of physiological response is encoded in the frequency of Ca^{2+} oscillations [40]. In this sense, results about frequency (shown in next section) were thought to clarify if this codification is present in our results.

In Figure 6.13 we show the individual secretion obtained for each mean $[Ca^{2+}]_i$ level shown in Figure 6.12. In this case, the predictions of the model are: seven cells of fourteen ($\sim 50\%$) clearly secrete more glucagon at 0.5G than at 11G, five cells ($\sim 36\%$) secrete almost equal at both levels, and two cells ($\sim 14\%$) secrete more glucagon at 11G than at 0.5G. However, average secretion rate at low glucose (0.198 pg/cell/hr) is still above the rate at high glucose (0.093 pg/cell/hr), i.e. there is still a 53% high-glucose-induced reduction on secretion. In contrast, for low glucose concentration -which most of the time induce Ca^{2+} oscillations- the secretion rate is higher for an oscillatory Ca^{2+} signal (0.241 pg/cell/hour) than for a constant Ca^{2+} signal with the same average (0.198 pg/cell/hour); that is, oscillations induce $\sim 21\%$ more secretion. Moreover, the distribution of individual participation to total release is different for a constant than for an oscillatory calcium level, as summarized in Table 6.3. The model thus predicts that upon low-glucose stimulation, α -cells that display Ca^{2+} oscillations secrete more glucagon than those exhibiting an increase of steady-state Ca^{2+} with the

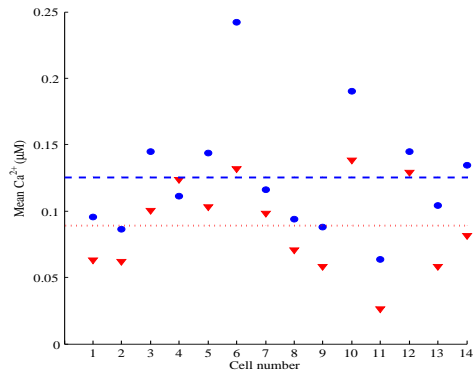


Figure 6.12: Mean Ca^{2+} corresponding to each of the 14 Ca^{2+} time-series, at 0.5G (dots) and 11G (triangles). Lines show that mean Ca^{2+} level at high glucose (0.088 μM) is lower than at low glucose (0.125 μM).

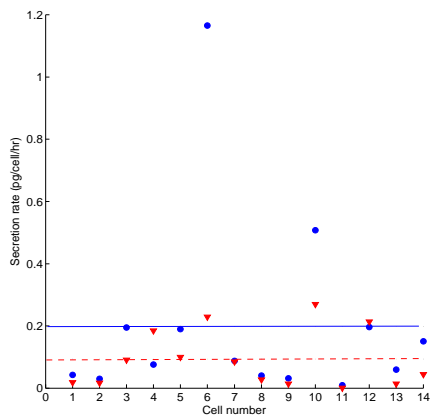


Figure 6.13: Secretion rates at 0.5G (dots) and 11G (triangles) induced by a constant Ca^{2+} level corresponding to the individual mean value of oscillations. Lines indicate that average secretion rate at low glucose (0.198 pg/cell/hr) is larger than at high glucose (0.093 pg/cell/hr). In this case, the model predicts that secretion rate is reduced 53% at high glucose.

same average.

6.4.3 Effect of oscillation frequency and mean $[Ca^{2+}]_i$ levels on secretion

The results shown in the preceding sections argue that oscillations have a clear impact on secretion. To unveil how oscillations are encoding relevant information for glucagon secretion, we have looked for the relationship between frequency and mean Ca^{2+} level of oscillations with individual glucagon release. In Figure 6.14 estimated frequencies for all oscillations are shown. Values are within the experimentally measured range, i.e., 0.3 to 1.6 per minute at 0.5mM glucose, with a mean value of 0.87 per minute [183]. In Figures 6.15 and 6.16 we looked for possible correlations between secretion

Table 6.3: Distribution of individual α -cell secretion.

	Percentage of cells		
Ca^{2+} dynamics	0.5G > 11G	0.5G = 11G	11G > 0.5G
Oscillations	57%	36%	7%
Constant	50%	36%	14%

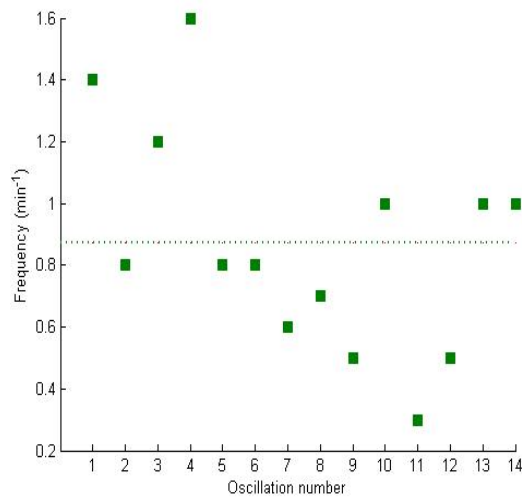


Figure 6.14: Computed frequency for the 14 Ca^{2+} time-series at 0.5mM glucose. Frequency was measured following the algorithm described in Section 6.3.1. Dotted line indicates the average frequency of all oscillations (0.87 min^{-1}).

and frequency and mean calcium level, respectively. Looking at these plots, we have found that there is no correlation between secretion and frequency, but there seems to be a correlation between secretion and mean $[Ca^{2+}]_i$ level. This observation suggests that there is no frequency coding phenomenon, which could be expected given the high level of irregularity of oscillations. However, it supports the possibility that oscillations allow the internal cell calcium level to go from time to time above a certain threshold that favours secretion.

In Figure 6.16, computed rates of secretion are shown as a function of calcium concentrations. The curves obtained at high and low glucose are different because the rates of resupply depend on the glucose concentration, hence the secretion rates. Interestingly, these curves are steep, which provides a clue to understand why oscillations favour secretion. Indeed, because of this highly non linear relationship between Ca^{2+} concentration and secretion rate, a small increase in Ca^{2+} concentration produces a large increase in secretion rate; thus, average secretion during oscillations is larger than the dynamic secretion that would be obtained over the same period of time with the average Ca^{2+} during oscillations. Such a type of oscillations-induced potentiation of a Ca^{2+} -activated response has been demonstrated experimentally for gene expression [36].

6.5 Discussion

In this study, we have developed a simple model that quantitatively reproduces the rates of glucagon secretion by alpha-cells undergoing glucose-induced Ca^{2+} oscillations. We have found that, although calcium oscillations are highly variable, the average secretion rates predicted by the model fall into the range of values reported in the literature both for high and low glucose. Besides providing a predictive tool to quantify glucagon release in conditions that have not yet been tested experimentally, the model leads to interesting hypotheses concerning the molecular mechanism that governs and regulates glucagon release. In particular, the model predicts that, in contrast to chromaffin cells, just one type of releasable pools manages glucose-induced glucagon secretion in

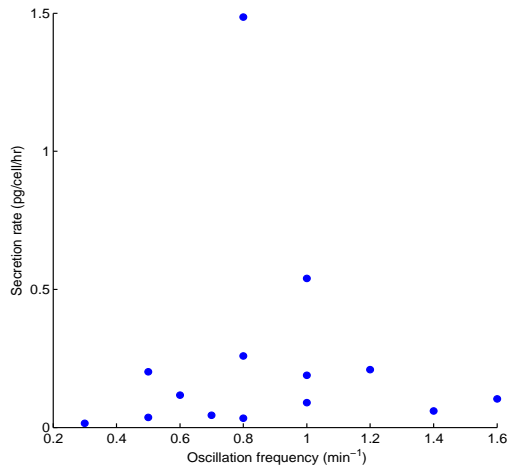


Figure 6.15: Secretion rates induced by Ca^{2+} oscillations, corresponding to the low glucose level, are plotted against the computed frequency of these oscillations. There is no correlation between secretion rate and frequency (correlation coefficient of 0.01).

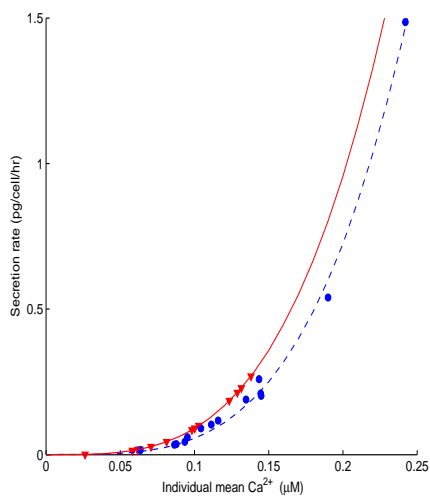


Figure 6.16: Secretion rates induced by Ca^{2+} oscillations at 0.5G (dots) and 11G (triangles) are plotted against the mean Ca^{2+} level of each cell. Best-fit curves for data sets are power functions ($n=3.69$ for 0.5G, and $n=3.41$ for 11G, correlation coefficients of 0.99). Notice that for a given value of individual mean Ca^{2+} , the presence of low glucose (dot) induces a lower secretion rate than the high glucose (triangle), because of the glucose-dependence of granule resupply.

alpha cells. Besides that, the secretory process is very similar between both cell types, involving three steps of Ca^{2+} binding. In both cases, a low affinity Ca^{2+} -sensing protein (known as Synaptotagmin) mediates the fusion of the secretory granules to the plasma membrane [97, 83]. This is similar to pancreatic beta cells as well [148].

Our modeling approach, however, suggests the existence of a regulation of the secretory pathway that would be rather specific to α -cells. As a matter of fact, it predicts that the resupply of releasable granules is not only controlled by cytoplasmic calcium, as in neuroendocrine cells, but also by the level of extracellular glucose. Here, we propose that resupply is a function of glucose concentration, which leads to a very good agreement between model-predicted and experimentally-measured rates of secretion, as well as resupply rates, at high and low glucose concentrations. Taking into account the maximal resupply rate estimated for mouse α -cells under depolarization-induced exocytosis (20 granules per second) [9], the model indeed predicts the observed steady-state secretion rate of glucose-induced glucagon secretion (0.8 to 1 pg/islet/minute) [83]. Moreover, glucose sensitivity of resupply also leads to a good estimation of granule mobilization for basal (high-glucose) conditions, that seems to be higher than for stimulated (low-glucose) conditions. We have found that granule mobilization, i.e. resupply rate in our model, is increased about 2.5-fold for high glucose (up to 51.5 granules per second), which well agrees with the 3.3-fold reported in [132].

The population of releasable granules at basal conditions was estimated with a constant calcium level corresponding to the average of all mean calcium levels observed at 11 mM glucose (shown in Figure 6.12). The estimation of the releasable population in the steady-state includes all primed granules in the Releasable stage (marked in Figure 6.5). The population predicted by the model, at high-glucose, is 63% in the Primed pool plus 3% in the +1Ca pool. The resultant percentage (66%) compares well with the 55% measured as the population of submembrane granules located in the first 300 nm below the plasma membrane in [83], suggesting that releasable granules in non-stimulated α -cells would be located between this distance, as in neuroendocrine cells [97]. In contrast, the predicted population of releasable granules at low-glucose conditions is 33% in the Primed pool plus 2% in the +1Ca pool. In both cases, the smallest percentage agrees well with estimations of the readily-releasable pool (RRP) in alpha cells (1 to 2%) [8, 9], that is slightly larger than in beta cells (0.2 to 1%) [148]. On the other hand, the distribution of primed (63%) and reserved (34%) granules at high glucose might be explained by the fact that under this condition, ATP levels should be higher so the priming step is favored, since it is ATP-dependent [148].

It is worth emphasizing that the model, in fact, leads to the prediction that low glucose levels have two counter-acting effects in α -cells. On the one hand, low glucose stimulates calcium oscillations that induce glucagon release. On the other hand, low glucose reduces the rate of resupply of the releasable pool. Our physiological interpretation of this apparent paradox is the following: during low glucose periods, there would be a well-controlled number of releasable granules refilled slowly from a huge reserve pool to ensure a steady-state secretion rate that could last for several minutes (as observed by [83]). This would be reasonable to avoid that α -cells would exhaust the releasable pool of granules, and could mean also that these cells have its own glucose-sensing mechanisms, as discussed in some previous works [146, 185]. Therefore, under normal functioning, the α -cell would be able to respond for long hypoglycemic

periods, as speculated in some works [8], but under pathological conditions as in diabetic patients, it may be unable to maintain the constant secretion rate probably due to abnormal blood glucose levels that would affect granule mobilization.

Overall, the present results all emphasize the crucial role played by glucose on the control of glucagon secretion in α -cells [185]. From our work, glucose control occurs both via a direct pathway that directly affects the resupply of secretory granules and whose molecular mechanisms remain to be elucidated, and via a control of $[Ca^{2+}]_i$ dynamics. As happens with other previous studies [56, 36], our modeling approach of glucose-induced glucagon secretion in α -cells also enlightens the potentiating role of calcium oscillations versus constant levels with the same average, as summarized in Table ???. Thus, at low glucose concentrations, whole-islet glucagon secretion may be increased not only by a higher average $[Ca^{2+}]_i$ in each α -cell, but also by the fact that up to 50% of these cells will display an oscillating level of $[Ca^{2+}]_i$ [114]. Such an observation suggests new therapeutic targets as the level of secretion might be manipulated by drugs affecting both, the levels and the dynamics of Ca^{2+} increases.

Alpha cells:
Electrical activity related to glucagon secretion

7.1 Introduction

The modeling work described in this chapter deals with the electrical activity in pancreatic alpha cells, and it has been based on the available data about ionic currents and channels. The usual experimental protocol to study electrical activity is to stimulate the cell with depolarization pulses, and then to measure the produced ionic currents [9, 75, 79]. However, from a physiological point of view, the electrical activity exhibited by alpha cells is initiated when they are exposed to low glucose levels. In this situation, the alpha cells generate action potentials (APs) which are related to glucagon secretion. These APs are supposed to be triggered by a low ATP/ADP ratio, because of the absence of glucose. In these ATP/ADP conditions, the K_{ATP} channels are opened what produce an ionic current; in turn, this current changes the membrane potential and APs are generated. This electrical activity chain is possible thanks to the Ca^{2+} and Na^+ channels that fire the depolarization stage of the APs. Then, cell depolarization finally activates the K^+ channels in order to repolarize the cell [80, 141].

7.2 Modeling ionic channels and electrical currents relevant to glucagon secretion

In this part, we define minimal state models and estimate their parameters for each ionic channel, towards simulating ionic currents associated with glucagon secretion in α -cells. Currently, we are only considering the relevant currents measured in mice, which are common animal models for alpha-cell experimentation, and which are the animals used in the research group we are collaborating with. We present a state modeling approach to simulate the dynamics of ionic currents commonly measured in voltage-clamp experiments on alpha cells. Voltage-dependent electrical currents that

Table 7.1: Fixed values for ionic channel models.

	Ca_T	Ca_N	Na	K_A	K_{DR}
Unitary conductance (pS)	8.4,4.2,2 [†]	13	12,4 [‡]	12	30
Activation voltage, V_{act} (mV)	-60	-20	-30	-40	-20
Inactivation voltage, V_{in} (mV)	-45	-31	-42	-68	—

[†]4.2pS if $V > -60$, 8.4pS if $V \leq -60$, 2pS if $V > 0$. See also section 7.2.4.

[‡]12pS if $V \leq 10$, otherwise 4pS. See also section 7.2.3.

Table 7.2: Fitted values for ionic channel models. All transition rates in ms^{-1} .

	Sodium	A-type potassium
Model	4-state	4-state
NC	2554	1631
q_{01}	$0.44 \exp(-0.06V_{th})$	$6.83 \exp(-0.02V_{th})$
q_{10}	$11.39 \exp(0.05V_{th})$	$30.77 \exp(0.03V_{th})^*$
q_{02}	0.81^*	$8.5 \cdot 10^{-5}$
q_{20}	$9.06/E_0^\dagger$	$0.01/E_0^\dagger^*$
q_{13}	0.004^*	0.008
q_{31}	$3.69/E_0^\dagger^*$	$0.12/E_0^\dagger^*$
q_{23}	$0.8 \exp(-0.06V_{th})$	$0.8 \exp(-0.02V_{th})$
q_{32}	$20.58 \exp(0.05V_{th})$	$3.6 \exp(0.03V_{th})^*$

	T-type calcium	N-type calcium	DR-type potassium
Model	3-state	3-state	2-state
NC	694	202	251
q_{01}	$0.03 \exp(-0.05V_{th})$	$0.22 \exp(-0.05V_{th})$	$2.6 \cdot 10^{-5} \exp(-0.2V_{th})$
q_{10}	$13.06 \exp(0.03V_{th})$	$0.67 \exp(0.04V_{th})$	$0.7 \exp(0.03V_{th})$
q_{02}	0.001	—	—
q_{20}	$8.94/E_1^\dagger$	—	—
q_{12}	$89.4/E_1^\dagger$	$6.9(\Delta Ca^\dagger/E_1)^*$	—
q_{21}	0.001	0.008^*	—

NC=Number of channels, $V_{th} = V - V_{act}$, $V_i = V - V_{in}$.

$$^\dagger \Delta Ca = \frac{[Ca]_i}{[Ca]_o}, E_0 = 1 + \exp(-0.01V_i), E_1 = 1 + \exp(-0.1V_i).$$

*Values modified to improve dynamic behaviour. See Section 1.1.1 for details.

control the sequence of events leading to glucagon secretion are I_{CaT} , I_{CaN} , I_{Na} , I_{K_A} and $I_{K_{DR}}$, and they all exhibit some common kinetic properties that make them suitable for modeling, as discussed in Section 1.1.1. Hence, state models of ionic channels that produce these currents, measured during electrophysiological experiments on alpha cells, may be a useful tool to unveil how electrical activity is coupled to glucagon secretion.

In what follows, we discuss the available experimental data for each ionic channel and current, and how we have used this information to define a particular channel model, having adopted the methodology detailed in Section 1.1.1. Tables 7.1 and 7.2 summarize the parameter values, fixed and fitted, of each state model proposed for each ionic channel. Sodium and A-type potassium channels were proposed as 4-state models, Ca^{2+} channels were proposed as 3-state models, and the DR-type potassium channels were modeled as a 2-state chain. These models, the corresponding notation for transitions between states, and the corresponding differential equations are shown in Figure 1.1. The following sections will show the obtained simulations for each ionic current, discussing briefly the available experimental information and the role of each current in α -cells. The final current-to-voltage (IV) curves obtained for all channel models using parameters given in Table 7.2, are shown in Figure 7.1.

7.2.1 A-type K^+ channels

We have considered two voltage-dependent potassium currents in this work: the $I_{K_{DR}}$ and the I_{K_A} . These currents are named "outward currents" since channels allow K^+ to go out of the cell when they are open, in contrast to calcium and sodium currents which are named "inward currents", I_{K_A} is due to $K_V4.3$ channels, a voltage-gated potassium channel type which is present in alpha cells, neurons and myocytes. In all these cell types, I_{K_A} plays a very important role since it regulates membrane potential and it initiates repolarisation after action potentials [4, 141]. Some sophisticated models simulate $K_V4.3$ channel behaviour in other cell types (not alpha cells) (see for example [191]). In all of these models there are several Closed states, one Open state and several Inactive states, including Open-Inactive and Closed-Inactive states. Because of its kinetics, it resembles voltage-gated sodium currents: it activates at negative membrane potentials, presents a sustained steady-state current and shows voltage-dependent rapid inactivation. In accordance, we propose a four-state minimal model for I_{K_A} (see figure 1.1(c)). In alpha cells, I_{K_A} activates above -50 to -40 mV and exponentially increases with depolarization. It exhibits voltage-dependent inactivation with half-maximum point at -68 mV [76]. In other cell types (not α -cells) unitary conductance of $K_V4.3$ channels has been established between 12 to 19 pS, for asymmetrical internal and external K^+ concentrations [4], so we assume a value of 12 pS for our simulations since alpha cells are commonly exposed to asymmetrical K^+ quantities. In Figure 7.1(a) we show the simulated I_{K_A} currents obtained for the activation and deactivation voltages proposed by [76], and with the parameters given in Table 7.2.

7.2.2 DR-type K^+ channels

$I_{K_{DR}}$ is produced by $K_V2.1$ channels which are potassium channels managed by voltage; these channels are found both in alpha and beta cells [80]. In beta cells, the activation threshold has been found at -20 mV and its IV curve shows that current grows as depolarization increases [175]. This current does not exhibit any inactivation so we propose a minimal two-state (Open-Close) model, as shown in Figure 1.1(a). The unitary conductance of $K_V2.1$ channels has been estimated in 30.1 ± 8.0 pS for neural stem cells [169]. Figure 7.1(b) shows the simulated $I_{K_{DR}}$ currents produced with the two-state model and the parameters given in Tables 7.1 and 7.2.

7.2.3 Na^+ channels

Na^+ channels are completely voltage driven, and they have been modelled with many Closed and Inactive states in addition to one Open state, so that the channel may inactivate from the Open or the Closed states [184]. Our minimal model then includes four states: one Closed, one Open and two Inactive states, as shown in Figure 1.1(c). Sodium channels activate and inactivate as a function of membrane potential with a threshold voltage in the range of -30 to -20 mV [76, 9, 186]. Single channel properties of these channels have not been estimated in α -cells. In Purkinje cells, a unitary conductance of 12 pS using 140 mM of external sodium concentration, as well as a channel population of 167 channels per square micron, have been estimated [164]. In squid axon, unitary conductance was estimated as 14 pS, with a channel population of 180 per square micron [184]. In alpha cells, an activation voltage of -30 mV has been reported as well as a half-maximal inactivation voltage of -42 mV [9]. This work also reports that approximately 200 pA are obtained for a depolarization of -70 to 0 mV, although a much larger current (about -545 pA) has been reported in other work [76]. On the basis of this, we take a unitary conductance of 12pS for voltages less than 10 mV, and 4 pS for greater voltages. Activation and inactivation voltages are taken from [9]. Estimated parameters are given in Table 7.2. In Figure 7.1(c) we show simulated I_{Na} currents with these values taking into account that the model should reproduce the fast activation-deactivation kinetics in a time scale below 5 ms, as observed in alpha-cell experiments [9, 76].

7.2.4 T-type Ca^{2+} channels

Two types of Ca^{2+} channels are considered: the T- and the N-. The T-type channels have been modelled as having one Open and many Inactive and Closed states, with possible transitions from/to Inactive to/from Open and Closed states [161]. So, a model should include Closed, Open and Inactive states, and should take into account that the channel may inactivate from the Open and the Closed states. Since these channels exhibit Open-state and Closed-state inactivation, and considering that both inactive states reach a fast equilibrium [161], we are proposing a minimal 3-state model (Figure 1.1(b) for which transitions to the Inactive state from the Open or the Closed states are similar.

There are two different experimental observations for T- currents in alpha cells concerning activation voltage: -40 mV [76, 101, 102] and -60 mV [101, 102]. Considering

these experimental works in order to define the parameters of our model, we are assuming that T-type calcium channels activate above -60 mV (in agreement with the proposed role of pacemakers for T- channels [141, 199]), and that the peak current (~ 27 pA) is reached at -20 mV . We are taking the unitary conductances reported for neurons: 4.2 pS for voltages above -60 mV (broader range), 8.4 pS below -60 mV, and 2 pS for positive voltages to obtain small currents [17].

It is well worth noticing that modeling inactivation for T- channels is not easy since inactivation and recovery could bypass the Open state [161]. In alpha cells, the I_{Ca_T} is transient, fast activated and seems to be rapidly inactivated in a voltage-dependent manner [102]. Moreover, T- currents exhibit an overcrossing behaviour over depolarization [17], so peak currents do not follow the hierarchy of steady-state currents. Thus, to estimate parameters for the T- channel model we used a routine `channel` that calculates dynamic solutions instead of steady-state values, considering a half maximal inactivation at -45mV [76]. Deactivation has to be fixed to achieve a transient behaviour in the first few milliseconds. Figure 7.1(d) shows the resultant I_{Ca_T} currents obtained with the parameters shown in Table 7.2.

7.2.5 N-type Ca^{2+} channels

N-type calcium channels do not exhibit transitions from the Open to the Inactive state, and they exhibit some calcium inactivation [94]. Hence, we propose a minimal model with Open, Closed and Inactive states with possible transitions only from the Open to the Closed and from the Inactive to the Closed, and viceversa, i.e., transitions q_{02} and q_{20} are zero. An important dependence included in the inactivation rate is $\Delta Ca = Ca_o/Ca_i$, which estimates the increase in the internal calcium concentration ($[Ca^{2+}]_i$) compared to the external concentration ($[Ca^{2+}]_o$). In this calculation we are assuming that $[Ca^{2+}]_o$ remains constant at 2.5mM, which is reasonable since the external medium is four orders of magnitude greater than the internal concentration (Basal $[Ca^{2+}]_i \sim 0.1\mu M$), and that $[Ca^{2+}]_i$ is varying each time step. This is done assuming local diffusion along 100 nm from the cell membrane without buffering. We have made some tests with buffered diffusion and the results have shown that inactivation only varies by a constant factor. So, it is valid to use our approximation to estimate an upper limit for calcium-dependent inactivation.

I_{Ca_N} activates between -40 and -20 mV [94]. Single-channel data has been measured in neurons (where unitary conductance is between 13 to 15 pS [94]) and in embryonic kidney cell lines (where unitary conductance is 12 pS [50]). In alpha cells, the N-current represents about one third of the total calcium current (the rest is L- and T-current), and it has been estimated in ~ 50 pA when the cell becomes depolarised from -70 to +10 mV [111]. In the cited paper, the activation and inactivation voltage have been estimated in -20 mV and -31 mV, respectively, so we take them as fixed values for the model, as well as 13 pS of unitary conductance. Simulated I_{Ca_N} currents, obtained with the parameters given in Table 7.2, are shown in Figure 7.1(e).

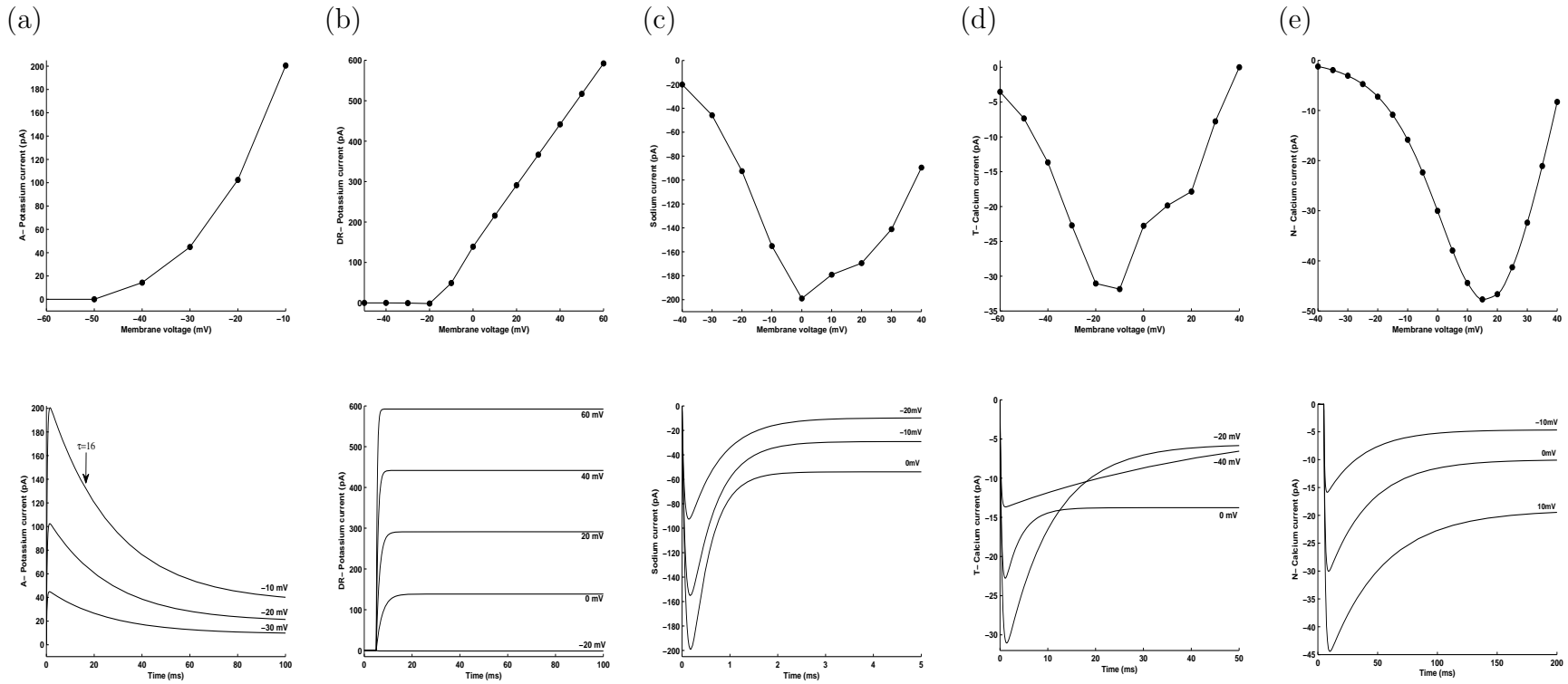


Figure 7.1: (TOP) Simulated current-to-voltage (IV) curves for all channels. (a) A-type potassium channels, (b) DR-type potassium channels, (c) Sodium channels, (d) T-type calcium channels, and (e) N-type calcium channels. (BOTTOM) Simulated dynamic currents following the experimental protocols reported in the references. Notice differences in time scales. (a) I_{K_A} . Arrow over the largest current indicates the value of our time constant ($\tau = 16ms$) which is in agreement with experimental findings [76]. (b) $I_{K_{DR}}$ [175]. (c) I_{Na} [9]. (d) I_{CaT} [102]. Currents overcross, as observed in experiments [17]. (e) I_{CaN} [111].

Table 7.3: Estimated conductances and channel densities in α -cells

	Ca_T	Ca_N	Na	K_A	K_{DR}
Estimated number of channels	694	202	2554	1631	251
Single-channel conductance (pS)	4.2	13	12	12	30
Max. Shell conductance (nS)	2.9	2.6	30.6	19.5	7.5
Density (channels per μm^2)	2.2	0.6	8.1	5.2	0.8

Density was estimated considering a spherical alpha cell of radius= $5 \mu m$.

7.3 Discussion

The ionic currents simulated here are based on minimal state models for those ionic channels related to glucagon secretion in pancreatic alpha cells [141]. The state model approach for channel kinetics could highlight information about the main independent variables controlling channel gating [155]. This is particularly interesting in relation to alpha cells, as it could explain how electrical activity is related to glucagon release, and how channel functioning could affect glucose regulation. In agreement with the experimental observations we have considered that channel activation and deactivation are functions of the membrane voltage. Moreover, we have fixed deactivation parameters for fast changing currents (I_{Ca_N} , I_{Ca_T} , I_{Na} , and I_{K_A}), to efficiently estimate model parameters. These constraints helped to improve model identifiability [124]. For channel inactivation, we have assumed that channels inactivate in a sigmoidal manner, considering the half-inactivation voltage values reported in alpha cell experiments. For N-type calcium channels, we also found it necessary to include a dependence on external and internal calcium concentrations to correctly simulate inactivation. This fact links N- calcium current to a main role in calcium influx and calcium homeostasis. This is interesting since this influx may trigger glucagon release, as discussed in [80, 141].

Another topic emerging from our analysis are whole-cell conductances and channel populations in alpha cells. Shell conductances are estimated as the maximal number of open channels multiplied by the unitary conductance. Although the unitary conductance is an intrinsic channel property, the maximal conductance depends on the cell type since it is a function of total channel population and opening probability. Based on our estimations, maximal whole-cell conductances for an alpha cell seem to be graded as follows: $g_{Na} \simeq g_K \gg g_{Ca}$, where each ion conductance g_x is calculated as the product of the estimated channel population and the unitary conductance, and $g_{Ca} = g_{Ca_T} + g_{Ca_N}$ and $g_K = g_{K_A} + g_{K_{DR}}$ (see Table 7.3). Our whole-cell conductance values highly agree with those used in a modelling work for alpha cells based on the Hodgkin-Huxley approach [34]. Our channel densities are also in the same magnitude order than values found in chromaffin and beta cells and used by some modelling works [98, 123]. We emphasize that our estimated conductances indicate that alpha cells are highly permeable to sodium and potassium which mainly manage action potentials, depolarising and repolarising the cell respectively [80]. Channel densities, as well as single-channel currents in alpha cells, are still not known. This is probably because these cells are scarce and it is difficult to isolate them [141]. To make a comparison, it has been reported that mouse pancreatic beta cells contain less than 500 L-type calcium

channels, which corresponds to a density of 0.9 channels per square micron [10]. It is well worth noticing that our estimated channel population for N-type calcium channels in alpha cells is in the same order, since we have ~ 200 , which would correspond to a density of 0.6 (see Table 7.3). This finding is strongly relevant since both, L-type and N-type calcium channels, play a main role in insulin and glucagon secretion, respectively [10, 141].

The present work attempts to bridge the gap between electrophysiological recordings and modeling related to glucagon secretion. Our final aim is to simulate the whole alpha-cell electrical activity observed during low-glucose periods, which involves all channel models working together; this complex simulation will be better understood keeping minimal models. These state models are able to simulate interesting experimental conditions, such as channel knocking or specific therapeutic inhibitions through changes in channel properties. Another interesting goal for the future is to model zinc influence on the alpha-cell electrical activity. This is relevant since it has been proposed that zinc ions, co-secreted with insulin from neighbouring beta cells, might be involved in the suppression of glucagon secretion [168]. This suppressive effect depends on the action of zinc on alpha-cell K_{ATP} channels, opening them and inducing membrane potential hyperpolarization, which leads to the inhibition of glucagon secretion. In order to study the electrical activity related to glucagon secretion following physiological protocols, the state modeling approach is adequate because these models are suitable to be used in microscopic simulations. These kind of simulations allow to understand secretion in exocytotic zones as well as the role of channel clustering, buffered Ca^{2+} diffusion and Ca^{2+} triggering in release, as discussed in Chapter 5, for human chromaffin cells.

Conclusions

Modeling cellular processes can be considered a powerful approach to study subcellular mechanisms that underly the physiological functions observed in humans and other animals. Cellular models allow researchers to link macroscopic behaviour with those biological elements that may be studied using a model prediction [125]. During the development of the present thesis, our main goals have been:

- To develop mathematical models, based on original or published experimental data on Ca^{2+} in each of the studied cell types, which allows us to unveil the role of main sub-cellular mechanisms in the observed Ca^{2+} behaviour.
- To implement models in an adequate geometry, based on experimental information, to study local and average Ca^{2+} dynamics, Ca^{2+} influx, and Ca^{2+} distribution in time and space.
- To simulate secretion occurring in specific time scales, and to relate vesicle or granule fusion and release with the underlying cellular features associated with Ca^{2+} signalling.

Models that study Ca^{2+} dynamics in simplified geometries as spheres or rectangular compartments, in various cell types such as synapses [166], neuroendocrine cells [98], and pancreatic beta cells [54], have been reported. In these geometries one may simulate an accurate Ca^{2+} distribution only when the quantity of Ca^{2+} can be considered homogeneous in a certain space, and for a time span. However, geometric simplifications may overlook realistic spatial Ca^{2+} distributions, that may lead to local secondary processes triggered by Ca^{2+} . Thus, recent works have studied spatiotemporal behaviour of intracellular Ca^{2+} considering inhomogeneous conditions [31]. For the studied cases in this thesis, we have implemented our models considering both approaches: for alpha cells, it was adequate to apply the Shell model for calculating $[Ca^{2+}]_i$ near the membrane, using the cytoplasmic Ca^{2+} concentration; for human chromaffin cells, Ca^{2+} dynamics for a long time scale was adequately simulated considering the same

approach, but this modeling tool was unable to explain the triggered secretion for a short time scale; and for bovine chromaffin cells, we applied a cylindrical model with non-homogenous distribution of subcellular mechanisms to reproduce the spatiotemporal Ca^{2+} distribution observed in experiments, so it was necessary to use microscopic models, as in the calyx of Held, to simulate fast secretion.

In a cell, when a Ca^{2+} channel opens in response to membrane depolarization, a Ca^{2+} microdomain is formed around the channel. Inside this microdomain, elevations of intracellular Ca^{2+} are steeper than in the cytosol, and these increments change very fast in synapses, but not so fast in neuroendocrine cells [147]. In synapses, nanodomains are formed because of the small distance (tens of nanometers) between channel clusters and vesicles, whereas in neuroendocrine cells the distance between these subcellular mechanisms is greater (hundreds of nanometers), leading to macrodomains. Nano- and micro-domains have gained importance since they seem to be responsible for the fast component of secretion evoked by action potentials [131]. Therefore, in order to study Ca^{2+} -triggered secretion in both cell types, and even in endocrine cells, models and computational implementations must be able to reproduce the actual spatial organization, and the characteristic response times. For synaptic terminals and for the fast secretion evoked in neuroendocrine cells, geometries that allow non-uniform location of channels and vesicles are needed, as well as an implementation with spatial resolution around nanometers, and temporal resolution around microseconds [7]. In contrast to these features, slow secretion exhibited by neuroendocrine and endocrine cells may be modeled in more regular geometries that cover the whole cell, where uniform distributions of channels and vesicles are assumed, since slow Ca^{2+} -triggered secretion is less sensitive to local Ca^{2+} increases, but more sensitive to the spatiotemporal Ca^{2+} dynamics that includes other Ca^{2+} controlling mechanisms [113]. Indeed, slow secretion is commonly induced by substances such as glucose or hormones, and this cellular process seems to be controlled by long timescale Ca^{2+} signals, i.e., Ca^{2+} oscillations [41, 142]. Then, models for slow Ca^{2+} and secretion dynamics could be implemented with a spatial resolution around microns and a higher time step, which open the possibility to simulate longer periods (up to minutes) in a reasonable computational time.

With regard to fast secretion, the required model features are well achieved using Monte Carlo methods in small-sized geometries that emulate an active zone, or a microdomain. Using these methods, some works simulate Ca^{2+} profiles close to Ca^{2+} channels, and the associated Ca^{2+} -triggered secretion occurring in the vicinity of Ca^{2+} channels in the time scale of microseconds [12, 13, 69, 72, 163]. However, these works implement a cubic or spherical domain, and consider a single channel or a uniform arrangement of channels and vesicles, which are not compatible with real microdomains and channel-to-vesicle organizations found in synaptic terminals [162]; in particular, in the calyx of Held [120]. Therefore, our Active-zone and Cytoskeleton-cage models are intended to improve these approaches by studying local Ca^{2+} dynamics when Ca^{2+} channels and vesicles are not uniformly distributed, and even more, in correlated locations. The implementation of our models in a three-dimensional grid allows us to compute how many calcium ions are moving, in a nanometer size scale and in a microsecond time scale. Local Ca^{2+} signal managed by channel organization and its effects on fast secretion have been analyzed.

For intermediate and slow secretion, an adequate model should incorporate not only Ca^{2+} channels but other Ca^{2+} sources, such as endoplasmic reticulum, exchangers or mitochondria. Depending on the particular cell type, each of these sources may have more influence on the Ca^{2+} dynamics associated with exocytosis. Indeed, it is important to define which steps of the exocytotic pathway will be modeled since Ca^{2+} modulates not only the final steps leading to vesicle fusion, through Ca^{2+} binding to the vesicle sensor (as discussed in Section 1.1.3), but it also participates in other intermediate steps [24]. Temporal and spatial scales are linked to this decision because if only the final steps are to be modeled, it can be enough to simulate the secretory response of an active zone in a short time scale. On the one hand, the binding and unbinding rates of the calcium sensor are in the order of tens to hundreds of reactions, per micromolar and per second, meaning that if $[Ca^{2+}]_i$ reaches one micromolar, then in ten milliseconds the fastest reaction will take place. On the other hand, the Ca^{2+} signal that triggers these reactions is mainly due to Ca^{2+} channels, so it is more important to have high resolution than a large size. These time and size scales are associated with the fast component of exocytosis in chromaffin cells, then, these cellular process is suitable to be modeled with Monte Carlo methods. However, when secretion is evoked by prolonged stimulations, and is mediated by a slow Ca^{2+} dynamics, many other mechanisms and exocytotic steps come into great importance.

In alpha cells, glucagon secretion is induced by keeping a low glucose level for several minutes, and the secretory response takes also some minutes to become stable, as observed experimentally [83], and as supported by our modeling results shown in Chapter 6. Then, the relevant simulation times are in the order of tens of minutes, but the rate constants in our glucagon secretion model for granule resupply, and Ca^{2+} binding and unbinding are in the order of 10 per second, and 1 per micromolar per second, respectively. These values imply that, if $[Ca^{2+}]_i$ reaches one micromolar, at most one reaction will occur in one tenth of second, i.e., a time step below 0.1 seconds will be enough, although it will take above 6,000 time steps to simulate just 10 minutes of secretion, without simulating the associated Ca^{2+} dynamics. The computational time of the simulation grows rapidly if one considers that to correctly simulate slow Ca^{2+} dynamics in alpha cells, i.e., Ca^{2+} oscillations, we may need to include at least, Ca^{2+} channels, the Na^+ - Ca^{2+} exchanger, the endoplasmic reticulum, and the buffered diffusion of Ca^{2+} , which are the main mechanisms participating in Ca^{2+} dynamics involved in β -cell secretion [29, 57]. As simulated and discussed in Chapter 7, the maximal open probability for Ca^{2+} channels are in the order of 10^{-1} to 10^{-2} per millisecond (from Table 7.2), so an acceptable time step should be less than 10 ms. Thus, if we try to couple the Ca^{2+} channel models to the secretion model to study the whole stimulus-secretion pathway in alpha-cells, the simulation of the same above-mentioned 10 minutes would take at least 60,000 time steps. Notice that this coupling implies working with time scales with a difference of four orders of magnitude (milliseconds to minutes). One of our future goals is intended to solve this impediment, because stimulus-secretion coupling in α cells remains uncertain [80], and it is interesting for the experimental group we are collaborating with. As a first idea, we have run some uncoupled simulations of electrical currents produced during an action potential, and some other simulations intended to unveil the main mechanisms involved in the generation of glucose-induced Ca^{2+} oscillations.

The study of secretion process in human chromaffin cells was highly remarkable from a multiscale perspective. Secretion evoked by pulse depolarizations in these cells shows two components, rapid and slow, as described for neuroendocrine cells in other species [97], although the relevant times for each component does not coincide with any of them. Our modeling study revealed that not only these two components can be related to two different populations of vesicles, as reported for other species [190], but they seemed to be influenced by different Ca^{2+} signals. Slow secretion could be reproduced by our Shell model that assumes homogeneity and a uniform distribution of Ca^{2+} channels and vesicles, but fast secretion was correctly predicted only by our Active-zone model, considering a cluster organization of Ca^{2+} channels, close to a small group of vesicles. For both models, the same basic Ca^{2+} -regulating mechanisms were considered (diffusion, buffering, and Ca^{2+} -binding by the vesicle sensor), so the differential equations to be solved were the same in both approaches. However, the Shell and the Active-zone model interpret these equations differently, in a deterministic and a stochastic manner, respectively, hence equations were solved with convenient mathematical methods, as discussed in Section 1.2. This may be understood as cellular secretion in this cell type is more influenced by stochastic or deterministic features of the Ca^{2+} signal, depending on the stimulation level, as discussed for other cell types [39].

Our results in human chromaffin cells indicate that the Ca^{2+} signals triggering the two secretory components are influenced by two different spatiotemporal features: fast secretion, by local Ca^{2+} elevations i.e., calcium microdomains, whereas slow secretion, by global Ca^{2+} behaviour. Secretion in these neuroendocrine cells are a nice example of a physiological phenomena underlying multiscale variables, making it necessary to be modeled in two time and size scales: short time scale, in the order of milliseconds, and long time scale, in the order of seconds. The time step used in most simulations (11 microseconds) implies a spatial resolution of 100 nm, which means that a 100-*ms* simulation takes about 10,000 time steps; but for a 5-s simulation, it takes 50 times more, because of the timescale difference of one order of magnitude. Moreover, since fast secretion evoked by the 10-*ms* pulse was accurately predicted only when the spatial resolution was fixed at 50 nm, reducing the time step to 2.8 microseconds, the differences in time scales were incremented, and the computing times too. It is important to emphasize that the same macroscopic behaviour exhibited by the cell in response to stimulation, i.e., hormone release, may be regulated in very different manners by mechanisms acting at different spatial levels, and with different characteristic times.

As discussed above, the study of three cell types, namely the calyx of Held, the chromaffin cell, and the alpha cell comprehends secretion processes taking place in milliseconds (fast secretion), seconds (intermediate secretion), and minutes (slow secretion). These time scales of secretion correspond in turn to small (active zone) up to large (whole cell) regions to be modeled, and lead finally to short up to long simulations. In Table 8.1 we show the studied cell types and the corresponding developed models for ionic channels. In Table 8.2 we summarize the proposed models, the subcellular mechanisms, and the mathematical methods used to solve them, as discussed in Section 1.3. As expressed in this table, the Active-zone and the Cytoskeleton-Cage models include Ca^{2+} channels, fixed and mobile buffers, and diffusion, in order to simulate Ca^{2+} dynamics. These subcellular mechanisms were used to study the spatiotemporal

aspects of exocytosis in the calyx of Held and in bovine chromaffin cells. In fact, the use of Monte Carlo methods makes it feasible to evidence intracellular processes occurring in the order of micro and milliseconds, as well as to study the spatial organization of the secretory machinery at the size of nanometers, as expressed in Table 8.3. On the other hand, the Shell model includes a fixed buffer, Ca^{2+} diffusion and Ca^{2+} extrusion, as stated in Table 8.1, to adequately simulate Ca^{2+} dynamics in a long timescale. This model was configured to simulate secretion in human chromaffin cells and in alpha cells considering a whole cell level, in the scale of microns. Since the experimental data in both cases range between seconds to minutes, useful simulations should be run in the same time scale, so continuous methods (such as finite differences and integration methods, named in Table 8.2) provide us an adequate way to solve the model in a reasonable computing time. Hence, we were able to study vesicle pool dynamics in human chromaffin cells in the scale of seconds, and to study glucose-induced glucagon secretion in alpha cells in the scale of minutes, as expressed in Table 8.3.

The main hypothesis of this thesis was that cellular secretion, mainly controlled by intracellular calcium dynamics, exhibit similitudes, even between different cell types, which makes it possible to share models without forgetting particular cell characteristics. Therefore, our proposed models were thought to cover: 1) The nature and characteristics of the stimulus needed to trigger an exocytotic event in experiments, and, 2) The dynamic behaviour of intracellular calcium, related to secretion, which determines the relevant time and size scales. These two aspects comprehend the coupling between the macroscopic phenomenon observed in experiments, where a particular stimulus induces secretion, and the microscopic events leading to the observed response. Then, the models would be acting as theoretical tools to infer knowledge about how the stimulus-secretion coupling is achieved inside a cell. Our approach has been to propose simple models that can be adapted to reproduce a specific experiment in a cell type, and at the same time, to share models of subcellular mechanisms involved in the exocytotic process. To follow this approach, we have chosen the mathematical methods to solve the models under a multiscale perspective, since the couple of several spatiotemporal scales need to be considered.

The process of creating a mathematical model, to be implemented on a computer, which could be of relevance for the interpretation of experimental data and for enlightening disease causes, requires several modeling tasks and feedback from experimental researchers. Modeling tasks can be summarized as collecting data about the proposed hypothesis (data mainly comes from experiments, databases and scientific papers), integrating data, proposing models and estimating parameters, and finally, validating the model, as suggested in [194]. Integration of biological models and solving methods is a delicate task that requires the use of special description languages, frameworks, and computational implementations. Moreover, when the biological phenomenon to be studied involves many spatiotemporal levels, leading to different time and size scales in model parameters. Some efforts have been reported, mainly in the recent years, about integrating all modeling levels. The basic level is the model description; to accomplish it, some description languages have been proposed to standardize the representation of biological models at cellular or subcellular levels, and to facilitate information exchange, such as SBML [88] and CellML [106]. At the second and third level, some examples of formal frameworks have been implemented, ranging from those

oriented to solve biochemical systems [133], cellular phenomena [107], and reaction pathways [52], to those that implement Shell models [176] and Monte Carlo schemes [118]. All these computational environments are nice examples of how diverse could be data on biological research, and how important the implementation of the modeling solution is. It is noticeable that all of them are general, user-friendly software developed and supported by a team, and each one provides its own possibilities to model a complex biological system. In contrast, our framework constitutes an original effort because it is an expert-defined solution intended to study cellular secretion along with Ca^{2+} dynamics, in a multiscale environment. As far as we know, there has been no previous study on secretion in several cell types, covering different spatial and temporal scales.

Integration of multiple spatiotemporal scales is also a clue factor to achieve data integration and model design. In this sense, examples of research efforts can be found on integrating multiscale physiology in the heart [23, 89], solving multiscale stochastic kinetic reactions [43], and integrating multiscale models of angiogenesis [144]. For the cell types studied in the present thesis, original data was produced following experimental protocols that pose many questions on the stimulus-secretion coupling in these cells. Each cell type was specific, with own values for size, secretion times, relevant stimulation, and Ca^{2+} dynamics. Therefore, our basic modeling frameworks were suited to fit these specifications and to simulate Ca^{2+} -triggered exocytosis. Up to now, we have not used any description language, but have shared common subcellular models between cells, and have used stochastic and deterministic solutions considering real cellular behaviour and features. This makes the integration not an easy task, although we have done it in a static manner, as a first step, giving priority to computational speed. However, we have considered as a future goal, to achieve a dynamic integration of models based on reported methodologies where a controlling module deals with data exchanging, program running and schedule [144]. We keep in mind that our biomedical engineering goal should be to participate along with experts to answer the posed questions and hypothesis, based on modeling tools, towards a thorough understanding of cellular secretion processes.

Table 8.1: Studied cell types and modeled ionic channels

CELL TYPE	CHANNEL TYPES
Calyx of Held	P-type Ca^{2+}
Bovine chromaffin cells	P- and L-type Ca^{2+}
Human chromaffin cells	—
Alpha cells	Ca^{2+} (N- and T-type), Na^+ , K^+ (A- and DR-type)

Table 8.2: Models and solving methods

MODEL	SUBCELLULAR PROCESS	SOLVING METHOD
Active-Zone (AZ) and Cytoskeleton-cage (CC)	Ca^{2+} -channel influx	Monte Carlo
	Ca^{2+} and buffer diffusion	Random walk
	Buffer kinetics†	Monte Carlo
	Vesicle-fusion kinetics	Monte Carlo
Shell (S)	Ca^{2+} diffusion	Crank-Nicholson
	Endogenous buffer kinetics	Crank-Nicholson
	Ca^{2+} extrusion	Finite differences
	Vesicle-fusion kinetics	Integration

† Fixed and mobile buffers.

Table 8.3: Cell types, spatiotemporal scales, and models

CELL TYPE	TIME SCALE	SIZE SCALE	MODEL
Calyx of Held	Tens of milliseconds	Nanometers	AZ
Bovine chromaffin cells	Hundreds of milliseconds	Few microns	CC
Human chromaffin cells	First milliseconds	Few microns	AZ
Human chromaffin cells	Seconds	Some microns	S
Alpha cells	Seconds to minutes	Some microns	S

Publications derived from this thesis

Papers in peer-reviewed journals

1. V. González-Vélez, G. Dupont, A. Gil, I. Quesada. Model for glucagon secretion by pancreatic α -cells (Submitted).
2. A. Albillos, A. Gil, V. González-Vélez, A. Pérez-Álvarez, J. Segura, A. Hernández-Vivanco, J.C. Caba-González. Exocytotic Dynamics in Human Chromaffin Cells: Experiments and Modeling (Submitted).
3. C.J. Torregrosa-Hetland, J. Villanueva, D. Giner, I. López-Font, A. Nadal, I. Quesada, S. Viniegra, G. Expósito-Romero, A. Gil, V. González-Vélez, J. Segura, L.M. Gutiérrez, The F-actin cortical network is a major factor influencing the organization of the secretory machinery in chromaffin cells, **J Cell Sci**(2011) 124: 727-734.
4. C.J. Torregrosa-Hetland, J. Villanueva, I. López-Font, V. García-Martínez, A. Gil, V. González-Vélez, J. Segura, S. Viniegra, L.M. Gutiérrez, Association of SNAREs and Calcium Channels with the Borders of Cytoskeletal Cages Organizes the Secretory Machinery in Chromaffin Cells, **Cell Mol Neurobiol**(2010) 30: 1315-1319.
5. V. González-Vélez, A. Gil, I. Quesada. Minimal state models for ionic channels involved in glucagon secretion, **Math Biosci Eng** (2010) 7(4): 793-807.
6. J. Villanueva, C.J. Torregrosa-Hetland, A. Gil, V. González-Vélez, J. Segura, S. Viniegra, L.M. Gutiérrez, The organization of the secretory machinery in chromaffin cells as a major factor in modeling exocytosis, **HFSP Journal**(2010) 4(2): 85-92.
7. A. Gil, V. González-Vélez, Exocytotic dynamics and calcium cooperativity effects in the calyx of Held synapse: A modelling study, **J Comput Neurosci** (2010)

28: 65-76.

Other publications

1. A.Gil, V. González-Vélez, J. Segura, C.J. Torregrosa-Hetland, J. Villanueva, I. Lpez, L.M. Gutierrez, Simulation of cytoskeleton influence on spatial Ca^{2+} dynamics in neuroendocrine cells, **BMC Neurosci** (2009) 10(Sup.1): 31.
2. A. Gil, V. González-Vélez, J. Segura, Monte Carlo modelling and simulation of cell exocytosis, **SMO 08: Proc. WSEAS Simulation, Modelling and Optimization, Math Comp Sci Eng** (2008): 122-126.

Oral presentations, posters, and conferences

1. *Modelado y simulación multiescala de la secreción celular controlada por Ca^{2+}* .
Poster presented in the **XXVIII Annual Congress of the Spanish Society of Biomedical Engineering (CASEIB 2010)**.
Universidad Carlos III, Madrid, Spain.
2. *Multiscale modelling of slow and fast exocytotic processes*
Oral presentation in the **Symposium on Interdisciplinary Approaches to Calcium and Secretory Dynamics in Cells: Mathematical Models and Experiments**. (2009)
Universidad de Cantabria, Santander, Spain.
3. *Simulation of cytoskeleton influence on spatial Ca^{2+} dynamics in neuroendocrine cells*
Poster presented in the **Annual Computational Neuroscience Meeting (CNS 2009)**.
Academy of Sciences, Berlin, Germany.
4. *Modelling the dynamics of calcium-triggered cell exocytosis: a Monte Carlo approach*
Oral presentation in the **Workshop and Advanced Course on Deterministic and Stochastic Modeling in Computational Neuroscience and other Biological Topics** (2009)
Centre de Recerca Matemàtica, Universidad de Barcelona, España.

5. *Dynamics of calcium-triggered cell exocytosis*
Oral presentation in the **3rd ESF Conference on Functional Dynamics** (FUNCDYN 2009).
Cascais, Portugal.
6. *Monte Carlo modelling and simulation of cell exocytosis*
Oral presentation in the **8th WSEAS International Conference on Simulation, Modelling and Optimization** (2008).
Universidad de Cantabria, Santander, Spain.
7. *El valor de la información experimental para el modelado de la regulación y la exocitosis controlados por Ca^{2+}*
Conference given in the Instituto de Bioingeniería, (2008).
Universidad Miguel Hernández, Elche, Spain.
8. *Stochastic modeling and simulation of presynaptic secretory dynamics*
Poster presented in **The Cold Spring Harbor/Wellcome Trust Meeting on Computational Cell Biology** (2008).
Wellcome Trust Conference Centre, Hinxton, UK.

B.1 Routines for parameter estimation of channel models

Figure 1.2 shows the main program used to find the best parameter set that fits experimental peak currents for each channel model. The called routines are: **randPar**, **channel**, **minChiDev**. Following, we describe the purpose and arguments of these routine.

randPar(numPar).

Purpose: Generate random values for each parameter, including the number of channels.

Arguments:

Inputs: **numPar**: Number of parameters.

Outputs: Array of random values for all parameters.

minChiDev(I,Iexp).

Purpose: Find the parameter set that gives minimal chi square deviation between the simulated and experimental currents.

Arguments:

Inputs: **I**: Array of simulated peak currents. **Iexp**: Array of experimental peak currents.

Outputs: Index of the best parameter set.

channel(V,p(j)).

Purpose: Calculate peak current at each membrane voltage.

Arguments:

Inputs: **V**: Array of membrane voltages. **p(j)**: The j th parameter set.

Outputs: Array of simulated peak currents at each voltage.

B.2 Routines for the Stochastic models

Figure 1.8 shows the main program used to solve the Stochastic models. The called routines are: **data**, **makegrid**, **chandis**, **vesdis**, **districa**, **chanmod**, **walk**, **kineves**. Following, we describe the purpose and arguments of these routines.

makegrid(imicro,ncomps,ncomph,jl,il,numcom,nt).

Purpose: Routine to make the grid for a conical or a cylindrical domain.

Arguments:

Inputs: **imicro**: selects the geometry of the domain. If **imicro**=1, the selected domain is conical while **imicro**=2 stands for a cylindrical domain. **ncomps**: number of grid points along the radius of the base of the domain. **ncomph**: number of grid points along the depth of the domain.

Outputs: **jl(1:ncomph)**, **il(1:ncomph,jl)**: range of the coordinates of the grid points as a function of depth. **numcom(1:ncomph)**: number of compartments as a function of depth. **nt**: total number of compartments of the domain.

data(deltax,difca,difbf,difbm,di0,fhz,tpulse,tsimul,nmaps,tmap) .

Purpose: transformation of the input data to microscopic quantities used in the simulation and setting of the initial conditions.

Arguments:

Inputs: **deltax**: selected resolution for the simulation. **difca**: diffusion coefficient of Ca^{2+} . **difbf**: diffusion coefficient of buffer 1. **difbm**: diffusion coefficient of buffer 2. **di0**: unitary current (per channel). **fhz**: frequency of delivery of ionic pulses. **tpulse**: duration of each pulse. **tsimul**: duration of the simulation. **nmaps**: number of 2-D calcium maps. **tmap(1:nmap)**: times at which the 2-D calcium maps are obtained.

Parameters: **charge**: number of charges of one ion (default: charge=2).

chandis(iseed,ncha,ie,je).

Purpose: generation of a uniform and random distribution of channels.

Arguments:

Inputs: **iseed**: seed for the simulation. **ncha**: number of calcium channels to be distributed.

Outputs: **ie(1:ncha),je(1:ncha)**: planar coordinates of each channel (the depth coordinate is $k = 1$).

vesdis(iseed,nves,iev,jev).

Purpose: generation of a uniform and random distribution of vesicles.

Arguments:

Inputs: **iseed**: seed for the simulation. **nves**: number of secretory vesicles.

Outputs: **iev(1:ncha),jev(1:ncha)**: planar coordinates of each vesicle (the depth coordinate is $k = 1$).

districa(iseed,numcom,inica,nt,ni).

Purpose: distributes a given species of particle (ions, free buffer molecules,...) all over the domain of simulation, being all compartments of the grid equally probable.

Arguments:

Inputs: **iseed**: seed for the simulation. **numcom(1:ncomph)**: number of compartments of the domain as a function of the depth. **inica**: number of particles to be distributed. **nt**: total number of compartments in the domain.

Outputs: **ni(-il(ncomph,jl):il(ncomph,jl),-jl(ncomph):jl(ncomph),ncomph)**: initial number of particles in each compartment of the grid.

chanmod(V,pchan).

Purpose: calculate the number of calcium ions entering into each compartment containing a channel.

Arguments:

Inputs: **V**: depolarization voltage. **pchan**: array of parameters for the channel model.

Outputs: **ienter(ie(1:ncha),je(1:ncha))**: number of ions for the compartment located at coordinates ie,je (the depth coordinate is $k = 1$).

walk(iseed,ni).

Purpose: implementation of a 3-D random walk algorithm for the movement of particles.

Arguments:

Inputs: **iseed**: seed for the simulation. **ni(-il(ncomph,jl):il(ncomph,jl),-jl(ncomph):jl(ncomph),ncomph)**: number of particles in each compartment of the domain.

Outputs: Updated input variables after the random walk has taken place.

kineves(iseed,ni,nb1,nb2,nbm1,nbm2,nbsf,nbsb,iev,jev).

Purpose: implementation of the kinetic reactions of the buffers (buffer 1 and buffer 2) and the vesicle sensor, in each compartment of the domain.

Arguments:

Inputs: **iseed**: seed for the simulation.

ni(-il(ncomph,jl):il(ncomph,jl),-jl(ncomph):jl(ncomph),ncomph): number of calcium ions in each compartment of the domain.

nb1(-il(ncomph,jl):il(ncomph,jl),-jl(ncomph):jl(ncomph),ncomph): number of free buffer molecules of type 1 in each compartment of the domain.

nb2(-il(ncomph,jl):il(ncomph,jl),-jl(ncomph):jl(ncomph),ncomph): number of free buffer molecules of type 2 in each compartment of the domain.

nbm1(-il(ncomph,jl):il(ncomph,jl),-jl(ncomph):jl(ncomph),ncomph): number of bound buffer molecules of type 1 in each compartment of the domain.

nbm2(-il(ncomph,jl):il(ncomph,jl),-jl(ncomph):jl(ncomph),ncomph): number of bound buffer molecules of type 2 in each compartment of the domain.

nbsf(-il():il(),-jl():jl()): number of free binding sites for each secretory vesicle.

nbsb(-il():il(),-jl():jl()): number of bound binding sites for each secretory vesicle.

iev(1:nves),jev(1:nves): planar coordinates of vesicles (depth is 1).

Outputs: Updated input variables after kinetic reactions.

B.3 Routines for the Deterministic model

Figure 1.9 shows the main program used to solve the Deterministic model. The called routines are: **difb**, **ica**, **secre**. Following, we describe the purpose and arguments of these routines.

difb(cai,b,dt).

Purpose: Update free Ca^{2+} and buffer concentrations in each shell.

Arguments:

Inputs: **cai**: Array of last free Ca^{2+} concentrations in all shells. **b**: Array of last free buffer concentration in all shells. **dt**: Time step.

Outputs: Updated **cai** and **b** arrays.

ica(dt,tsim).

Purpose: Read experimental data of Ca^{2+} current, and adequate it to the specified time step and simulation time.

Arguments:

Inputs: **dt**: Time step. **tsim**: Simulation time.

Output: Array of Ca^{2+} current values at each \mathbf{dt} , computed using a spline interpolation of experimental values.

secre(**cap**,**tsim**).

Purpose: Calculate the number of fused vesicles along the simulation time.

Arguments:

Inputs: **cap**: Cell capacitance. **tsim**: Simulation time.

Outputs: Arrays of fused vesicles and times.

Bibliography

- [1] M. Alber, T. Hou, J.A. Glazier, and Y. Jiang. Special issue on multiscale modeling in biology: Introduction. *Multiscale Model Simul*, 3:vii–viii, 2005. [Cited in p. 1].
- [2] N.L. Allbritton, T. Meyer, and L. Stryer. Range of messenger action of calcium ion and inositol 1,4,5-trisphosphate. *Science*, 258:1812–1815, 1992. [Cited in p. 13].
- [3] Y.D. Álvarez and F.D. Marengo. The immediately releasable vesicle pool: highly coupled secretion in chromaffin cells and other neuroendocrine cells. *J Neurochem*, 116:155–163, 2011. [Cited in pp. 51, 55, 63, and 64].
- [4] G.C. Amberg, S.D. Koh, Y. Imaizumi, S. Ohya, and K.M. Sanders. A-type potassium currents in smooth muscle. *Am J Physiol Cell Physiol*, 284:583–595, 2003. [Cited in p. 90].
- [5] G.J. Augustine. How does calcium trigger neurotransmitter release? *Curr Opinion Neurobiol*, 11:320–326, 2001. [Cited in p. 28].
- [6] G.J. Augustine, M.P. Charlton, and S.J. Smith. Calcium entry and transmitter release at voltage clamped nerve terminals of squid. *J Physiol*, 367:163–181, 1985. [Cited in p. 51].
- [7] G.J. Augustine, F. Santamaria, and K. Tanaka. Local calcium signaling in neurones. *Neuron*, 40:331–346, 2003. [Cited in pp. vi, 13, and 97].
- [8] S. Barg. Mechanisms of exocytosis in insulin-secreting B-cells and glucagon-secreting A-cells. *Pharmacol Toxicol*, 92:3–13, 2003. [Cited in pp. 72, 73, 77, 86, and 87].
- [9] S. Barg, J. Galvanovskis, S.O. Göpel, P. Rorsman, and L. Eliasson. Tight coupling between electrical activity and exocytosis in mouse glucagon-secreting α -cells. *Diabetes*, 49:1500–1510, 2000. [Cited in pp. 10, 67, 73, 74, 77, 78, 86, 88, 91, and 93].

- [10] S. Barg, X. Ma, and L. Eliasson et al. Fast exocytosis with few ca channels in insulin-secreting mouse pancreatic b cells. *Biophys J*, 81:3308–3323, 2001. [Cited in p. 95].
- [11] M.R. Bennett. The concept of a calcium sensor in transmitter release. *Prog Neurobiol*, 59:243–277, 1999. [Cited in p. v].
- [12] M.R. Bennett, L. Farnell, and W.G. Gibson. The probability of quantal secretion near a single calcium channels of an active zone. *Biophys J*, 78:2201–2221, 2000. [Cited in p. 97].
- [13] M.R. Bennett, L. Farnell, and W.G. Gibson. The probability of quantal secretion within an array of calcium channels of an active zone. *Biophys J*, 78:2222–2240, 2000. [Cited in pp. 2, 13, 28, 29, and 97].
- [14] M.J. Berridge, M. Bootman, and H. Roderick. Calcium signaling: Dynamics, homeostasis and remodeling. *Nat Rev Mol Cell Biol*, 4:517–529, 2003. [Cited in pp. 4, 5, and 12].
- [15] R. Bertram, G.D. Smith, and A. Sherman. Modeling study of the effects of overlapping Ca^{2+} microdomains on neurotransmitter release. *Biophys J*, 76:735–750, 1999. [Cited in p. 29].
- [16] A. Berts, A. Ball, E. Gylfe, and B. Hellman. Suppression of Ca^{2+} oscillations in glucagon-producing α_2 -cells by insulin/glucose and amino acids. *Biochimica et Biophysica Acta*, 1310:212–216, 1996. [Cited in pp. 67 and 68].
- [17] K.C. Bittner and D.A. Hanck. The relationship between single-channel and whole-cell conductance in the T-type Ca^{2+} channel $ca_v3.1$. *Biophys J*, 95:931–941, 2008. [Cited in pp. 92 and 93].
- [18] H.P. Bode, S. Weber, H-C Fehmann, and B. Göke. A nutrient-regulated cytosolic calcium oscillator in endocrine pancreatic glucagon-secreting cells. *Pflugers Arch-Eur J Physiol*, 437:324–334, 1999. [Cited in pp. 67, 68, and 73].
- [19] J.H. Bollmann and B. Sakmann. Control of synaptic strength and timing by the release-site Ca^{2+} signal. *Nat. Neurosci.*, 8:426–434, 2005. [Cited in p. 28].
- [20] J.H. Bollmann, B. Sakmann, and J.G.G. Borst. Calcium sensitivity of glutamate release in a calyx-type terminal. *Science*, 289:953–957, 2000. [Cited in pp. 16, 29, 30, 31, 35, and 36].
- [21] J.G.G. Borst and B. Sakmann. Calcium influx and transmitter release in a fast CNS synapse. *Nature*, 383:431–434, 1996. [Cited in pp. 28, 30, 31, and 33].
- [22] J.L. Bossu, M. De Waard, and A. Feltz. Inactivation characteristics reveal two calcium currents in adult bovine chromaffin cells. *J Physiol*, 437:603–620, 1991. [Cited in p. 46].

- [23] T. Brennan, M. Fink, and B. Rodríguez. Multiscale modelling of drug-induced effects on cardiac electrophysiological activity. *Eur J Pharmac Sci*, 36:6277, 2009. [Cited in p. 101].
- [24] R.D. Burgoyne and A. Morgan. Secretory granule exocytosis. *Physiol Rev*, 83:581–632, 2003. [Cited in pp. vi, 1, 15, and 98].
- [25] R.C. Cannon and G. D’Alessandro. The ion channel inverse problem: Neuroinformatics meets biophysics. *PLoS Computational Biology*, 2:862–869, 2006. [Cited in pp. 7 and 8].
- [26] W.A. Catterall. Structure and regulation of voltage-gated Ca^{2+} channels. *Annu Rev Cell Dev Biol*, 16:521–555, 2000. [Cited in pp. 7 and 28].
- [27] T. Cens, M. Rousset, J.P. Leyris, P. Fesquet, and P. Charnet. Voltage- and calcium-dependent inactivation in high voltage-gated Ca^{2+} channels. *Prog Biophys Mol Biol*, 90:104–117, 2006. [Cited in p. 30].
- [28] S.C. Chapra and R.P. Canale. *Numerical methods for engineers*, chapter Finite difference: Parabolic equations. McGraw-Hill International, New York, 5th. edition, 2006. [Cited in pp. 13, 23, and 25].
- [29] L. Chen, D-S Koh, and B. Hille. Dynamics of calcium clearance in mouse pancreatic β -cells. *Diabetes*, 52:1723–1731, 2003. [Cited in p. 98].
- [30] Y. Chen, S. Wang, and A. Sherman. Identifying the targets of the amplifying pathway for insulin secretion in pancreatic β -cells by kinetic modeling of granule exocytosis. *Biophys J*, 95:2226–2241, 2008. [Cited in pp. 72 and 73].
- [31] Y. Cheng, Z. Yu, M. Hoshijima, M.J. Holst, A.D. McCulloch, J.A. McCammon, and A.P. Michailova. Numerical analysis of Ca^{2+} signaling in rat ventricular myocytes with realistic transverse-axial tubular geometry and inhibited sarcoplasmic reticulum. *PLoS Comput Biol*, 6:e1000972, 2010. [Cited in p. 96].
- [32] T. Collin and et al. Developmental changes in parvalbumin regulate presynaptic Ca^{2+} signaling. *J Neurosci*, 25(1):96–107, 2005. [Cited in pp. 28 and 29].
- [33] A.P.H. de Jong and M. Verhage. Presynaptic signal transduction pathways that modulate synaptic transmission. *Curr Opin Neurobiol*, 19:245–253, 2009. [Cited in p. 33].
- [34] P.M. Diderichsen and S.O. Göpel. Modelling the electrical activity of pancreatic α -cells based on experimental data from intact mouse islets. *J Biol Phys*, 32:209–229, 2006. [Cited in pp. 2 and 94].
- [35] FA Dodge and R Rahamimoff. Co-operative action of calcium ions in transmitter release at the neuromuscular junction. *J Physiol*, 193:419–432, 1967. [Cited in p. 28].

- [36] R. Dolmetsch, K. Xu, and R. Lewis. Calcium oscillations increase the efficiency and specificity of gene expression. *Nature*, 392:933–936, 1998. [Cited in pp. 84 and 87].
- [37] W.W. Douglas. Stimulus-secretion coupling: the concept and clues from chromaffin and other cells. *Br J Pharmacol*, 34:453–474, 1968. [Cited in p. v].
- [38] L.S. Dove, L.C. Abbott, and W.H. Griffith. Whole-cell and single-channel analysis of P-type calcium currents in cerebellar purkinje cells of leaner mutant mice. *J Neurosci*, 18:7687–7699, 1998. [Cited in p. 31].
- [39] G. Dupont, A. Abou-Lovergne, and L. Combettes. Stochastic aspects of oscillatory Ca^{2+} dynamics in hepatocytes. *Biophys J*, 95:2193–2202, 2008. [Cited in p. 99].
- [40] G. Dupont, G. Houart, and P. De Koninck. Sensitivity of CaM kinase II to the frequency of Ca^{2+} oscillations : a simple model. *Cell Calcium*, 34:485–497, 2003. [Cited in p. 82].
- [41] G. Dupont, S. Swillens, C. Clair, T. Tordjmann, and L. Combettes. Hierarchical organization of calcium signals in hepatocytes: from experiments to models. *Biochim Biophys Acta*, 1498:134–152, 2000. [Cited in p. 97].
- [42] S.N. Duffy E.M. Adler, G.J. Augustine and M.P. Charlton. Alien intracellular calcium chelators attenuate neurotransmitter release at the squid giant synapse. *J Neurosci*, 11(6):1496–1507, 1991. [Cited in p. 32].
- [43] S. Engblom. Parallel in time simulation of multiscale stochastic chemical kinetics. *Multiscale Model Simul*, 8:46–68, 2009. [Cited in p. 101].
- [44] J. Gromada et al. ATP-sensitive K^+ channel-dependent regulation of glucagon release and electrical activity by glucose in wild-type and $SUR1^{-/-}$ mouse α -cells. *Diabetes*, 53(Suppl.3):S181–S189, 2004. [Cited in p. 68].
- [45] C.P. Fall, E.S. Marland, J.M. Wagner, and J.J. Tyson. *Computational Cell Biology*. Springer-Verlag, New York, 1st edition, 2002. [Cited in pp. 7 and 8].
- [46] L. Farnell and W.G. Gibson. Monte carlo simulation of diffusion in a spatially nonhomogenous medium: A biased random walk on an asymmetrical lattice. *J Comp Phys*, 208:253–265, 2005. [Cited in p. 20].
- [47] M.J. Fedchyshyn and L.-Y. Wang. Developmental transformation of the release modality at the calyx of Held synapse. *J. Neurosci.*, 25(16):4131–4140, 2005. [Cited in pp. 28 and 38].
- [48] L. Fedrizzi, D. Lim, and E. Carafoli. Calcium and signal transduction. *Biochem Mol Biol Edu (BAMBED)*, 36(3):175–180, 2008. [Cited in pp. v and 14].
- [49] F. Felmy and R. Schneggenburger. Developmental expression of the Ca^{2+} -binding proteins calretinin and parvalbumin at the calyx of Held of rats and mice. *Eur J Neurosci*, 20:1473–1482, 2004. [Cited in p. 29].

- [50] Z.-P. Feng, J. Hamid, C. Doering, S.E. Jarvis, G.M. Bosey, E. Bourinet, T.P. Snutch, and G.W. Zamponi. Amino acid residues outside of the pore region contribute to N-type calcium channel permeation. *J Biol Chem*, 276:5726–5730, 2001. [Cited in p. 92].
- [51] E.M. Fenwick, A. Marty, and E. Neher. Sodium and calcium channels in bovine chromaffin cells. *J Physiol*, 331:599–635, 1982. [Cited in pp. 57 and 62].
- [52] Max Planck Institute for Molecular Genetics. A tool for modeling and simulation of cellular systems. <http://pybios.molgen.mpg.de/>. [Cited in p. 101].
- [53] K.M. Franks, T.M. Bartol Jr., and T.J. Sejnowski. A Monte Carlo model reveals independent signaling at central glutamatergic synapses. *Biophys J*, 83:2333–2348, 2002. [Cited in p. 21].
- [54] L.E. Fridlyand, N. Tamarina, and L.H. Philipson. Modeling of Ca^{2+} flux in pancreatic β -cells: role of the plasma membrane and intracellular stores. *Am J Physiol Endocrinol Metab*, 285:E138–E154, 2003. [Cited in p. 96].
- [55] C.J. Gadgil. Size-independent differences between the mean of discrete stochastic systems and the corresponding continuous deterministic systems. *Bull Math Biol*, 71:1599–1611, 2009. [Cited in p. 15].
- [56] D. Gall, E. Baus, and G. Dupont. Activation of the liver glycogen phosphorylase by Ca^{2+} oscillations: A theoretical study. *J Theor Biol*, 207:445–454, 2000. [Cited in pp. 82 and 87].
- [57] D. Gall, J. Gromada, I. Susa, P. Rorsman, A. Herchuelz, and K. Bokvist. Significance of Na/Ca exchange for Ca buffering and electrical activity in mouse pancreatic β -cells. *Biophys J*, 76:2018–2028, 1999. [Cited in p. 98].
- [58] A.G. García, A.M. García de Diego, L. Gandía, R. Borges, and J. García-Sancho. Calcium signaling and exocytosis in adrenal chromaffin cells. *Physiol Rev*, 86:1093–1131, 2006. [Cited in pp. vii, 41, 45, and 51].
- [59] L. Gentile and E.F. Stanley. A unified model of presynaptic release site gating by calcium channel domains. *Eur J Neurosci*, 21:278–282, 2005. [Cited in pp. 2 and 30].
- [60] W.G. Gibson, L. Farnell, and M.R. Bennett. A Monte Carlo analysis of calcium dynamics and facilitation in nerve terminals. *Neurocomputing*, 38-40:17–22, 2001. [Cited in pp. 2 and 21].
- [61] A. Gil and V. González-Vélez. Exocytotic dynamics and calcium cooperativity effects in the calyx of held synapse: a modelling study. *J Comput Neurosci*, 28:65–76, 2010. [Cited in p. 7].
- [62] A. Gil, J. Rueda, S. Viniegra, and L.M. Gutiérrez. The cytoskeleton modulates slow secretory components rather than readily releasable vesicle pools in bovine chromaffin cell. *Neurosci*, 98:605–614, 2000. [Cited in p. 42].

- [63] A. Gil and J. Segura. Ca3D: a Monte Carlo code to simulate 3D buffered calcium diffusion of ions in sub-membrane domains. *Comput Phys Commun*, 136:269–293, 2001. [Cited in p. 21].
- [64] A. Gil and J. Segura. Ca3d: a monte carlo code to simulate 3d buffered calcium diffusion of ions in sub-membrane domains. *Comput Phys Commun*, 136:269–293, 2001. [Cited in p. 23].
- [65] A. Gil, J. Segura, V. González-Vélez, and M. Heckmann. Calcium thresholds and release probability as a result of non-cooperative binding schemes in a calyx-type terminal. In progress. [Cited in p. 17].
- [66] A. Gil, J. Segura, J.A.G. Pertusa, and B. Soria. Monte Carlo simulation of 3 – D buffered Ca^{2+} diffusion in neuroendocrine cells. *Biophys. J.*, 78(1):13–33, 2000. [Cited in pp. 13, 15, 38, and 40].
- [67] A. Gil, S. Viniegra, P. Neco, and L.M. Gutiérrez. Co-localization of vesicles and P/Q Ca^{2+} -channels explains the preferential distribution of exocytotic active zones in neurites emitted by bovine chromaffin cells. *Eur J Cell Biol*, 80:358–365, 2001. [Cited in pp. 42 and 45].
- [68] K.D. Gillis, R. Mössner, and E. Neher. Protein kinase C enhances exocytosis from chromaffin cells by increasing the size of the readily releasable pool of secretory granules. *Neuron*, 16:1209–1220, 1996. [Cited in p. 54].
- [69] I.R. Gilmanov, D.V. Samigullin, F. Vyskocil, E.E. Nikolsky, and E.A. Bukharaeva. Modeling of quantal neurotransmitter release kinetics in the presence of fixed and mobile calcium buffers. *J Comput Neurosci*, 25(2):296–307, 2008. [Cited in pp. 13 and 97].
- [70] D. Giner, I. López, J. Villanueva, V. Torres, S. Viniegra, and L.M. Gutiérrez. Vesicle movements are governed by the size and dynamics of f-actin cytoskeletal structures in bovine chromaffin cells. *Neurosci*, 146:659–669, 2007. [Cited in pp. 42, 43, 46, 48, and 62].
- [71] D. Giner, P. Neco, M.M. Francés, I. López, S. Viniegra, and L.M. Gutiérrez. Real-time dynamics of the f-actin cytoskeleton during secretion from chromaffin cells. *J Cell Sci*, 118:2871–2880, 2005. [Cited in p. 43].
- [72] M.I. Glavinović and H.R. Rabie. Monte Carlo evaluation of quantal analysis in the light of Ca^{2+} dynamics and the geometry of secretion. *Pflug Arch-Eur J Physiol*, 443:132–145, 2001. [Cited in pp. 2, 21, and 97].
- [73] V. González-Vélez and J.R. Godínez-Fernández. Simulation of five intracellular Ca^{2+} -regulation mechanisms in response to voltage-clamp pulses. *Comp Biol Med*, 34(4):279–292, 2004. [Cited in pp. 15, 20, 26, and 73].
- [74] V. González-Vélez and H. González-Vélez. Parallel stochastic simulation of macroscopic calcium currents. *J. Bioinf. Comput. Biol.*, 5(3):755–772, 2007. [Cited in pp. 11 and 30].

- [75] S. Göpel, Q. Zhang, L. Eliasson, X.-S. Ma, J. Galvanovskis, T. Kanno, A. Salehi, and P. Rorsman. Capacitance measurements of exocytosis in mouse pancreatic α -, β - and δ -cells within intact islets of Langerhans. *J Physiol*, 556.3:711–726, 2004. [Cited in pp. 67 and 88].
- [76] S.O. Göpel, T. Kanno, S. Barg, X-G. Weng, J. Gromada, and P. Rorsman. Regulation of glucagon release in mouse α -cells by K_{ATP} channels and inactivation of TTX-sensitive Na^+ channels. *J Physiol*, 528(3):509–520, 2000. [Cited in pp. 90, 91, 92, and 93].
- [77] J.D. Goutman and E. Glowatzki. Time course and calcium dependence of transmitter release at a single ribbon synapse. *PNAS*, 104(41):16341–16346, 2007. [Cited in p. 14].
- [78] B.P. Graham, A.Y.C. Wong, and I.D. Forsythe. A multi-component model of depression at the calyx of Held. *Neurocomp*, 58-60:449–454, 2004. [Cited in pp. 2 and 29].
- [79] J. Gromada, K. Bokvist, W.-G. Ding, S. Barg, K. Buschard, E. Renström, and P. Rorsman. Adrenaline stimulates glucagon secretion in pancreatic A-cells by increasing the Ca^{2+} current and the number of granules close to the L-type Ca^{2+} channels. *J Gen Physiol*, 110:217–228, 1997. [Cited in pp. 67 and 88].
- [80] J. Gromada, I. Franklin, and C.B. Wollheim. α -cells of the endocrine pancreas: 35 years of research but the enigma remains. *Endocrine Rev*, 28(1):84–116, 2007. [Cited in pp. 66, 67, 68, 88, 91, 94, and 98].
- [81] G. Grynkiewicz, M. Poenie, and R.Y. Tsien. A new generation of Ca^{2+} indicators with greatly improved fluorescence properties. *J Biol Chem*, 260:3440–3450, 1985. [Cited in p. 32].
- [82] M. Gurkiewicz and A. Korngreen. A numerical approach to ion channel modelling using whole-cell voltage-clamp recordings and a genetic algorithm. *PLoS Computational Biology*, 3:1633–1647, 2007. [Cited in p. 7].
- [83] N. Gustavsson, S-H Wei, D.N. Hoang, Y. Lao, Q. Zhang, G.K. Radda, P. Rorsman, T.C. Sdhof, and W. Han. Synaptotagmin-7 is a principal Ca^{2+} sensor for Ca^{2+} -induced glucagon exocytosis in pancreas. *J Physiol*, 587:1169–1178, 2009. [Cited in pp. 67, 71, 73, 86, and 98].
- [84] M. Haller, C. Heinemann, R.H. Chow, R. Heidelberg, and E. Neher. Comparison of secretory responses as measured by membrane capacitance and by amperometry. *Biophys J*, 74:2100–2113, 1998. [Cited in p. 2].
- [85] C. Heinemann, R.H. Chow, E. Neher, and R.S. Zucker. Kinetics of the secretory response in bovine chromaffin cells following flash photolysis of caged Ca^{2+} . *Biophys J*, 67:2546–2557, 1994. [Cited in pp. 16 and 51].
- [86] M.H. Hennig and et al. A biophysical model of short-term plasticity at the calyx of Held. *Neurocomputing*, 70:1626–1629, 2007. [Cited in pp. 2 and 29].

- [87] F.T. Horrigan and R.J. Bookman. Releasable pools and the kinetics of exocytosis in rat adrenal chromaffin cells. *Neuron*, 13:1119–1129, 1994. [Cited in p. 54].
- [88] M. Hucka, A. Finney, and H.M. Sauro. The systems biology markup language (SBML): a medium for representation and exchange of biochemical network models. *Bioinformatics*, 19:524–531, 2003. [Cited in p. 100].
- [89] P.J. Hunter and T.K. Borg. Integration from proteins to organs: the physiome project. *Nature Rev Mol Cell Biol*, 4:237–243, Mar 2003. [Cited in p. 101].
- [90] H. Ishihara, P. Maechler, A. Gjnovci, P.L. Herrera, and C.B. Wollheim. Islet β -cell secretion determines glucagon release from neighbouring α -cells. *Nature Cell Biol*, 5:330–335, 2003. [Cited in pp. 68 and 77].
- [91] S. Iwasaki and et al. Developmental changes in calcium channel types mediating central synaptic transmission. *J Neurosci*, 20:59–65, 2000. [Cited in p. 28].
- [92] S. Iwasaki and T. Takahashi. Developmental changes in calcium channel types mediating synaptic transmission in rat auditory brainstem. *J Physiol*, 509:419–423, 1998. [Cited in p. 28].
- [93] M. Juhaszova, P. Church, M.P. Blaustein, and E.F. Stanley. Location of calcium transporters at presynaptic terminals. *Eur J Neurosci*, 12:839–846, 2000. [Cited in p. 18].
- [94] H. Kasai and E. Neher. Dihydropyridine-sensitive and omega-conotoxin-sensitive calcium channels in a mammalian neuroblastoma-glioma cell line. *J Physiol*, 448:161–188, 1992. [Cited in p. 92].
- [95] J. Keener and J. Sneyd. *Mathematical Physiology I: Cellular physiology*, volume 8/I of *Interdisciplinary Applied Mathematics*, chapter Biochemical reactions, pages 1–48. Springer, 2nd. edition, 2009. [Cited in p. 14].
- [96] M.H. Kim, N. Korogod, R. Schneggenburger, W.K. Ho, and S.H. Lee. Interplay between Na^+/Ca^{2+} exchangers and mitochondria in Ca^{2+} clearance at the calyx of Held. *J Neurosci*, 25(26):6057–6065, 2005. [Cited in p. 29].
- [97] K.S. Kits and H.D. Mansvelder. Regulation of exocytosis in neuroendocrine cells: spatial organization of channels and vesicles, stimulus-secretion coupling, calcium buffers and modulation. *Brain Res Rev*, 33:78–94, 2000. [Cited in pp. 2, 51, 56, 72, 86, and 99].
- [98] J. Klingauf and E. Neher. Modeling buffered Ca^{2+} diffusion near the membrane: Implications for secretion in neuroendocrine cells. *Biophys J*, 72:674–690, 1997. [Cited in pp. 2, 11, 13, 32, 46, 51, 54, 56, 62, 64, 74, 94, and 96].
- [99] R.M. Leao and H. von Gersdorff. Synaptic vesicle pool size, release probability and synaptic depression are sensitive to Ca^{2+} buffering capacity in the developing rat calyx of Held. *Braz. J. Med. Biol. Res.*, 42(1):94–104, 2009. [Cited in p. 33].

- [100] A. Lee, T. Scheuer, and W.A. Catterall. Ca^{2+} /calmodulin-dependent facilitation and inactivation of P/Q-type Ca^{2+} channels. *J Neurosci*, 20:6830–6838, 2000. [Cited in p. 28].
- [101] Y.M. Leung, I. Ahmed, L. Sheu, R.G. Tsushima, N.E. Diamant, and H.Y. Gaisano. Two populations of pancreatic islet α -cells displaying distinct Ca^{2+} channel properties. *Biochem Biophys Res Comm*, 345:340–344, 2006. [Cited in p. 91].
- [102] Y.M. Leung, I. Ahmed, L. Sheu, R.G. Tsushima, N.E. Diamant, M. Hara, and H.Y. Gaisano. Electrophysiological characterization of pancreatic islet cells in the mouse insulin promoter-green fluorescent protein mouse. *Endocrinology*, 146:4766–4775, 2005. [Cited in pp. 91, 92, and 93].
- [103] Y.J. Liu, E. Vieira, and E. Gylfe. A store-operated mechanism determines the activity of the electrically excitable glucagon-secreting pancreatic α -cell. *Cell Calcium*, 35:357–365, 2004. [Cited in p. 67].
- [104] R. Llinás, A. Steinberg, and K. Walton. Relationship between presynaptic calcium current and postsynaptic potential in squid giant synapse. *Biophys J*, 33:323–351, 1981. [Cited in p. 51].
- [105] R.R. Llinás, M. Sugimori, and R.B. Silver. The concept of calcium concentration microdomains in synaptic transmission. *Neuropharm*, 34:1443–1451, 1995. [Cited in p. 28].
- [106] C.M. Lloyd, M.D.B. Halstead, and P.F. Nielsen. CellML: its future, present and past. *Prog Biophys Mol Biol*, 85:433–450, 2004. [Cited in p. 100].
- [107] L.M. Loew and J.C. Schaff. The virtual cell: a software environment for computational cell biology. *Trends Biotechnol*, 19:401–406, 2001. <http://vcell.org>. [Cited in p. 101].
- [108] I. López-Font, C.J. Torregrosa-Hetland, J. Villanueva, and L.M. Gutiérrez. t-SNARE cluster organization and dynamics in chromaffin cells. *J Neurochem*, 114:1550–1556, 2010. [Cited in p. 42].
- [109] X.L. Lou, V. Scheuss, and R. Schneggenburger. Allosteric modulation of the presynaptic Ca^{2+} sensor for vesicle fusion. *Nature*, 435:497–501, 2005. [Cited in pp. 2, 16, 28, and 29].
- [110] E.A. Lukyanetz and E. Neher. Different types of calcium channels and secretion from bovine chromaffin cells. *Eur J Neurosci*, 11:2865–2873, 1999. [Cited in p. 45].
- [111] P.E. MacDonald, Y.Z. De Marinis, R. Ramracheya, A. Salehi, X. Ma, P.R.V. Johnson, R. Cox, L. Eliasson, and P. Rorsman. A K_{ATP} channel-dependent pathway within α cells regulates glucagon release from both rodent and human islets of Langerhans. *PLoS Biology*, 5:1236–1247, June 2007. [Cited in pp. 67, 92, and 93].

- [112] I. Manno. Introduction into the monte-carlo method. Report, CERN-INFN, 1994. [Cited in p. 20].
- [113] H.D. Mansvelder and K.S. Kits. Calcium channels and the release of large dense core vesicles from neuroendocrine cells: spatial organization and functional coupling. *Prog Neurobiol*, 62:427–441, 2000. [Cited in p. 97].
- [114] S.J. Le Marchand and D.W. Piston. Glucose supression of glucagon secretion: Metabolic and calcium responses from α -cells in intact mouse pancreatic islets. *J Biol Chem*, 285:14389–14398, 2010. [Cited in pp. 67, 68, 82, and 87].
- [115] F.D. Marengo. Calcium gradients and exocytosis in bovine adrenal chromaffin cells. *Cell Calcium*, 38:87–99, 2005. [Cited in pp. 2, 51, 54, 55, and 57].
- [116] F.D. Marengo and J.R. Monck. Development and dissipation of Ca^{2+} gradients in adrenal chromaffin cells. *Biophys J*, 79:1800–1820, 2000. [Cited in p. 63].
- [117] V. Matveev, R.S. Zucker, and A. Sherman. Facilitation through buffer saturation: Constraints on endogenous buffering properties. *Biophys J*, 86:2691–2709, 2004. [Cited in p. 29].
- [118] Salk Institute for Biological Studies MCell Team. A monte carlo simulator of cellular microphysiology. <http://www.mcell.cnl.salk.edu>. [Cited in p. 101].
- [119] C.J. Meinrenken, J.G.G. Borst, and B. Sakmann. Calcium secretion coupling at calyx of Held goverened by nonuniform channel-vesicle topography. *J. Neurosci*, 22:1648–1667, 2002. [Cited in pp. 2, 27, and 29].
- [120] C.J. Meinrenken, J.G.G. Borst, and B. Sakmann. Local routes revisited: the space and time dependence of the Ca^{2+} signal for phasic transmitter release at the rat calyx of Held. *J Physiol*, 547:665–689, 2003. [Cited in pp. 2, 29, 31, 37, 40, and 97].
- [121] A. Meir and et al. Ion channels in presynaptic nerve terminals and control of transmitter release. *Physiol Rev*, 79(3):1019–1088, 1999. [Cited in pp. vi, 7, and 31].
- [122] N. Metropolis. The beginning of the monte carlo method. *Los Alamos Science (Special issue)*, 1:125–130, 1987. [Cited in p. 20].
- [123] M.E. Meyer-Hermann. The electrophysiology of the β -cell based on single transmembrane protein characteristics. *Biophys J*, 93:2952–2968, 2007. [Cited in pp. 11 and 94].
- [124] L.S. Milesco, G. Akk, and F. Sachs. Maximum likelihood estimation of ion channel kinetics from macroscopic currents. *Biophys J*, 88:2494–2515, 2005. [Cited in pp. 8 and 94].
- [125] I.I. Moraru and L.M. Loew. Intracellular signaling: Spatial and temporal control. *Physiology*, 20:169–179, 2005. [Cited in p. 96].

- [126] T. Moser and E. Neher. Rapid exocytosis in single chromaffin cells recorded from mouse adrenal slices. *J Neurosci*, 17:2314–2323, 1997. [Cited in p. 54].
- [127] A. Nadal, I. Quesada, and B. Soria. Homologous and heterologous asynchronicity between identified α -, β -, and δ -cells within intact islets of Langerhans in the mouse. *J Physiol*, 517.1:85–93, 1999. [Cited in p. 82].
- [128] E. Neher. Concentration profiles of intracellular calcium in the presence of a diffusible chelator. *Exp. Brain Res.*, 14:80–96, 1986. [Cited in p. 32].
- [129] E. Neher. Vesicle pools and Ca^{2+} microdomains: New tools for understanding their roles in neurotransmitter release. *Neuron*, 20:389–399, 1998. [Cited in pp. 4 and 51].
- [130] E. Neher. A comparison between exocytotic control mechanisms in adrenal chromaffin cells and a glutamatergic synapse. *Pflug Arch-Eur J Physiol*, 453:261–268, 2006. [Cited in pp. vi, 41, 52, and 54].
- [131] M. Oheim, F. Kirchhoff, and W. Sthmer. Calcium microdomains in regulated exocytosis. *Cell Calcium*, 40:423–439, 2006. [Cited in pp. 28 and 97].
- [132] H.L. Olsen, S. Theander, K. Bokvist, K. Buschard, C.B. Wollheim, and J. Gromada. Glucose stimulates glucagon release in single rat α -cells by mechanisms that mirror the stimulus-secretion coupling in α -cells. *Endocrinology*, 146:4861–4870, 2005. [Cited in pp. 77 and 86].
- [133] Mendes P. Gepasi: a software package for modelling the dynamics, steady states and control of biochemical and other systems. *Comput Appl Biosci*, 9:563571, 1993. <http://www.gepasi.org>. [Cited in p. 101].
- [134] E. Renstrom P. Rorsman, L. Eliasson, J. Gromada, S. Barg, and S. Gopel. The cell physiology of biphasic insulin secretion. *News Physiol Sci*, 14:72–77, 2000. [Cited in p. 72].
- [135] P. Pearle, B. Collett, K. Bart, D. Bilderback, D. Newman, and S. Samuels. What Brown saw and you can too. *Am J Phys*, 78:1278–1289, 2010. [Cited in p. 20].
- [136] M.G. Pedersen and A. Sherman. Newcomer insulin secretory granules as a high calcium-sensitive pool. *PNAS*, 106:18–22, 2009. [Cited in pp. 72 and 73].
- [137] A. Pérez-Alvarez and A. Albillos. Key role of the nicotinic receptor in neurotransmitter exocytosis in human chromaffin cells. *J Neurochem*, 103:2281–2290, 2007. [Cited in pp. 42 and 52].
- [138] J.A.G. Pertusa, J.V. Sánchez-Andrés, F. Martín, and B. Soria. Effects of calcium buffering on glucose-induced insulin release in mouse pancreatic islets: an approximation to the calcium sensor. *J Physiol*, 520.2:473–483, 1999. [Cited in pp. 17, 73, and 74].
- [139] F. Qin. Principles of single-channel kinetic analysis. *Meth Mol Biol*, 288:253–286, 2007. [Cited in p. 7].

- [140] I. Quesada, M.G. Todorova, P. Alonso-Magdalena, M. Beltrá, E.M. Carneiro, F. Martin, A. Nadal, and B. Soria. Glucose induces opposite intracellular Ca concentration oscillatory patterns in identified α - and β -cells within intact human islets of Langerhans. *Diabetes*, 55:2463–2469, 2006. [Cited in pp. 67, 68, and 70].
- [141] I. Quesada, E. Tudurí, C. Ripoll, and A. Nadal. Physiology of the pancreatic α -cell and glucagon secretion: role in glucose homeostasis and diabetes. *J Endocrin*, 199:5–19, 2008. [Cited in pp. vii, 66, 67, 68, 77, 88, 90, 92, 94, and 95].
- [142] I. Quesada, C. Villalobos, L. Núñez, P. Chamero, M.T. Alonso, A. Nadal, and J. García-Sancho. Glucose induces synchronous mitochondrial calcium oscillations in intact pancreatic islets. *Cell Calcium*, 43:39–47, 2008. [Cited in pp. 67 and 97].
- [143] N. Quoix, R. Cheng-Xue, L. Mattart, Z. Zeinoun, Y. Guiot, M.C. Beauvois, J-C Henquin, and P. Gilon. Glucose and pharmacological modulators of ATP-sensitive K^+ channels control $[Ca^{2+}]_c$ by different mechanisms in isolated mouse α -cells. *Diabetes*, 58(2):412–421, 2009. [Cited in pp. 67, 68, 73, and 82].
- [144] A.A. Qutub, F. Mac Gabhann, E.D. Karagiannis, P. Vempati, and A.S. Popel. Multiscale models of angiogenesis. *IEEE Eng Med Biol*, 28:14–31, 2009. [Cited in p. 101].
- [145] P. Rangamani and R. Iyengar. Modelling spatio-temporal interactions within the cell. *J. Biosci.*, 32:157167, 2006. [Cited in p. 1].
- [146] M.A. Ravier and G.A. Rutter. Glucose or insulin, but not zinc ions, inhibit glucagon secretion from mouse pancreatic α -cells. *Diabetes*, 54:1789–1797, 2005. [Cited in p. 86].
- [147] R. Rizzuto and T. Pozzan. Microdomains of intracellular Ca^{2+} : Molecular determinants and functional consequences. *Physiol rev*, 86:369–408, 2006. [Cited in p. 97].
- [148] P. Rorsman and E. Renstrom. Insulin granule dynamics in pancreatic beta cells. *Diabetologia*, 46:1029–1045, 2003. [Cited in p. 86].
- [149] P. Rorsman, S.A. Salehi, F. Abdulkader, M. Braun, and P.E. MacDonald. K_{ATP} -channels and glucose-regulated glucagon secretion. *Trends Endocrinol Metab*, 19:277–284, 2008. [Cited in p. 67].
- [150] K. Sätzler and et al. Three-dimensional reconstruction of a calyx of Held and its postsynaptic principal neuron in the medial nucleus of the trapezoid body. *J Neurosci*, 22:10567–10579, 2002. [Cited in pp. 27, 28, 29, and 31].
- [151] T. Sakaba and E. Neher. Calmodulin mediates rapid recruitment of fast-releasing synaptic vesicles at a calyx-type synapse. *Neuron*, 32:1119–1131, 2001. [Cited in pp. 28, 29, 32, and 33].

- [152] T. Sakaba and E. Neher. Quantitative relationship between transmitter release and calcium current at the calyx of Held synapse. *J Neurosci*, 21(2):462–476, 2001. [Cited in pp. 28, 29, 30, 32, and 33].
- [153] F. Sala and A. Hernández-Cruz. Calcium diffusion modeling in a spherical neuron. relevance of buffering properties. *Biophys J*, 57:313–324, 1990. [Cited in pp. 13 and 62].
- [154] A. Salehi, E. Vieira, and E. Gylfe. Paradoxical stimulation of glucagon secretion by high glucose concentrations. *Diabetes*, 55(8):2318–2323, 2006. [Cited in pp. 67, 68, and 77].
- [155] M.S.P. Sansom, F.G. Ball, C.J. Kerry, R. McGee, R.L. Ramsey, and P.N.R. Usherwood. Markov, fractal, diffusion, and related models of ion channel gating. *Biophys J*, 56:1229–1243, 1989. [Cited in pp. 8 and 94].
- [156] S. Calvo, R. Granja, C. González-García, and V. Ceña. Catecholamine secretion, calcium levels and calcium influx in response to membrane depolarization in bovine chromaffin cells. *Neurosci*, 68:265–272, 1995. [Cited in p. 46].
- [157] A. Schmid, S. Hallermann, R.J. Kittel, O. Khorramshahi, A.M.J. Frolich, C. Quentin, T.M. Rasse, S. Mertel, M. Heckmann, and S.J. Sigrist. Activity-dependent site-specific changes of glutamate receptor composition in vivo. *Nature Neurosci*, 11:659–666, 2008. [Cited in p. vi].
- [158] R. Schneggenburger and I.D. Forsythe. The calyx of Held. *Cell Tissue Res*, 326:311–337, 2006. [Cited in pp. 11, 27, and 32].
- [159] R. Schneggenburger and E. Neher. Intracellular calcium dependence of transmitter release rates at a fast central synapse. *Nature*, 406:889–893, 24 Aug 2000. [Cited in pp. 16, 29, 30, 31, 35, and 36].
- [160] J. Segura, A. Gil, and B. Soria. Modeling study of exocytosis in neuroendocrine cells: Influence of the geometrical parameters. *Biophys J*, 79:1771–1786, 2000. [Cited in pp. 2, 19, 21, 51, 54, 58, and 72].
- [161] J.R. Serrano, E. Pérez-Reyes, and S.W. Jones. State-dependent inactivation of the $\alpha 1G$ T-type calcium channel. *J Gen Physiol*, 114:185–201, 1999. [Cited in pp. 91 and 92].
- [162] Y. Serulle, M. Sugimori, and R.R. Llinás. Imaging synaptosomal calcium concentration microdomains and vesicle fusion by using total internal reflection fluorescent microscopy. *PNAS*, 104:1697–1702, 2007. [Cited in p. 97].
- [163] V. Shahrezaei and K.R. Delaney. Consequences of molecular-level Ca^{2+} channel and synaptic vesicle colocalization for the Ca^{2+} microdomain and neurotransmitter exocytosis: A monte carlo study. *Biophys J*, 87:2353–2364, 2004. [Cited in pp. 2, 13, 29, and 97].

- [164] M.F. Sheets, B.E. Scanley, D.A. Hanck, J.C. Makielski, and H.A. Fozzard. Open sodium channel properties of single canine cardiac purkinje cells. *Biophys J*, 52:13–22, 1987. [Cited in p. 91].
- [165] J.C. Sible and J.J. Tyson. Mathematical modeling as a tool for investigating cellular cycle control networks. *Methods*, 41:238–247, 2007. [Cited in p. 14].
- [166] S.M. Simon and R.R. Llinás. Compartmentalization of the submembrane calcium activity during calcium influx and its significance in transmitter release. *Biophys J*, 48(3):485–498, 1985. [Cited in p. 96].
- [167] B.M. Slepchenko, J.C. Schaff, J.H. Carson, and L.M. Loew. Computational cell biology: Spatiotemporal simulation of cellular events. *Annu Rev Biophys Biomol Struct*, 31:423–441, 2002. [Cited in p. 3].
- [168] M. Slucca, J.S. Harmon, E.A. Oseid, J. Bryan, and R.P. Robertson. ATP-sensitive k^+ channel mediates the zinc switch-off signal for glucagon response during glucose deprivation. *Diabetes*, 59:128–134, 2010. [Cited in p. 95].
- [169] D.O. Smith, J.L. Rosenheimer, and R.E. Kalil. Delayed rectifier and a-type potassium channels associated with $K_V2.1$ and $K_V4.3$ expression in embryonic rat neural progenitor cells. *PLoS one*, 3:1–9, 2008. [Cited in p. 91].
- [170] A.F. Strassberg and L.J. DeFelice. Limitations of the Hodgkin-Huxley formalism: Effects of single channel kinetics on transmembrane voltage dynamics. *Neural Comp*, 5:843–855, 1993. [Cited in p. 7].
- [171] T.C. Sudhof. Synaptotagmins: Why so many? *J Biol Chem*, 277:7629–7632, 2002. [Cited in pp. 15, 16, and 77].
- [172] J. Sun, Z.P. Pang, D.Qin, A.T. Fahim, R. Adachi, and T.C. Sudhof. A dual- Ca^{2+} -sensor model for neurotransmitter release in a central synapse. *Nature*, 450:676–683, 29 Nov 2007. [Cited in pp. 2, 16, 28, and 29].
- [173] A. Takahashi, P. Camacho, J.D. Lechleiter, and B. Herman. Measurement of intracellular calcium. *Physiol Rev*, 79:1089–1125, 1999. [Cited in pp. 4 and 14].
- [174] A.E. Takesian, V.C. Kotak, and D.H. Sanes. Developmental hearing loss disrupts synaptic inhibition: implications for auditory processing. *Future Neurol*, 4:331–349, 2009. [Cited in p. vii].
- [175] N.A. Tamarina, A. Kuznetsov, L.E. Fridlyand, and L.H. Philipson. Delayed-rectifier ($k_v2.1$) regulation of pancreatic β -cell calcium responses to glucose: inhibitor specificity and modeling. *Am J Physiol Endocrinol Metab*, 289:E578–E585, 2005. [Cited in pp. 91 and 93].
- [176] M. Tomita, K. Hashimoto, K. Takahashi, T.S. Shimizu, Y. Matsuzaki, F. Miyoshi, K. Saito, S. Tanida, K. Yugi, J.C. Venter, and C.A. Hutchison. E-cell: software environment for whole-cell simulation. *Bioinformatics*, 15:72–84, 1999. <http://www.e-cell-org>. [Cited in p. 101].

- [177] T.L. Török. Electrogenic Na^+/Ca^{2+} -exchange of nerve and muscle cells. *Prog Neurobiol*, 82:287–347, 2007. [Cited in p. 17].
- [178] C.J. Torregrosa-Hetland, J. Villanueva, D. Giner, I. López-Font, A. Nadal, I. Quesada, S. Viniegra, G. Expósito-Romero, A. Gil, V. González-Vélez, J. Segura, and L.M. Gutiérrez. The F-actin cortical network is a major factor influencing the organization of the secretory machinery in chromaffin cells. *J Cell Sci*, 124:727–734, 2011. [Cited in p. 44].
- [179] C.J. Torregrosa-Hetland, J. Villanueva, I. López-Font, V. García-Martínez, A. Gil, V. González-Vélez, J. Segura, S. Viniegra, and L.M. Gutiérrez. Association of SNAREs and calcium channels with the borders of cytoskeletal cages organizes the secretory machinery in chromaffin cells. *Cell Mol Neurobiol*, 30:1315–1319, 2010. [Cited in p. 43].
- [180] T.I. Tóth and V. Crunelli. Estimation of the activation and kinetic properties of i_{Na} and i_k from the time course of the action potential. *J Neurosci Meth*, 111:111–126, 2001. [Cited in p. 8].
- [181] J. Trommersháuser, R. Schneggenburger, A. Zippelius, and E. Neher. Heterogeneous presynaptic release probabilities: Functional relevance for short-term plasticity. *Biophys J*, 84:1563–1579, 2003. [Cited in p. 29].
- [182] E. Tudurí, E. Filiputti, E.M. Carneiro, and I. Quesada. Inhibition of Ca^{2+} signaling and glucagon secretion in mouse pancreatic α -cells by extracellular ATP and purinergic receptors. *Am J Physiol Endocrinol Metab*, 294:E952–E960, 2008. [Cited in pp. 67 and 78].
- [183] E. Tudurí, L. Marroquí, S. Soriano, A.B. Roperro, T.M. Batista, S. Piquer, M.A. López-Boado, E.M. Carneiro, R. Gomis, A. Nadal, and I. Quesada. Inhibitory effects of leptin on pancreatic α -cell function. *Diabetes*, 58:1–9, 2009. [Cited in pp. 67, 68, and 83].
- [184] C.A. Vandenberg and F. Bezanilla. A sodium channel gating model based on single channel, macroscopic ionic, and gating currents in the squid giant axon. *Biophys J*, 60:1511–1533, 1991. [Cited in p. 91].
- [185] E. Vieira, A. Salehi, and E. Gylfe. Glucose inhibits glucagon secretion by a direct effect on mouse pancreatic alpha cells. *Diabetologia*, 50:370–379, 2007. [Cited in pp. 67, 68, 86, and 87].
- [186] S. Vignali, V. Leiss, R. Karl, F. Hofmann, and A. Welling. Characterization of voltage-dependent sodium and calcium channels in mouse pancreatic a- and b-cells. *J Physiol*, 572.3:691–706, 2006. [Cited in p. 91].
- [187] J. Villanueva, C.J. Torregrosa-Hetland, A. Gil, V. González-Vélez, J. Segura, S. Viniegra, and L.M. Gutiérrez. The organization of the secretory machinery in chromaffin cells as a major factor in modeling exocytosis. *HFSP Journal*, 4:85–92, 2010. [Cited in pp. 50 and 58].

- [188] J. Villanueva, C.J. Torregrosa-Hetland, A. Gil, V. González-Vélez, J. Segura, S. Viniegra, and L.M. Gutiérrez. The organization of the secretory machinery in neuroendocrine chromaffin cells as a major factor to model exocytosis. *HFSP Journal*, 4(2):85–92, 2010. [Cited in p. 7].
- [189] T. Voets. Dissection of three Ca^{2+} -dependent steps leading to secretion in chromaffin cells from mouse adrenal slices. *Neuron*, 29:537–545, 2000. [Cited in pp. 2, 51, 54, 55, 56, 58, 63, 64, 72, 73, and 78].
- [190] T. Voets, E. Neher, and T. Moser. Mechanisms underlying phasic and sustained secretion in chromaffin cells from mouse adrenal slices. *Neuron*, 23:607–615, 1999. [Cited in pp. 54, 55, 58, and 99].
- [191] S. Wang, V.E. Bondarenko, Y. Qu, M.J. Morales, R.L. Rasmusson, and H.C. Strauss. Activation properties of $K_V4.3$ channels: time, voltage and $[k^+]_o$ dependence. *J Physiol*, 557.3:705–717, 2004. [Cited in p. 90].
- [192] A. Warashina and T. Ogura. Modeling of stimulation-secretion coupling in a chromaffin cell. *Pflug Arch-Eur J Physiol*, 448:161–174, 2004. [Cited in pp. 2 and 51].
- [193] J.F. Whitfield and B. Chakravarthy. *Calcium: The grand-master cell signaler*. NRC Research Press, Ottawa, 2001. [Cited in p. v].
- [194] C. Wierling, R. Herwig, and H. Lehrach. Resources, standards and tools for systems biology. *Brief Funct Genomic Proteomic*, 6:240–251, 2007. [Cited in p. 100].
- [195] A.R. Willms. Neurofit: software for fitting Hodgkin-Huxley models to voltage-clamp data. *J Neurosci Meth*, 121:139–150, 2002. [Cited in p. 7].
- [196] A.R. Willms, D.J. Baro, R.M. Harris-Warrick, and J. Guckenheimer. An improved parameter estimation method for Hodgkin-Huxley models. *J Comp Neurosci*, 6:145–168, 1999. [Cited in p. 7].
- [197] L.G. Wu and et al. Calcium channel types with distinct presynaptic localization couple differentially to transmitter release in single calyx-type synapses. *J Neurosci*, 19:726–736, 1999. [Cited in pp. 28 and 30].
- [198] W.M. Yamada and R.S. Zucker. Timer course of transmitter release calculated from simulations of a calcium diffusion model. *Biophys J*, 61:671–682, 1992. [Cited in pp. 2, 13, and 29].
- [199] G. Zamponi. *Voltage-gated calcium channels*. Landes Bioscience. Kluwer Academic/Plenum Publishers, New York, 2005. [Cited in pp. 5, 8, 28, 30, 40, and 92].
- [200] Q. Zheng and J. Ross. Comparison of deterministic and stochastic kinetics for nonlinear systems. *J Chem Phys*, 94:3644–3648, 1991. [Cited in p. 15].

-
- [201] L. Zylinska and M. Soszynski. Plasma membrane Ca^{2+} -ATPase in excitable and nonexcitable cells. *Acta Biochim Polonica*, 47(3):529–539, 2000. [Cited in p. 17].